THE HONG KONG
POLYTECHNIC UNIVERSITY
香港理工大學
Pao Yue-kong Library
包玉剛圖書館

Copyright Undertaking

This thesis is protected by copyright, with all rights reserved.

By reading and using the thesis, the reader understands and agrees to the following terms:

1. The reader will abide by the rules and legal ordinances governing copyright regarding the use of the thesis.
2. The reader will use the thesis for the purpose of research or private study only and not for distribution or further reproduction or any other purpose.
3. The reader agrees to indemnify and hold the University harmless from and against any loss, damage, cost, liability or expenses arising from copyright infringement or unauthorized usage.

If you have reasons to believe that any materials in this thesis are deemed not suitable to be distributed in this form, or a copyright owner having difficulty with the material being included in our database, please contact lbsys@polyu.edu.hk providing details. The Library will look into your claim and consider taking remedial action upon receipt of the written requests.

Pao Yue-kong Library, The Hong Kong Polytechnic University, Hung Hom, Kowloon, Hong Kong

http://www.lib.polyu.edu.hk

A SUB-GRIDDING SCHEME WITH PERFECTLY MATCHED INTERFACE FOR MRTD METHOD

CHOI KAI YIP

THE DEGREE OF MASTER OF PHILOSOPHY

THE HONG KONG POLYTECHNIC UNIVERSITY

2001

Pao Yue-Kong Library
PolyU • Hong Kong

Abstract

Recently, the multiresolution time domain method (MRTD) has been applied to many microwave problems. There are two different MRTD schemes. They are MRTD with scaling functions only (S-MRTD) and MRTD with scaling functions and wavelet functions (W-MRTD). In S-MRTD scheme, all the fields are expanded by Battle-Lemarie scaling function with respect to space. In W-MRTD scheme, all the fields are expanded by Battle-Lemarie scaling functions and Battle-Lemarie wavelet functions with respect to space. However, when the W-MRTD is applied to air-filled cavities, spurious mode is found in other published literature. In deriving the updating equations of the W-MRTD, it is necessary to compute several integrals. By modifying one of these integrals, spurious mode of the W-MRTD is removed.

Since wavelet is sensitive to sudden change, the W-MRTD will be used when a field problem involves instantaneous strong field variation. Hence, when it is necessary to compute the field accurately within an area, W-MRTD will be used. However, this results in increasing in both computational and memory resources as it is not necessary to have a high level of refinement in all regions. Hence, based on the need of calculating the fields accurately without wasting any unnecessary computer resources, the sub-gridding MRTD is proposed.

In sub-gridding MRTD scheme, the whole region is divided into dense grid regions and coarse grid regions. In the dense grid regions, the fields are expanded by both scaling functions and wavelet functions with respect to space. For the

coarse grid regions, fields are expanded by scaling functions only. However, non-physical reflection occurs in the boundary between the dense grid region and the coarse grid region. The non-physical reflection is due to the numerical wave of the wavelet coefficients at the boundary, which can be removed by the Anisotropic Perfectly Matched Layer (APML).

A sub-gridding MRTD scheme is applied to the two-dimensional problems. The propagation of the electromagnetic wave inside the cavity is considered. The time response are recorded and compared with the results obtained by the S-MRTD and W-MRTD. Also, we have applied the sub-gridding MRTD to study the resonant frequencies of an air-filled cavity. The memory resources and computation time of the sub-gridding MRTD are compared with the traditional FDTD, S-MRTD and the W-MRTD. It is found that the sub-gridding MRTD provides a good accuracy in measuring the resonant frequencies of the cavity, while it consumes less memory resources and fast computation time, compared with FDTD, S-MRTD and W-MRTD.

Acknowledgment

I wish to express my deep sense of gratitude to my supervisor Dr. W.Y. Tam. I am most grateful for his guidance, patience and support. This made me easier to go through some of the difficult times during this two years. Also, he gives me many valuable opinions in my graduate thesis. Besides, I would like to thanks the Department of Electronic and Information Engineering of the Hong Kong Polytechnic University and the Research Grant Committee of the University Grant Council for their facility and financial support.

Deepest appreciation is given to my parents for their unlimited patience and support. Also, I would like to thank my friends, C.K. Lee, Kenny Ho and Tommy Chan for their support. Finally, I would like to thank Christine Lau, who encourage me much during these days.

Contents

Statements of Originality

The following points are claimed to be original in this work:

1. Removal of the spurious mode of the multiresolution time domain method with wavelet (W-MRTD). (Chapter 1)

The multiresolution time domain method with wavelet (W-MRTD) is derived by expanding the unknown fields with the Battle-Lemarie scaling function and Battle-Lemarie wavelet functions for the spatial coordinates. Spurious mode of the MRTD is found in other published literature when the MRTD is applied to air-filled cavities. In deriving the updating equations of the MRTD, it is necessary to compute several integrals. By modifying one of these integrals, spurious mode of the W-MRTD is removed.

2. A sub-gridding MRTD (Chapter 2)

In the sub-gridding MRTD scheme, the whole region is divided into dense grid regions and coarse grid regions. In the dense grid regions, the fields are expanded by both scaling functions and wavelet functions with respect to space. For the coarse grid regions, fields are expanded by scaling functions only. Anisotropic Perfectly Matched Layer (APML) is placed at the boundary between the dense grid region and coarse grid region for the removal of non-physical reflection contributed by the wavelet coefficients.

3. Application of the sub-gridding MRTD for two-dimensional field problems (Chapter 3)

The sub-gridding MRTD is used to analysis the propagation of the electromagnetic pulse inside an extra large two-dimensional cavity. Different grid sizes have been used. The results are compared with the multiresolution time domain with scaling functions only (S-MRTD) and multiresolution time domain method with wavelets (W-MRTD).

Also, we have studied the resonant frequency of a small size two-dimensional cavity using sub-gridding MRTD. By keeping the percentage error below 1%, the memory resources and computation time of the sub-gridding MRTD are compared with the traditional FDTD, S-MRTD and W-MRTD.

Author's Publications

International Conference Paper

K. Y. Choi, W.Y. Tam, "The theory of sub-gridding MRTD," Proceedings, IEEE International Symposium on Antennas and Propagation Signal Processing, Vol1, pp.240-243, July 2000, Utah, USA.

K. Y. Choi, W.Y. Tam, "Numerical dispersion of Multiresolution Time Domain Method (W-MRTD)," Proceedings, IEEE International Symposium on Antennas and Propagation Signal Processing, Vol1, pp.256-259, July 2000, Utah, USA.

K. Y. Choi, W.Y. Tam, "The two-dimensional sub-gridding MRTD," Proceedings, The First IEEE Hong Kong MTT/AP/LEOS Postgraduate Conference, pp.37-38, September 2000, Hong Kong.

International Journal Paper

K. Y. Choi, W.Y. Tam, " A sub-gridding MRTD: new scheme of combining the S-MRTD and W-MRTD," (in preparation)

List of figures

List of tables

Chapter 1

Introduction

The electromagnetic field is governed by the Maxwell's equations, which were stated in 1870. Since then, both engineers and scientists have sought a way to solve them. The reason is that the solution of Maxwell's equations can help to understand many engineering purposes such as waveguide and antenna [1-6]. To solve the partial differential equations (PDE), initial conditions and boundary conditions have to be specified. In most of the cases, Maxwell's equations cannot be solved analytically. Hence, many numerical methods are developed for solving Maxwell's equations, such as the method of moments (MoM) [7], Yee's Finite Difference Time Domain Method (FDTD) [8] and the Multiresolution time domain method (MRTD) [9].

1.1 Background of the problem

In 1966, Kane Yee proposed the finite difference time domain method (FDTD) for solving the Maxwell's equations. In FDTD algorithm, the Maxwell's equations are discretized by the central difference schemes. Because of its simplicity and modeling versality, FDTD is now one of the most popular numerical methods for the solution of the electromagnetic problems. However, FDTD suffers from limitations that are required large computational resources, especially when the electromagnetic problems involve large structure or high frequency signal. In order to solve those problems, many techniques are developed such as local gridding [10-12]. Instead of improving the FDTD, a new computational scheme, which is called multiresolution time domain method (MRTD) [9], was published in 1994. Comparing with the FDTD, MRTD, which has highly linear dispersion characteristics, consumes less computer resources [9].

The MRTD comes from the concept of wavelet analysis, which is a newly developed mathematics concept over the last thirty years. Since the first paper of the MRTD was published, many papers from worldwide, concerning this new computational scheme, have been published [12-26]. The MRTD updating scheme is resulted from discretizing the Maxwell's equations by method of moment (MoM) [7] with scaling functions and wavelets functions as the basis functions [33]. Two different kinds of MRTD have been reported. They are MRTD with scaling functions only (S-MRTD) and MRTD with both scaling functions and wavelet functions (W-MRTD). Compared

with the FDTD, the formulation of MRTD is more complicated. However, it has been shown that the MRTD can be generalizd into the Yee's FDTD [28-29]. Also, MRTD saves lot of computer resources in terms of the number of grid points and simulation time steps.

One of the properties of wavelet is that it is sensitive to sudden change [30]. Hence, W-MRTD is used especially when the field problem involves instantaneous strong field variations. Compared with the S-MRTD, it requires more grids and smaller time steps [9]. Hence, when it is necessary to compute the field accurately within an area, W-MRTD will be used. However, this results in increasing both computational and memory resources as it is not necessary to have a high level of refinement in all regions. In most situations, we only need refined grids in certain regions while coarse grids are used in other regions. Since both W-MRTD and S-MRTD compute the electromagnetic fields by uniform grid discretization, it is desirable to develop a new computational method so that the refined grids exist only in regions, which require dense discretization.

1.2. Research methodology

The object of this dissertation is to develop a new MRTD scheme, which contains both refined grids and coarse grids in different regions. Instead of using an adaptive grid [25], we are looking for a structural grid so that wavelet is used to expand the

field components within certain regions only. This new MRTD scheme should have a similar order of accuracy with W-MRTD.

In this dissertation, a sub-gridding MRTD is proposed. The sub-gridding MRTD consists of regions with different cell sizes. The coarse grid region corresponds to the S-MRTD and the dense grid region corresponds to the W-MRTD. However, non-physical reflection occurs at the boundary between the coarse grids and the dense grids. The non-physical reflection is due to the numerical wave of the wavelet coefficients at the boundary. To remove the numerical wave introduced by the wavelet coefficients, an Anisotropic Perfectly Matched Layer (APML) is placed at the boundary.

1.3 Overview of Yee's finite difference time domain method

The finite difference time domain method (FDTD), which was proposed by Kane Yee in 1966 [8], is one of the most popular numerical methods for the solution of the electromagnetic problems. The solution of the electromagnetic problems is governed by the Maxwell's equations, which can be solved by the use of the FDTD algorithm. The FDTD algorithm is derived by discretizing the Maxwell's equations using a central difference scheme [31]. In this section, we will discuss briefly the FDTD algorithm.

In FDTD algorithm, space and time are discretized into discrete space points and time steps. As seen in figure 1.1, the continuous space is discretized into discrete space with space increments Δx, Δy and Δz in the x, y and z coordinates respectively.

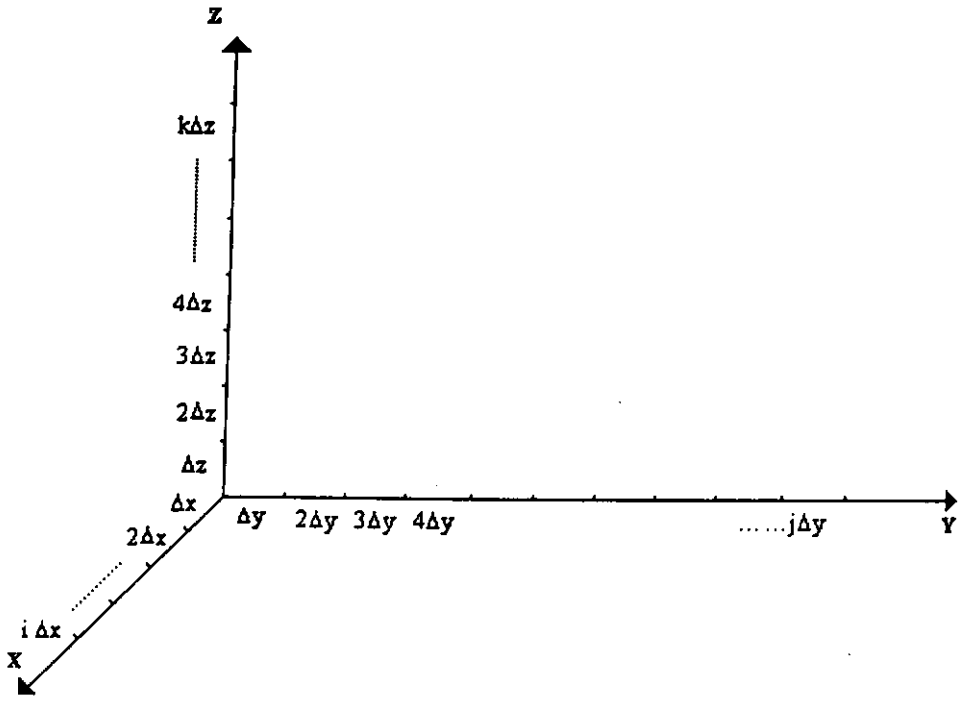

Figure 1.1. The FDTD discretization of the continuous space.

Hence, a continuous function in the spatial domain is discretized into a discrete function in FDTD algorithm. To illustrate this concept, let u be a function of space and time.

$$u = u(x, y, z, t) \tag{1.1}$$

In FDTD, the function u is discretized and it is denoted as $u^n_{i,j,k}$, which is given by

$$u^n_{i,j,k} = u(i\Delta x, j\Delta y, k\Delta z, n\Delta t) \tag{1.2}$$

where Δt is the time increment in t coordinate. i, j, k and n are integers. To obtain the FDTD scheme, the partial differentials in Maxwell's equations are discretized by central difference scheme as follows.

$$\frac{\partial u}{\partial x}(i\Delta x, j\Delta y, k\Delta z, n\Delta t) = \frac{u^n_{i+1/2,j,k} - u^n_{i-1/2,j,k}}{\Delta x} + [(\Delta x)^2] \tag{1.3}$$

$$\frac{\partial u}{\partial t}(i\Delta x, j\Delta y, k\Delta z, n\Delta t) = \frac{u^{n+1/2}_{i,j,k} - u^{n-1/2}_{i,j,k}}{\Delta t} + [(\Delta t)^2] \tag{1.4}$$

As seen in equation (1.3) and (1.4), central difference scheme is second order accurate. Making use the central difference scheme stated at equation (1.3) and (1.4), we can derive the FDTD scheme. We start from the Maxwell's equations. For a homogeneous loseless medium, the Maxwell's Equations are

$$\nabla \times E = -\mu \frac{\partial}{\partial t} H \tag{1.5}$$

$$\nabla \times H = \varepsilon \frac{\partial}{\partial t} E \tag{1.6}$$

where E is the electric field, H is the magnetic field, μ is the magnetic permeability, and ε is the electric permittivity. In matrix form,

$$\begin{bmatrix} 0 & -\partial_z & \partial_y \\ \partial_z & 0 & -\partial_x \\ -\partial_y & \partial_x & 0 \end{bmatrix} \begin{bmatrix} E_x \\ E_y \\ E_z \end{bmatrix} = -\mu \frac{\partial}{\partial t} \begin{bmatrix} H_x \\ H_y \\ H_z \end{bmatrix} \tag{1.7}$$

$$\begin{bmatrix} 0 & -\partial_z & \partial_y \\ \partial_z & 0 & -\partial_x \\ -\partial_y & \partial_x & 0 \end{bmatrix} \begin{bmatrix} H_x \\ H_y \\ H_z \end{bmatrix} = \varepsilon \frac{\partial}{\partial t} \begin{bmatrix} E_x \\ E_y \\ E_z \end{bmatrix} \tag{1.8}$$

Hence, there are six equations, which are equivalent to the Maxwell's equations in the three- dimensional coordinates. For simplicity of discussion, we only consider the FDTD updating equation of the following equation.

$$\frac{\partial}{\partial z} E_y - \frac{\partial}{\partial y} E_z = \mu \frac{\partial}{\partial t} H_x \tag{1.9}$$

In the three-dimensional rectangular coordinates, H_x field is a function of x, y, z and t. H_x is represented as $H_x(x, y, z, t)$. In FDTD algorithm, H_x is represented as $H_x(i\Delta x, j\Delta y, k\Delta z, n\Delta t)$. Using the central difference scheme as stated in equation (1.3) and equation (1.4), the R.H.S. of equation (1.9) becomes

$$\mu \frac{\partial}{\partial t} H_x = \mu \frac{H_x^{n+1/2}(i, j, k) - H_x^{n-1/2}(i, j, k)}{\Delta t} \tag{1.10}$$

and the L.H.S. of equation (1.9) becomes

$$\frac{\partial}{\partial z}E_y - \frac{\partial}{\partial y}E_z = \frac{E_y^n(i,j,k+1/2) - E_y^n(i,j,k-1/2)}{\Delta z} - \frac{E_z^n(i,j+1/2,k) - E_z^n(i,j-1/2,k)}{\Delta y} \tag{1.11}$$

By substituting the equation (1.10) and equation (1.11) into equation (1.9), we get the FDTD updating equation of H_x field as follows.

$$H_x^{n+1/2}(i,j,k) = H_x^{n-1/2}(i,j,k) + \frac{\Delta t}{\mu}\left(\frac{E_y^n(i,j,k+1/2) - E_y^n(i,j,k-1/2)}{\Delta z} - \frac{E_z^n(i,j+1/2,k) - E_z^n(i,j-1/2,k)}{\Delta y} \right) \tag{1.12}$$

The FDTD updating equation of the remaining electric fields (E) and magnetic fields (H) can be obtained using the same method. Taking E_x as an example, the FDTD updating equation of E_x is

$$E_x^{n+1}(i,j+1/2,k+1/2) = E_x^n(i,j+1/2,k+1/2) + \frac{\Delta t}{\varepsilon}\left(\frac{H_z^n(i,j+1,k+1/2) - H_z^n(i,j,k+1/2)}{\Delta y} - \frac{H_y^n(i,j+1/2,k+1) - H_y^n(i,j+1/2,k)}{\Delta z} \right) \tag{1.13}$$

One of the characteristics of the FDTD is the time step of the magnetic fields (H) shifted ½ from the time step of the electric fields (E). Also, the electric fields (E) grid offset spatially from magnetic fields (H) grids. This can be seen in figure 1.2. In order to have a stable result, Δt must be chosen as

$$\Delta t \leq \frac{1}{c\sqrt{\left(\frac{1}{\Delta x}\right)^2+\left(\frac{1}{\Delta y}\right)^2+\left(\frac{1}{\Delta z}\right)^2}} \tag{1.14}$$

[31] where c is the velocity of electromagnetic wave in free space. Besides, the grid size (Δ) is usually chosen from 0.02 to 0.05 of the wavelength of the electromagnetic wave.

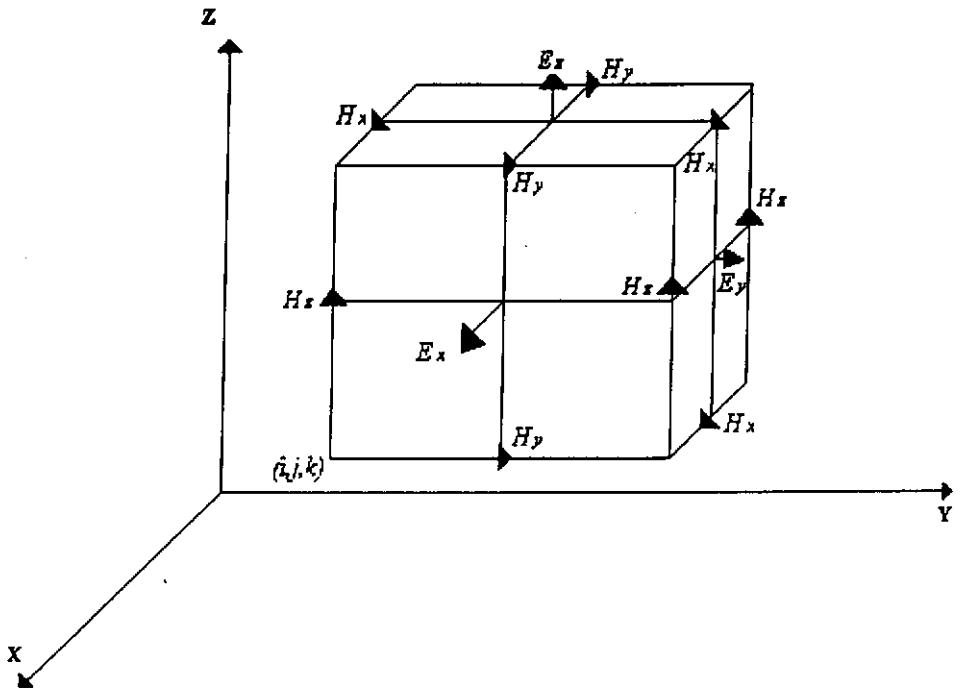

Figure 1.2. The position of the electric fields and magnetic fields in FDTD grid

As the grid size is proportional to the wavelength of the signal under simulation, this leads to the increase of the computational resources when the electromagnetic problems involve large structure or high frequency signal. In order to solve this problem, many techniques are developed such as local gridding [10-12]. In the next chapter, we will introduce a new computational scheme, which is called multiresolution time domain method (MRTD) [9]. Compared with the FDTD, MRTD consumes less computational and memory resources [9].

Chapter 2

Introduction to Multiresolution Time Domain Method (MRTD)

In last chapter, we have discussed briefly the FDTD algorithm, which is now one of the most popular numerical methods for the solution of the electromagnetic problems. Since the FDTD suffers from a limitation that large computational resources are required especially when the electromagnetic problems involve large structure or high frequency signal. In this chapter, we will introduce the Multiresolution Time Domain Method (MRTD), which is based on the orthogonal expansion of the fields in terms of scaling functions and wavelets. Comparing with the FDTD, the formulation of the MRTD is rather complicated. However, it requires less computational and memory resources. In order to understanding the concepts of MRTD, we will also discuss the concepts of wavelet expansion.

2.1 Introduction to wavelet expansion

Two functions, y_1 and y_2 are orthogonal, if they satisfy the following conditions. That is,

$$\int_{-\infty}^{+\infty} y_1(x) \cdot y_2(x) dx = 0 \ . \tag{2.1}$$

The most famous example is the Fourier series, which compose of a series of harmonics. That is,

$$F(x) = \sum_{n=-\infty}^{+\infty} F_n e^{jn\omega x} \ . \tag{2.2}$$

These harmonics are orthogonal to each other because

$$\int_{-\infty}^{+\infty} e^{j\omega x(n-m)} dx = \delta_{n,m} \tag{2.3}$$

$$\text{where } \delta_{n,m} = \begin{cases} 1 & \text{when } n = m \\ 0 & \text{otherwise} \end{cases} .$$

In general, a function $F(x)$ can be expanded in terms of any complete set of orthogonal functions. That is, it can be written as

$$F(x) = \sum_{n=-\infty}^{+\infty} F_n \phi(x-n) \tag{2.4}$$

where n=0,1,2,3,4,... and $\phi(x)$ satisfies the following condition.

$$\int_{-\infty}^{+\infty} \phi(x-m)\phi(x-n)dx = \delta_{n,m} \tag{2.5}$$

By the property of orthogonality, the coefficient of F_n can be obtained by the following relationship:

$$F_n = \int_{-\infty}^{\infty} F(x)\phi(x-n)dx \tag{2.6}$$

where n=0, 1 ,2 ,3 ,4 ,5,...

2.1.1 Multiresolution Analysis

Another concept, which is necessary in our proposed method, is the idea of multiresolution analysis [30,32]. In brief, multiresolution analysis (MRA) consists of orthogonal basis of $\{\phi_{mn}(x) = 2^{m/2}\phi(2^m x - n); n \in Z\}$ and $\{\psi_{mn}(x) = 2^{m/2}\psi(2^m x - n); n \in Z\}$, which, respectively, generates a scaling space V_m and a complementary space W_m, so that they satisfy the following properties:

$$\cdots \subseteq V_{-m} \subseteq V_{-m+1} \cdots \subseteq V_{-2} \subseteq V_{-1} \subseteq V_0 \subseteq V_1 \subseteq V_2 \subseteq \cdots \subseteq V_m \subseteq V_{m+1} \cdots \tag{2.7}$$

$$\overline{\bigcup_{j \in Z} V_j} = L^2(R) \tag{2.8}$$

$$\bigcap_{j \in Z} V_j = \{0\} \tag{2.9}$$

$$V_{j+1} = V_j \oplus W_j \tag{2.10}$$

$$W_j \cap W_m = \{0\} \tag{2.11}$$

$$f(x) \in V_0 \Leftrightarrow f(2^j x) \in V_j \tag{2.12}$$

For simplicity, we denote the first orthogonal basis set $\{\phi_{mn}(x) = 2^{m/2}\phi(2^m x - n); n \in Z\}$ as Φ_m. That is,

$$\Phi_m = \{\phi_{mn}(x) = 2^{m/2}\phi(2^m x - n); n \in Z\}. \tag{2.13}$$

We denote the latter set of orthogonal basis $\{\psi_{mn}(x) = 2^{m/2}\psi(2^m x - n); n \in Z\}$ as Ψ_m. That is,

$$\Psi_m = \{\psi_{mn}(x) = 2^{m/2}\psi(2^m x - n); n \in Z\}. \tag{2.14}$$

The orthogonal basis Φ_m belongs to the scaling space V_m while the orthogonal basis of Ψ_m belongs to the complementary space W_m. Mathematically, we can state these as

$$\Phi_m \in V_m \tag{2.15}$$

$$\text{and } \Psi_m \in W_m \ . \tag{2.16}$$

Since the orthogonal basis Φ_m belongs to V_m, any function, which belongs to V_m, can be expanded by this orthogonal basis Φ_m. Let $f(x)$ be the function, which belongs to the scaling space V_m, we can expand it by the orthogonal basis Φ_m as

$$f(x) = 2^{m/2} \sum_{n=-\infty}^{\infty} f_n^m \phi(2^m x - n) \tag{2.17}$$

where f_n^m is the scaling coefficient of $f(x)$, which is given by

$$f_n^m = 2^{m/2} \int_{-\infty}^{+\infty} f(x)\phi(2^m x - n)\mathrm{d}x\,. \tag{2.18}$$

From the property of multiresolution analysis stated in equation (2.10), the scaling space V_m is equal to the direct sum of the scaling space V_{m-1} and the complementary space W_{m-1}. This can be illustrated by following figure.

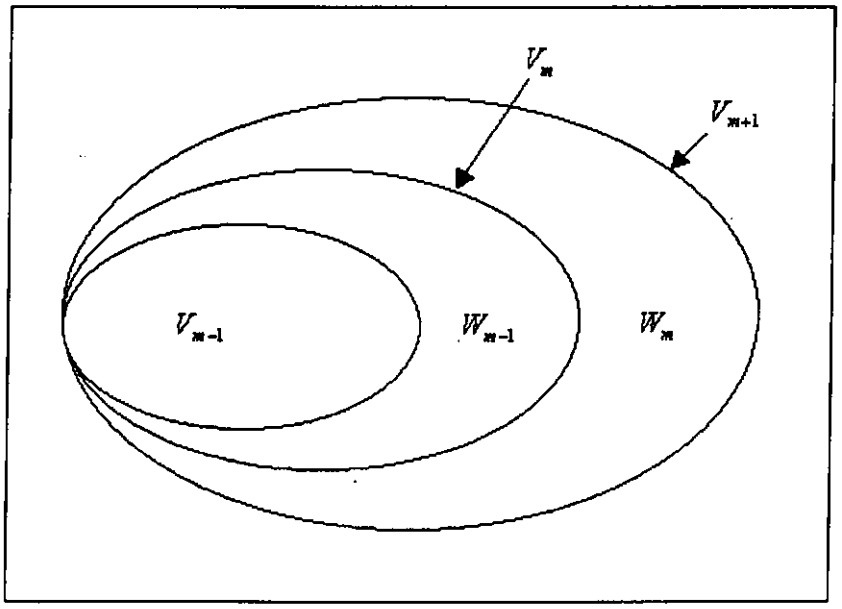

Figure 2.1. The relationship of the successive scaling spaces

From figure 2.1, the scaling space V_m is composed of the scaling space V_{m-1} and its complementary space W_{m-1}. In other words, the function which belongs to V_m can also be expanded by the orthogonal basis in V_{m-1} and W_{m-1}. The orthogonal basis in V_{m-1} and W_{m-1} are Φ_{m-1} and Ψ_{m-1} respectively. As stated in equation (2.13) and equation (2.14),

$$\Phi_{m-1} = \left\{\phi_{m-1n}(x) = 2^{(m-1)/2}\phi(2^{m-1}x - n); n \in \mathrm{Z}\right\} \tag{2.19}$$

and

$$\Psi_{m-1} = \left\{\psi_{m-1n}(x) = 2^{(m-1)/2}\psi(2^{m-1}x - n); n \in \mathrm{Z}\right\}. \tag{2.20}$$

Let $f(x)$ be a function belongs *to* V_m, the function $f(x)$ can be expanded by Φ_{m-1} and Ψ_{m-1}. Therefore, we can write

$$f(x) = 2^{(m-1)/2}\sum_{n=-\infty}^{\infty} C_n^{m-1}\phi(2^{m-1}x - n) + 2^{(m-1)/2}\sum_{n=-\infty}^{\infty} D_n^{m-1}\psi(2^{m-1}x - n) \tag{2.21}$$

where C_n^{m-1} is the scaling coefficient of $f(x)$, which is given by

$$C_n^{m-1} = 2^{(m-1)/2}\int_{-\infty}^{+\infty} f(x)\phi(2^{m-1}x - n)dx \tag{2.22}$$

and D_n^{m-1} is the wavelet coefficient of $f(x)$, which is given by

$$D_n^{m-1} = 2^{(m-1)/2}\int_{-\infty}^{+\infty} f(x)\psi(2^{m-1}x - n)dx. \tag{2.23}$$

The orthogonal basis Φ_{m-1} in the scaling space is called scaling functions. The orthogonal basis Ψ_{m-1} in the complementary space is called the wavelets [30,32].

The idea of this multiresolution analysis, which consists of scaling functions and wavelets, allows the possibility of representing a function with different order of approximations. Assuming there is a function $f(x)$ belonging to a scaling space V_{m-1}, the function can be expanded by the basis Φ_{m-1}. That is,

$$f(x) = 2^{(m-1)/2} \sum_{n=-\infty}^{\infty} C_n^{m-1} \phi(2^{m-1}x - n). \tag{2.24}$$

The same function $f(x)$, which belongs to a scaling space V_m, can be expanded by the basis Φ_m. That is,

$$f(x) = 2^{m/2} \sum_{n=-\infty}^{\infty} f_n^m \phi(2^m x - n). \tag{2.25}$$

The function $f(x)$ can also be expanded by the orthogonal basis Φ_{m-1} and Ψ_{m-1}. Therefore, we have

$$f(x) = 2^{(m-1)/2} \sum_{n=-\infty}^{\infty} C_n^{m-1} \phi(2^{m-1}x - n) + 2^{(m-1)/2} \sum_{n=-\infty}^{\infty} D_n^{m-1} \psi(2^{m-1}x - n). \tag{2.26}$$

The function, which belongs to scaling space, V_m is expanded by both $\phi_{m-1n}(x)$ and $\psi_{m-1n}(x)$ while the function belongs to V_{m-1} is expanded by $\phi_{m-1n}(x)$ only. Hence, the

function which belongs to V_m will have better approximation when it is compared with the function belongs to V_{m-1}. The reason is that the scaling space V_m samples the function with more points, when it is compared with the scaling space V_{m-1}. Theoretically, any the function can be expressed as

$$f(x) = 2^{m/2} \sum_{j=-\infty}^{\infty} C_j^m \phi(2^m x - n) + \sum_{p=m}^{+\infty} 2^{p/2} \sum_{n=-\infty}^{\infty} D_k^p \psi(2^p x - n) \ . \qquad (2.27)$$

In practice, when we want to have a very good approximation of a function, we express the function with more basis functions. This is equally assuming that the function belongs to a scaling space with higher order. Instead, if we want to have an acceptable level of approximation, the function will be expressed with fewer basis functions. In order words, the function corresponds to the scaling space with lower order.

As seen in the architecture of the successive scaling space, the complementary space W_m, which carries detailed information, plus the scaling space V_m with rough information to form a scaling space of higher scale. This can be illustrated by the figure 2.2. A function $f(x)$ on scaling space V_1 is constituted by the local information of $f(x)$ given by the wavelet in W_0 together with global information of $f(x)$ provided by V_0.

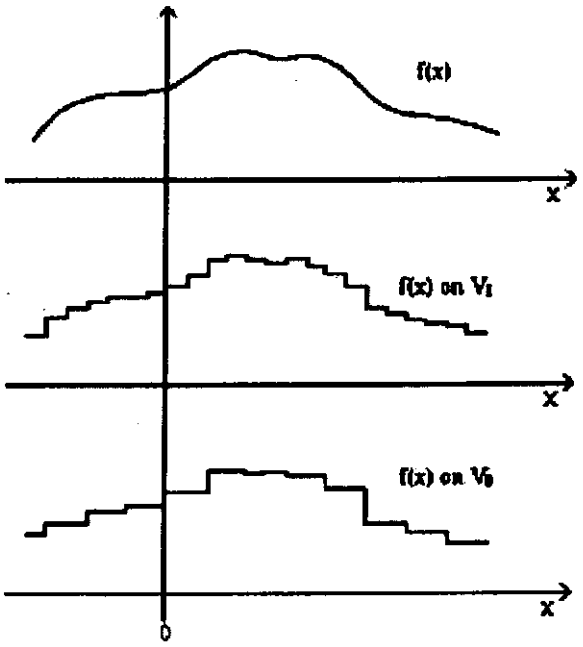

Figure 2.2. A function $f(x)$ on V_1 and V_0

In simple terms, the scaling space V_m provides the skeleton of the global information while the complementary space W_m gives the detailed local information, which is characterized by the wavelet basis. Hence, wavelet is sensitive to sudden sharp change and it has been applied in many areas for sharp change detection [34-35].

2.1.2 Battle-Lemarie System

There are many different kinds of wavelet systems such as, the Haar system and the Battle-Lemarie System. The Haar system is constructed by the Haar scaling function and Haar wavelet function, which are shown in figure 2.3 and 2.4. The Battle-Lemarie

system, which is constructed by the Battle-Lemarie scaling function and Battle-Lemarie wavelet function, has been used in the MRTD for the expansion of the field [9].

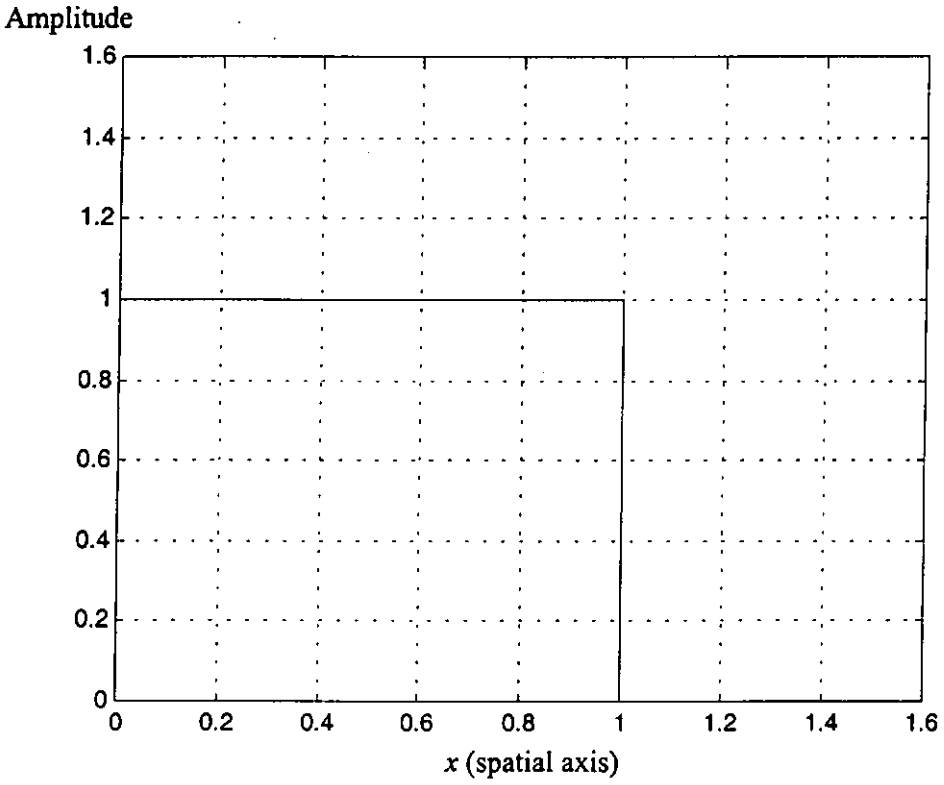

Figure 2.3. Haar scaling function in spatial domain

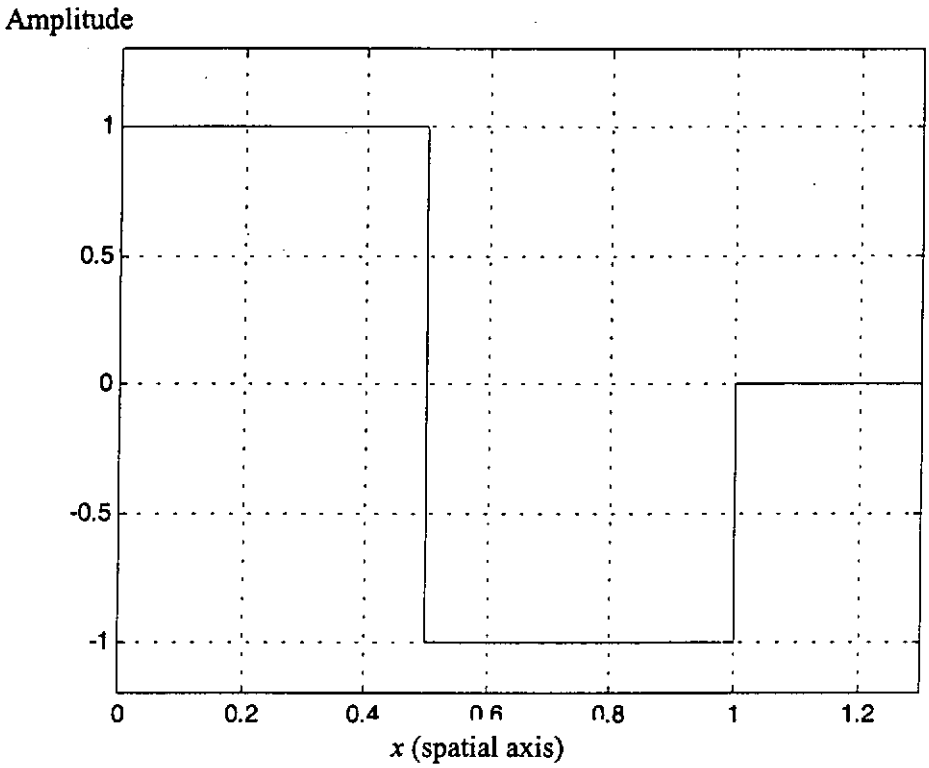

Figure 2.4. Haar wavelet function in spatial domain

Battle-Lemarie scaling function $\phi(x)$ is formed by cubic spline $N_3(x)$, which is defined as

$$N_3(x) = \begin{cases} \dfrac{4-6x^2+3|x|^3}{6} & \text{for } |x| \le 1 \\ \dfrac{(2-|x|)^3}{6} & \text{for } 1<|x| \le 2 \\ 0 & \text{for } |x| \ge 2 \end{cases} . \qquad (2.28)$$

The Battle-Lemarie scaling function $\phi(x)$ doesn't have a closed form in spatial domain. The spectral domain of the Battle-Lemarie scaling function $\phi(x)$ is governed by the following expression.

$$\hat{\phi}(\lambda) = \frac{\hat{N}_3(\lambda)}{\sqrt{\sum_{k=-\infty}^{\infty} \left|\hat{N}_3(\lambda + 2\pi k)\right|^2}} \tag{2.29}$$

where $\hat{\phi}(\lambda)$ is the Fourier transform of $\phi(x)$ and it is determined by

$$\hat{\phi}(\lambda) = \int_{-\infty}^{\infty} \phi(x) e^{-j\lambda x} dx \tag{2.30}$$

and $\hat{N}_3(\lambda)$ is the Fourier transform of $N_3(x)$ and it is determined by

$$\hat{N}_3(\lambda) = \int_{-\infty}^{\infty} N_3(x) e^{-j\lambda x} dx . \tag{2.31}$$

The denominator of (2.29) is resulted from the orthonormalization trick as in [32]. Hence, $\hat{\phi}(\lambda)$ is determined by the following equation.

$$\hat{\phi}(\lambda) = \frac{\left[\frac{\sin(\lambda/2)}{\lambda/2}\right]^4}{\sqrt{\left(1 - \frac{4}{3}\sin^2(\frac{\lambda}{2}) + \frac{2}{5}\sin^4(\frac{\lambda}{2}) - \frac{4}{315}\sin^6(\frac{\lambda}{2})\right)}} \tag{2.32}$$

It can be seen that this function has low pass characteristic as shown in figure 2.5.

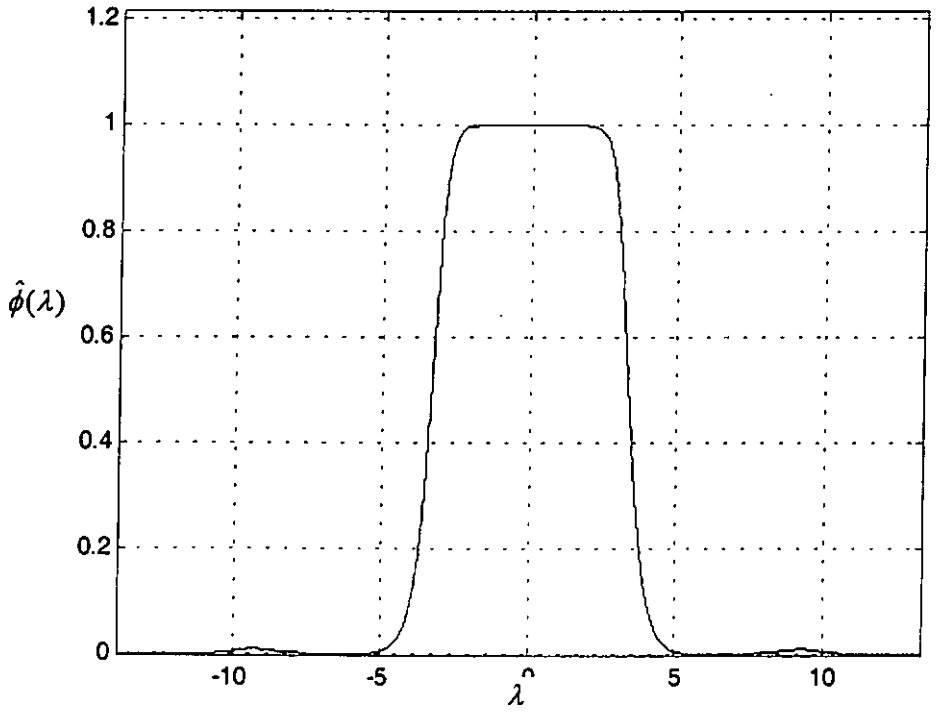

Figure 2.5. Battle-Lemarie scaling function in frequency domain

The Battle-Lemarie scaling function $\phi(x)$ can be determined by setting

$$\left(\sum_{k=-\infty}^{\infty} \left| \hat{N}_3(\lambda + 2\pi k) \right|^2 \right)^{-1/2} = \sum_{n=-\infty}^{+\infty} C_n e^{-jn\lambda} \quad . \tag{2.33}$$

Then, the equation (2.33) is substituted to equation (2.29). The equation (2.29) becomes

$$\hat{\phi}(\lambda) = \sum_{n=-\infty}^{+\infty} C_n e^{-jn\lambda} \hat{N}_3(\lambda) \quad . \tag{2.34}$$

The inverse Fourier transform is defined as

$$\phi(x) = \frac{1}{2\pi} \int_{-\infty}^{\infty} \hat{\phi}(\lambda) e^{j\lambda x} dx \, . \tag{2.35}$$

Then, taking inverse Fourier transform at both sides of equation (2.34), the equation (2.34) becomes

$$\phi(x) = \sum_{n=-\infty}^{+\infty} C_n N_3(x-n) \tag{2.36}$$

where C_n can be calculated by

$$C_n = \frac{1}{2\pi} \int_0^{2\pi} \left(\sum_{k=-\infty}^{\infty} \left| \hat{N}_3(\lambda + 2\pi k) \right|^2 \right)^{-1/2} e^{+jn\lambda} d\lambda \quad . \tag{2.37}$$

Some of the coefficients C_n are given by Table 2.1. The spatial characteristic of the Battle-Lemarie scaling function $\phi(x)$ is shown in figure 2.6

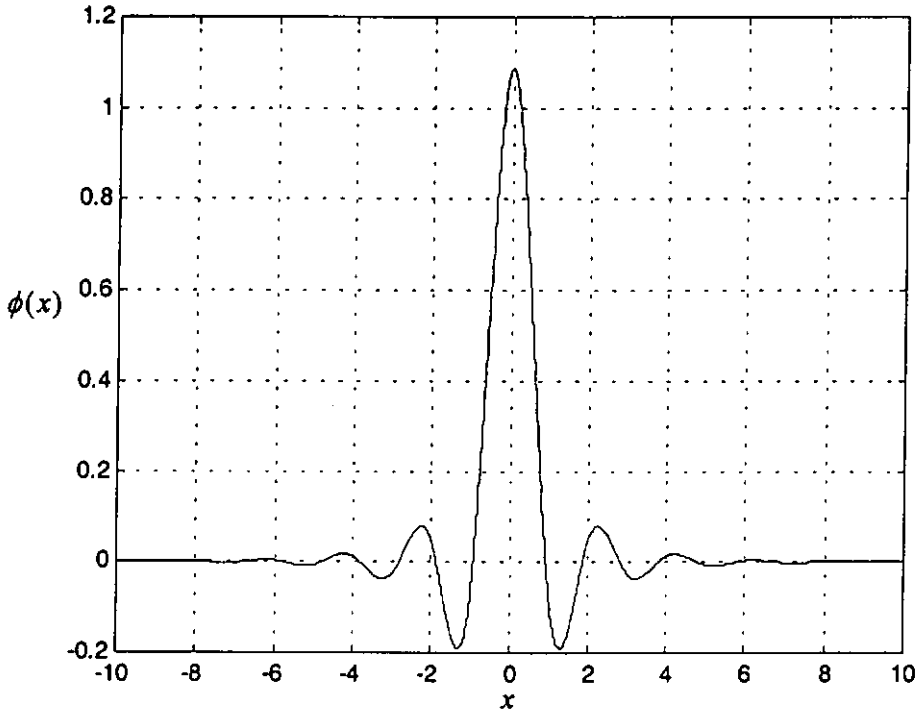

Figure 2.6. Battle-Lemarie scaling function in spatial domain

. Similarly, the Battle-Lemarie wavelet function $\psi(x)$ is determined by

$$\psi(x) = \sum_{n=-\infty}^{\infty} D_n N_3(2x-n) \tag{2.38}$$

where the coefficient D_n are given in Table 2.1. The spatial characteristic of the Battle-Lemarie wavelet function $\psi(x)$ is shown in figure 2.7. The spectrum domain of the Battle-Lemarie wavelet function $\psi(x)$ is determined by [30,32]

$$\hat{\psi}(\lambda) = e^{j\lambda/2} \frac{\hat{\phi}(\lambda+2\pi)}{\hat{\phi}(\lambda/2+2\pi)} \hat{\phi}(\lambda/2) \tag{2.39}$$

and the high pass characteristic of this wavelet function is seen in figure 2.8.

Comparing with the Haar system, the Battle-Lemarie scaling function has low pass characteristics with steep rejection outside the passband. With the same level of the resolution, the Battle-Lemarie scaling function sample more points compared with the Haar scaling function. Also, the bandpass characteristics of Battle-Lemarie wavelet function allows accurate sampling of the high frequency content of the signal without increasing the resolution level of the scaling functions [35].

In next section, we can see the advantages of using Battle-Lemarie system for the MRTD discretization. Because the Battle-Lemarie scaling functions and Battle-Lemarie wavelet functions have closed form expressions and band limited characteristics, these simplify the derivation of the MRTD.

n	C_n	D_n
0	1.9697616	0
1	-0.6724304	2.8917339
2	0.2687042	-2.0052104
3	-0.1185199	0.5422788
4	0.0551914	-0.0120712
5	-0.0265203	0.1440885
6	0.0129981	-0.1459123
7	-0.0064574	0.0030182
8	0.0032398	0.0283441
9	-0.0016377	0.0191491
10	0.0008328	-0.0224618

Table 2.1 The coefficients of C_n and D_n

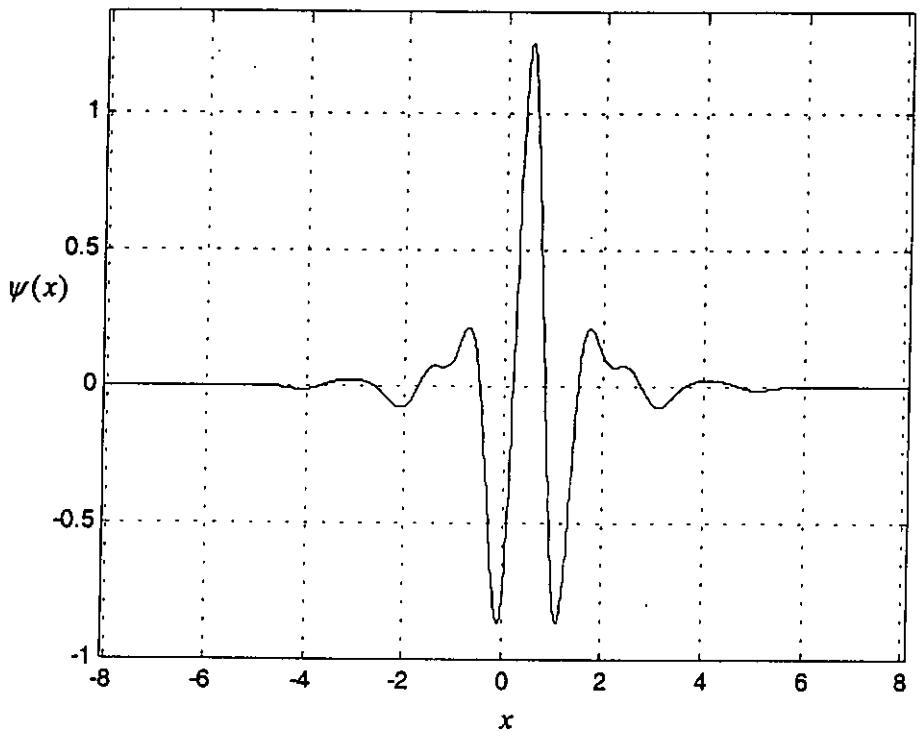

Figure 2.7 Battle-Lemarie wavelet function in spatial domain

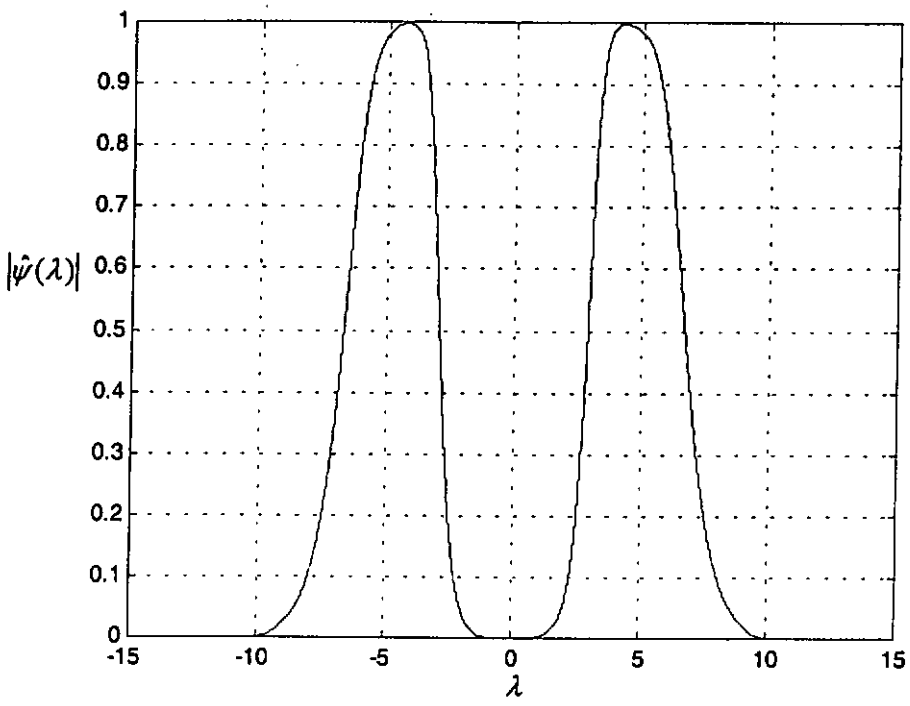

Figure 2.8. Battle-Lemarie wavelet function in frequency domain

2.2 Multiresolution Time Domain Method

Combining the multiresolution analysis and Battle-lemarie system mentioned in section 2.1, the multiresolution time domain method (MRTD) has been developed [9]. This computational scheme named Multiresolution Time domain Method (MRTD) is resulted by expanding the unknown fields with the Battle-Lemarie scaling functions and Battle-Lemarie wavelet functions [9,35] for the spatial coordinates and the pulse function is used for the expansion of the time coordinates.

2.2.1 Formulation

For a homogeneous loseless medium,.the Maxwell's Equations in differential form are

$$\nabla \times \boldsymbol{E} = -\mu \frac{\partial}{\partial t} \boldsymbol{H} \tag{2.40}$$

$$\nabla \times \boldsymbol{H} = \varepsilon \frac{\partial}{\partial t} \boldsymbol{E} \tag{2.41}$$

After expanding equation (2.40) in Cartesian coordinates, it becomes

$$\frac{\partial}{\partial z} E_y - \frac{\partial}{\partial y} E_z = \mu \frac{\partial}{\partial t} H_x \tag{2.42}$$

$$\frac{\partial}{\partial x} E_z - \frac{\partial}{\partial z} E_x = \mu \frac{\partial}{\partial t} H_y \tag{2.43}$$

$$\frac{\partial}{\partial y}E_x - \frac{\partial}{\partial x}E_y = \mu\frac{\partial}{\partial t}H_z \tag{2.44}$$

After expanding equation (2.41) in Cartesian coordinates, equation (2.41) becomes

$$\frac{\partial}{\partial y}H_z - \frac{\partial}{\partial z}H_y = \varepsilon\frac{\partial}{\partial t}E_x \tag{2.45}$$

$$\frac{\partial}{\partial z}H_x - \frac{\partial}{\partial x}H_z = \varepsilon\frac{\partial}{\partial t}E_y \tag{2.46}$$

$$\frac{\partial}{\partial x}H_y - \frac{\partial}{\partial y}H_x = \varepsilon\frac{\partial}{\partial t}E_z \tag{2.47}$$

In S-MRTD, all the field components are expanded by the Battle-Lemarie scaling functions in spatial axis and pulse functions in time axis. Using E_z field as an example, E_z field is written in terms of the Battle-Lemarie scaling functions and pulse functions in equation (2.48). In expanding the H field, the coefficients of H field are shifted by half a discrtetization level in space and time step with respect to electric field components. Using H_x field as an example, H_x field is written in terms of the Battle-Lemarie scaling functions and pulse functions in equation (2.49). The expansion of the other fields components are similar and can be found in [9].

$$E_z(r,t) = \sum_{k,l,m,n=-\infty}^{\infty} {}_k E^{\phi x}_{l,m,n+1/2}\,\phi_l(x)\phi_m(y)\phi_{n+1/2}(z)h_k(t) \tag{2.48}$$

$$H_x(r,t) = \sum_{k,l,m,n=-\infty}^{\infty} {}_{k+1/2} H^{\phi x}_{l,m+1/2,n+1/2}\,\phi_{m+1/2}(y)\phi_l(x)\phi_{n+1/2}(z)h_{k+1/2}(t) \tag{2.49}$$

where ${}_{k}E^{\phi x}_{l,m,n+1/2}$ and ${}_{k+1/2}H^{\phi x}_{l,m+1/2,n+1/2}$ are the coefficients for the field expansions in terms of scaling functions. The spatial indexes, l, m and n correspond to the discrete space, which is related to the spatial coordinates by the following relationship.

$$\begin{aligned} x &= l\Delta x \\ y &= m\Delta y \\ z &= n\Delta z \end{aligned} \tag{2.50}$$

where Δx , Δy and Δz are the space discretization intervals in x-direction, y-direction and z-direction respectively. The time index, k, corresponds to discrete time, which is related to the time axis by the following relationship.

$$t = k\Delta t \tag{2.51}$$

where Δt is the time discretization interval in time axis. The function $\phi_m(x)$ is the dilated and translated version of the Battle-Lemarie scaling function. It is defined as,

$$\phi_m(x) = \phi(\frac{x}{\Delta x} - m). \tag{2.52}$$

The function $h_k(t)$ is defined as

$$h_m(t) = h(\frac{t}{\Delta t} - m) \tag{2.53}$$

where $h(t)$ is a pulse function. It is defined as

$$h(t) = \begin{cases} 1 & \text{for } |t| < 1/2 \\ 1/2 & \text{for } |t| = 1/2 \\ 0 & \text{for } |t| > 1/2 \end{cases}. \tag{2.54}$$

For W-MRTD, all the fields are expanded by the Battle-Lemarie scaling functions and Battle-Lemarie wavelet functions. For simplicity, we only use wavelet to expand the y-direction and only one resolution level of wavelet is considered. Using E_z field as an example, E_z field is expanded in terms of the Battle-Lemarie scaling functions, Battle-Lemarie wavelet functions and pulse functions in equation (2.55). The expansion of other components are similar and has been derived by Krumpholz[9].

$$E_z(r,t) = \sum_{k,l,m,n=-\infty}^{\infty} [\, {}_k E^{\phi\phi}_{l,m,n+1/2} \phi_m(y) + {}_k E^{\psi\phi}_{l,m+1/2,n+1/2} \psi_{m+1/2}(y)] \phi_l(x) \phi_{n+1/2}(z) h_k(t) \tag{2.55}$$

where ${}_k E^{\psi\phi}_{l,m+1/2,n+1/2}$ are the coefficients for the field expansions in terms of wavelet functions. The function $\psi_{m+1/2}(y)$ is the dilated and translated version of the Battle-Lemarie wavelet function. It is defined as,

$$\psi_{m+1/2}(y) = \psi(\frac{y}{\Delta y} - m). \tag{2.56}$$

Since Battle-Lemarie wavelet function $\psi(y)$ has an even symmetry with respect to y=½., the spatial index $m+1/2$ is used.

In deriving the MRTD scheme, the following orthogonal relationship of scaling function and wavelet are used for discretizing the Maxwell's equations in time and space.

$$\int_{-\infty}^{+\infty}\psi_m(x)\psi_{m'}(x)dx = \delta_{m,m'}\Delta x \tag{2.57}$$

$$\int_{-\infty}^{+\infty}h_m(x)h_{m'}(x)dx = \delta_{m,m'}\Delta x \tag{2.58}$$

$$\int_{-\infty}^{+\infty}\phi_m(x)\psi_{m'+1/2}(x)dx = 0 \tag{2.59}$$

$$\int_{-\infty}^{+\infty}\phi_m(x)\phi_{m'}(x)dx = \delta_{m,m'}\Delta x \tag{2.60}$$

$$\int_{-\infty}^{\infty}\frac{\partial}{\partial t}h_{m'+1/2}(t)\cdot h_m(t)dt = \delta_{m,m'} - \delta_{m,m'+1} \tag{2.61}$$

Besides, in discretizing the Maxwell's equations, the following integrals are necessary. These integrals can be calculated by the closed form representation of the Battle-Lemarie scaling function and Battle-Lemarie wavelet function in spectral domain.

$$\int_{-\infty}^{\infty}\frac{\partial}{\partial x}\psi_{m'+1/2}(x)\cdot\psi_m(x)dx = \frac{1}{\pi}\int_0^{\infty}|\hat{\psi}(w)|^2\ w\sin(w(j+\tfrac{1}{2}))dw \tag{2.62}$$

$$\int_{-\infty}^{\infty}\frac{\partial}{\partial x}\phi_{m'+1/2}(x)\cdot\psi_{m+1/2}(x)dx = \frac{1}{\pi}\int_0^{\infty}|\hat{\phi}(w)\,\|\,\hat{\psi}(w)|\ w\sin(w(m'-m+1))dw \tag{2.63}$$

$$\int_{-\infty}^{\infty}\frac{\partial}{\partial x}\phi_{m'+1/2}(x)\cdot\phi_m(x)dx = \frac{1}{\pi}\int_0^{\infty}|\hat{\phi}(w)|^2\ w\sin(w(j+\tfrac{1}{2}))dw \tag{2.64}$$

$$\int_{-\infty}^{\infty}\frac{\partial}{\partial x}\psi_{m'+1/2}(x)\cdot\psi_m(x)dx = \frac{1}{\pi}\int_0^{\infty}|\hat{\psi}(w)|^2\ w\sin(w(j+\tfrac{1}{2}))dw \tag{2.65}$$

The integral in equation (2.63) is different from that in [9] so that the spurious mode of the W-MRTD reported in [9] is removed.

These integrals can be expressed in a series form with the impulse function as the basis function. The series is theoretically sum up from the minus infinity to positive infinity. However, because of the exponential decay of the Battle-Lemarie scaling function and Battle-Lemarie wavelet function in figure 2.6 and figure 2.7, the coefficients of the series are too small beyond certain range, hence the series are only sum up within certain range as follows:

$$\sum_{i=-9}^{8} b(i) \cdot \delta_{m+i,m'} = \int_{-\infty}^{\infty} \frac{\partial}{\partial x} \psi_{m'+1/2}(x) \cdot \psi_m(x) dx \tag{2.66}$$

$$\sum_{i=-9}^{8} a(i) \cdot \delta_{m+i,m'} = \int_{-\infty}^{\infty} \frac{\partial}{\partial x} \phi_{m'+1/2}(x) \cdot \phi_m(x) dx \tag{2.67}$$

$$\sum_{i=-9}^{9} c(i) \cdot \delta_{m+1+i,m'} = \int_{-\infty}^{\infty} \frac{\partial}{\partial x} \phi_{m'+1/2}(x) \cdot \psi_{m+1/2}(x) dx \tag{2.68}$$

$$\sum_{i=-9}^{9} c(i) \cdot \delta_{m+1+i,m'} = \int_{-\infty}^{\infty} \frac{\partial}{\partial x} \phi_{m'+1/2}(x) \cdot \psi_{m+1/2}(x) dx \tag{2.69}$$

The coefficients of $a(i)$, $b(i)$ and $c(i)$ are tabulated in the table 2.2.

i	$a(i)$	$b(i)$	$c(i)$
0	1.29185	2.47254	0
1	-0.15608	0.95623	-0.04660
2	0.05964	0.16606	0.05454
3	-0.02931	0.09392	-0.03700
4	0.01537	0.00314	0.02057
5	-0.00818	0.01349	-0.01115
6	0.00438	-0.00286	0.00598
7	-0.00234	0.00278	-0.00320
8	0.00125	-0.00113	0.00171
9	-0.00067	0.00071	-0.00092

Table 2.2. The Coefficients of $a(i)$, $b(i)$ and $c(i)$

Since the derivation of the W-MRTD scheme can be generalized to the S-MRTD scheme by setting all the wavelet coefficients to zero, we only demonstrate the derivation of the W-MRTD scheme. To derive the W-MRTD scheme, we start from the Maxwell's equations. Taking E_x field as an example, the time dependent Maxwell's equation of the E_x field is

$$\frac{\partial}{\partial y}H_z - \frac{\partial}{\partial z}H_y = \varepsilon\frac{\partial}{\partial t}E_x \,. \tag{2.70}$$

In W-MRTD scheme, E_x, H_z and H_y are expanded in terms of the Battle-Lemarie wavelet functions and Battle-Lemarie scaling functions. That is,

$$E_x(r,t) = \sum_{k,l,m,n=-\infty}^{\infty}[\,{}_{k}E^{\phi\phi}_{l+1/2,m,n}\phi_m(y) + {}_{k}E^{\psi\phi}_{l+1/2,m+1/2,n}\psi_{m+1/2}(y)]\phi_{l+1/2}(x)\phi_n(z)h_k(t)$$

$$H_y(r,t) = \sum_{k,l,m,n=-\infty}^{\infty}[\,{}_{k+1/2}H^{\phi\psi}_{l+1/2,m,n+1/2}\phi_m(y) + {}_{k+1/2}H^{\psi\psi}_{l+1/2,m+1/2,n+1/2}\psi_{m+1/2}(y)]\phi_{l+1/2}(x)\phi_{n+1/2}(z)h_{k+1/2}(t)$$

$$H_z(r,t) = \sum_{k,l,m,n=-\infty}^{\infty}[\,{}_{k+1/2}H^{\phi\phi}_{l+1/2,m+1/2,n}\phi_{m+1/2}(y) + {}_{k+1/2}H^{\psi\phi}_{l+1/2,m,n}\psi_m(y)]\phi_{l+1/2}(x)\phi_n(z)h_{k+1/2}(t)$$

(2.71)

To discretize the equation (2.70), we multiply the equation (2.70) by $\phi_{l+1/2}(x)\cdot\phi_m(y)\cdot\phi_n(z)\cdot h_{k+1/2}(t)$ in both sides and integrate with respect to x, y, z and t. Hence, the R.H.S. of equation (2.70) becomes

$$\int_{-\infty}^{\infty}\int_{-\infty}^{\infty}\int_{-\infty}^{\infty}\int_{-\infty}^{\infty}\varepsilon\frac{\partial}{\partial t}E_x \cdot \phi_{l+1/2}(x)\cdot\phi_m(y)\cdot\phi_n(z)\cdot h_{k+1/2}(t)dxdydzdt$$

$$= \varepsilon\left({}_{k+1}E^{\phi x}_{l+1/2,m,n} - {}_{k}E^{\phi x}_{l+1/2,m,n}\right)\Delta x\Delta y\Delta z \ . \tag{2.72}$$

The L.H.S. of the equation (2.70) becomes

$$\int_{-\infty}^{\infty}\int_{-\infty}^{\infty}\int_{-\infty}^{\infty}\int_{-\infty}^{\infty}\left(\frac{\partial}{\partial y}H_z - \frac{\partial}{\partial z}H_y\right)\cdot\phi_{l+1/2}(x)\cdot\phi_m(y)\cdot\phi_n(z)\cdot h_{k+1/2}(t)dxdydzdt$$

$$\begin{aligned}
&= \sum_{k,l,m=-\infty}^{\infty}\Big[{}_{k'+1/2}H^{\phi z}_{l'+1/2,m'+1/2,n'}\cdot\delta_{l,l'}\cdot\delta_{n,n'}\cdot\delta_{k,k'}\cdot\sum_{i=-9}^{+8}a(i)\cdot\delta_{m+i,m'} \\
&\qquad + {}_{k'+1/2}H^{\psi z}_{l'+1/2,m',n'}\cdot\delta_{l,l'}\cdot\delta_{n,n'}\cdot\delta_{k,k'}\cdot\sum_{i=-9}^{+9}c(i)\cdot\delta_{m+i+1,m'}\Big]\Delta x\Delta z\Delta t \\
&\quad - \sum_{k,l,m=-\infty}^{\infty}\Big[{}_{k'+1/2}H^{\phi y}_{l'+1/2,m',n'+1/2}\cdot\delta_{l,l'}\cdot\delta_{m,m'}\cdot\delta_{k,k'}\cdot\sum_{i=-9}^{+8}a(i)\cdot\delta_{n+i,n'}\Big]\Delta x\Delta y\Delta t
\end{aligned}$$

$$= \frac{\Delta t}{\varepsilon\Delta y}\Big[\sum_{i=-9}^{+8}a(i)_{k+1/2}H^{\phi z}_{l+1/2,m+1/2+i,n} + \sum_{i=-9}^{+9}c(i)_{k+1/2}H^{\psi z}_{l+1/2,m+1+i,n}\Big]\Delta x\Delta y\Delta z$$

$$\begin{aligned}
&= \frac{\Delta t}{\varepsilon\Delta y}\Big[\sum_{i=-9}^{+8}a(i)_{k+1/2}H^{\phi z}_{l+1/2,m+1/2+i,n} + \sum_{i=-9}^{+9}c(i)_{k+1/2}H^{\psi z}_{l+1/2,m+1+i,n}\Big]\Delta x\Delta y\Delta z \\
&\quad - \frac{\Delta t}{\varepsilon\Delta z}\Big[\sum_{i=-9}^{+8}a(i)_{k+1/2}H^{\phi y}_{l+1/2,m,n+1/2+i}\Big]\Delta x\Delta y\Delta z
\end{aligned} \tag{2.73}$$

The orthogonal relations, equation (2.62) to (2.65) and equation (2.66) to (2.69), are used for calculating the above integrals. Combining the L.H.S. of equation (2.70) in (2.72) and the R.H.S. of equation (2.70) in (2.73), we get the W-MRTD update equation of scaling coefficients of the equation (2.70).That is,

$$
\begin{aligned}
{}_{k+1}E^{\phi x}_{l+1/2,m,n} = {}_{k}E^{\phi x}_{l+1/2,m,n} &+ \frac{\Delta t}{\varepsilon \Delta y}\Big[\sum_{i=-9}^{+8} a(i)_{\,k+1/2}\, H^{\phi z}_{l+1/2,m+1/2+i,n} \\
&+ \sum_{i=-9}^{+9} c(i)_{\,k+1/2}\, H^{\psi z}_{l+1/2,m+1+i,n}\Big] \\
&- \frac{\Delta t}{\varepsilon \Delta z}\Big[\sum_{i=-9}^{+8} a(i)_{\,k+1/2}\, H^{\phi y}_{l+1/2,m,n+1/2+i}\Big]
\end{aligned}
\tag{2.74}
$$

To reconstruct the total field of E_x at particular space point r_0 at time t_0, we can use the delta function to sample the field expansion of E_x (2.75).

$$
\begin{aligned}
E_x(r_0,t_0) &= \int_{-\infty}^{+\infty}\int_{-\infty}^{+\infty}\int_{-\infty}^{+\infty}\int_{-\infty}^{+\infty} E_x(r_0,t_0)\delta(x-x_0)\delta(y-y_0)\delta(z-z_0)\delta(t-t_0)dxdydzdt \\
&= \sum_{k,l,m,n=-\infty}^{\infty}\Big[{}_{k}E^{\phi x}_{l+1/2,m,n}\phi_m(y_0) + {}_{k}E^{\psi x}_{l+1/2,m+1/2,n}\psi_{m+1/2}(y_0)\Big]\phi_{l+1/2}(x_0)\phi_n(z_0)
\end{aligned}
\tag{2.75}
$$

Because of the exponential decay of the Battle-Lemarie scaling function and its wavelet function, only finite terms of the sequence are enough to reconstruct the fields.

2.2.2 Numerical Dispersion

Numerical dispersion is a key factor in MRTD modeling that indicates the accuracy limits. Because of the discretization of space and time, the numerical dispersion of MRTD schemes deviates from the linear dispersion of the Maxwell's equations.

Theoretically, the dispersion relation of Maxwell's equations for a continuous loseless medium in two-dimensional space is given by

$$\frac{\omega^2}{c^2} = k^2$$
$$k = \sqrt{k_x^2 + k_x^2} \tag{2.76}$$

where ω is the angular frequency, k is the wavenumber and c is the speed of light. In S-MRTD, the dispersion relation is

$$\left(\frac{1}{c\Delta t}\right)^2 \sin^2\left(\frac{\omega\Delta t}{2}\right) = \left(\frac{1}{\Delta x}\sum_{i=-9}^{+8} a(i)\sin\left(\frac{k_x\Delta x(i+1/2)}{2}\right)\right)^2 + \left(\frac{1}{\Delta y}\sum_{i=-9}^{+8} a(i)\sin\left(\frac{k_y\Delta y(i+1/2)}{2}\right)\right)^2 \tag{2.77}$$

To investigate the dispersion relation (2.77), we use the square grid size. Therefore,

$$\Delta x = \Delta y = \Delta \ . \tag{2.78}$$

The wave propagates at an angle θ with respect to the positive x-axis. We have,

$$\begin{aligned} k_x &= k\cos\theta \\ k_y &= k\sin\theta \end{aligned} \tag{2.79}$$

Substituting the equation (2.78) and (2.79) into equation (2.77), the equation (2.77) becomes

$$\left(\frac{\Delta}{c\Delta t}\right)^2 \sin^2\left(\frac{\omega\Delta t}{2}\right) = \left(\sum_{i=-9}^{+8} a(i)\sin\left(\frac{k\cos\theta\cdot\Delta(i+1/2)}{2}\right)\right)^2 + \left(\sum_{i=-9}^{+8} a(i)\sin\left(\frac{k\sin\theta\cdot\Delta(i+1/2)}{2}\right)\right)^2 \tag{2.80}$$

Since it is impossible to separate the k and θ in either side, we can only solve the numerical k-vector at any propagation angle θ by means of numerical method, such as Newton's method. When the grid size is less than 0.3 of the wavelength, the percentage error of the S-MRTD scheme is less than 0.5% as seen in figure 2.9. In order to get a stable and accurate result, grid size (Δx) is usually choose as 1/10 of the wavelength and the time step Δt is chosen as

$$\Delta t = \Delta t_{max} / 5 \tag{2.81}$$

where $\Delta t_{max} \le \dfrac{1}{c\left(\sum_{i=0}^{+8}|a(i)|\right)\sqrt{\left(\frac{1}{\Delta x}\right)^2+\left(\frac{1}{\Delta y}\right)^2+\left(\frac{1}{\Delta z}\right)^2}}$

[35].

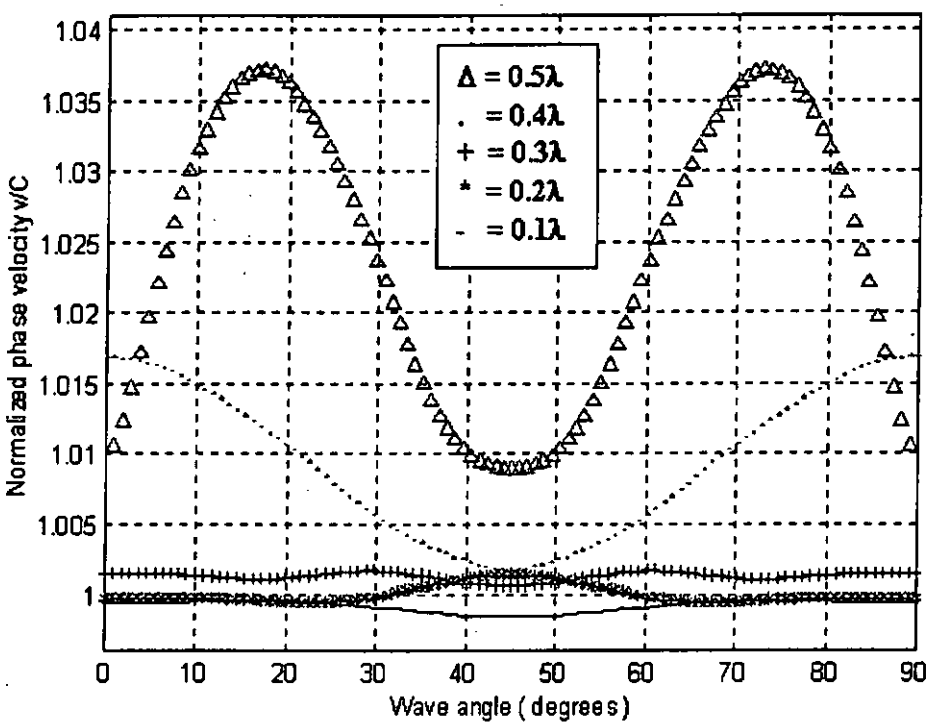

Figure 2.9 The normalized phase velocity against wave angle with different grid sizes for two dimensional S-MRTD.

Chapter 3

A sub-gridding MRTD

The concepts of wavelets have brought many scientists and engineers attentions. It has been applied for solving Maxwell's equation since 1992 [38]. This finally led to the multiresolution time-domain scheme (MRTD) in 1994 [9]. Based on the concepts of multiresolution, two different MRTD schemes were reported. They are the S-MRTD and W-MRTD. As introduced in previous chapter, the fields are expanded by scaling functions only in S-MRTD scheme. In W-MRTD, the fields are expanded by scaling functions and wavelet functions.

One of the advantages of using wavelet is that wavelet coefficients characterize sudden change fields. In practice, however, only some regions of the environment need wavelet for strong field characterization. This leads to the trade off between accuracy and computation resource: S-MRTD requires less grids to compute the fields while W-MRTD uses more grids but it has better field characterization. Hence, based on the need of calculating the field accurately without wasting any unnecessary computer resources, the sub-gridding MRTD is proposed.

In the sub-gridding MRTD scheme, the whole region is divided into dense grid regions and coarse grid regions. Unlike W-MRTD, the fields, expanded by both scaling functions and wavelet functions, are only confined to the dense grid regions. For the coarse grid regions, fields are expanded by scaling functions only. In this chapter, we will first discuss the numerical wave propagation of both the S-MRTD and W-MRTD. It can be shown that the W-MRTD updating equations can be changed to the S-MRTD updating equations if the wavelet coefficients are removed. This idea leads to the use of the Anisotropic Perfectly Matched layer (APML) as an selective absorbing material so that the non-physical solution at the boundaries between the regions of different scales can be removed.

3.1 Basic idea

In spatial space, the propagation of electromagnetic wave is governed by Maxwell's equation. If we consider a two-dimensional space, the propagation of electromagnetic

wave in TM mode inside a homogenous loseless medium, is governed by the following sets of equation,

$$\frac{\partial}{\partial x}H_y - \frac{\partial}{\partial y}H_x = \varepsilon\frac{\partial}{\partial t}E_z \tag{3.1}$$

$$-\frac{\partial}{\partial y}E_z = \mu\frac{\partial}{\partial t}H_x \tag{3.2}$$

$$\frac{\partial}{\partial x}E_z = \mu\frac{\partial}{\partial t}H_y \tag{3.3}$$

That is, a TM electromagnetic wave, which propagates in a two-dimensional space, consists of E_z , H_x and H_y only. When the Maxwell's equations are discretized using the S-MRTD scheme, the electromagnetic wave is expressed in terms of scaling coefficients. The scaling coefficients are governed by the following updating equations.

$$\begin{aligned} {}_{k+1}E^{\phi x}_{l,m} = {}_{k}E^{\phi x}_{l,m} + \frac{\Delta t}{\varepsilon}\Big[\frac{1}{\Delta x}\sum_{i=-9}^{+8} a(i)_{k+1/2}H^{\phi y}_{l+1/2+i,m} \\ -\frac{1}{\Delta y}\sum_{i=-9}^{+8} a(i)_{k+1/2}H^{\phi x}_{l,m+1/2+i}\Big] \end{aligned} \tag{3.4}$$

$${}_{k+1/2}H^{\phi x}_{l,m+1/2} = {}_{k-1/2}H^{\phi x}_{l,m+1/2} - \frac{\Delta t}{\mu\Delta y}\sum_{i=-9}^{+8} a(i)_k E^{\phi z}_{l,m+1+i} \tag{3.5}$$

$${}_{k+1/2}H^{\phi y}_{l+1/2,m} = {}_{k-1/2}H^{\phi y}_{l+1/2,m} + \frac{\Delta t}{\mu\Delta x}\sum_{i=-9}^{+8} a(i)_k E^{\phi z}_{l+1+i,m} \tag{3.6}$$

Then, when the Maxwell's equation is discretized by the S-MRTD scheme, the TM mode electromagnetic wave is mapped to the S-MRTD computational domain from spatial domain. Instead of propagating in spatial domain, the numerical wave, which constitutes ${}_{k}E^{\phi x}_{l,m}$, ${}_{k+1/2}H^{\phi x}_{l,m+1/2}$ and ${}_{k+1/2}H^{\phi y}_{l+1/2,m}$, propagate in the S-MRTD computational domain, which is filled with the S-MRTD unit cells. The S-MRTD unit cell contains the scaling coefficients of the E_z , H_y and H_x as in following figure.

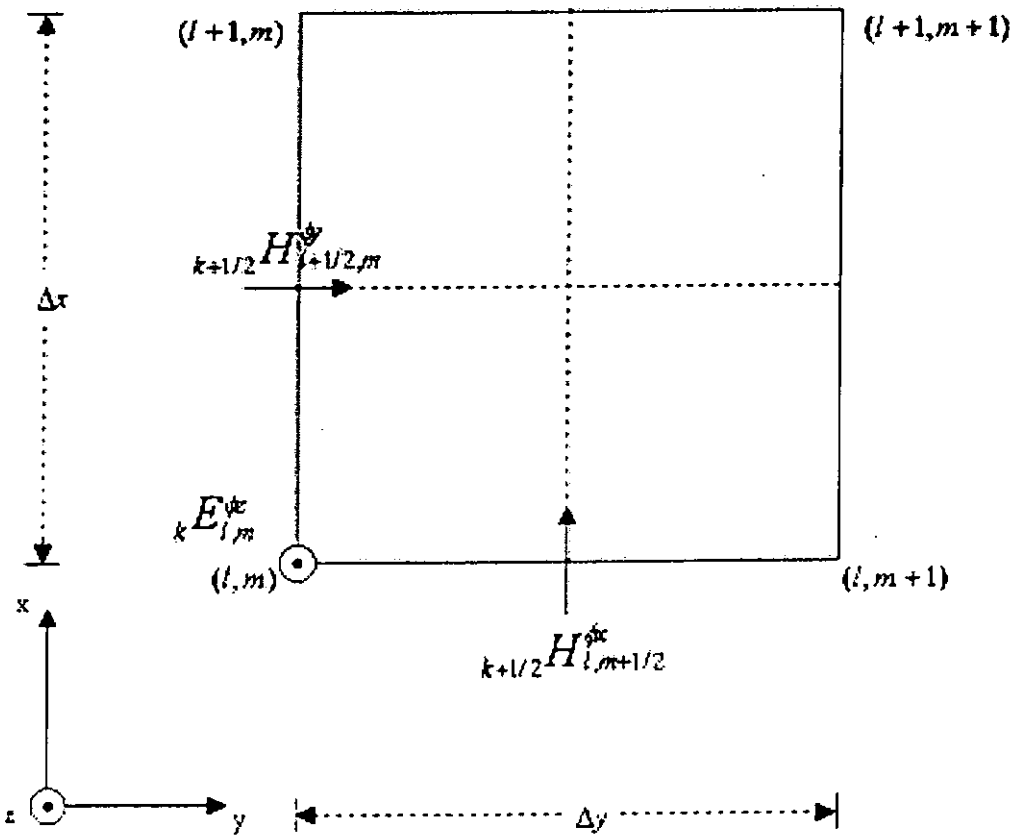

Figure 3.1. A unit cell of the S-MRTD scheme

Similarly, when the Maxwell's equation is discretized using the W-MRTD scheme, the numerical wave, which constitutes ${}_{k}E^{\phi x}_{l,m}$, ${}_{k+1/2}H^{\phi x}_{l,m+1/2}$, ${}_{k+1/2}H^{\phi y}_{l+1/2,m}$, ${}_{k}E^{\psi z}_{l,m+1/2}$, ${}_{k+1/2}H^{\psi x}_{l,m}$ and ${}_{k+1/2}H^{\psi y}_{l+1/2,m+1/2}$, propagates in the W-MRTD computational domain. The W-MRTD computational domain is filled with W-MRTD unit cells, which contain all the scaling coefficients and wavelet coefficients of the E_z, H_y and H_x as in following figure.

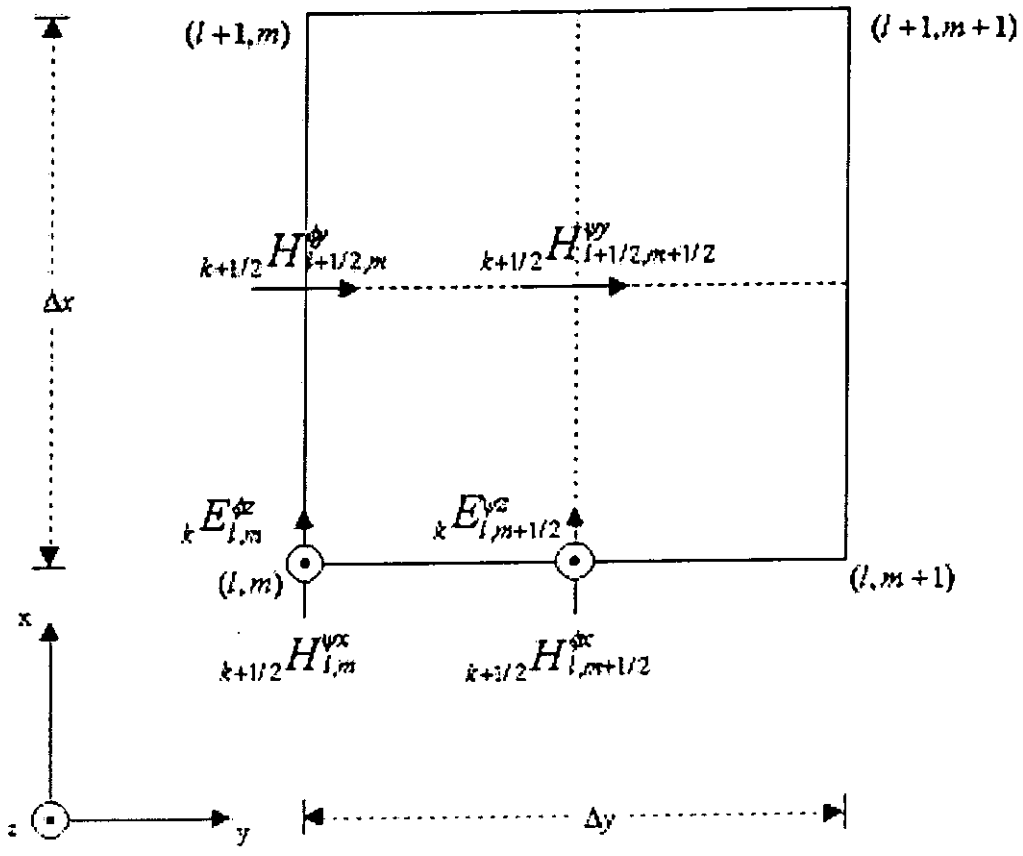

Figure 3.2. A unit cell of the W-MRTD scheme

In W-MRTD computational domain, the scaling coefficients of the E_z , H_y and H_x are governed by the following equations.

$$
\begin{aligned}
{}_{k+1}E^{\phi z}_{l,m} = {}_{k}E^{\phi z}_{l,m} + \frac{\Delta t}{\varepsilon}\Big[\frac{1}{\Delta x}\sum_{i=-9}^{+8} a(i)_{k+1/2} H^{\phi y}_{l+1/2+i,m} \\
- \frac{1}{\Delta y}\Big(\sum_{i=-9}^{+8} a(i)_{k+1/2} H^{\phi x}_{l,m+1/2+i} \\
+ \sum_{i=-9}^{+9} c(i)_{k+1/2} H^{\psi x}_{l,m+1+i}\Big)\Big]
\end{aligned}
\tag{3.7}
$$

$$
{}_{k+1/2}H^{\phi x}_{l,m+1/2} = {}_{k-1/2}H^{\phi x}_{l,m+1/2} - \frac{\Delta t}{\mu \Delta y}\Big(\sum_{i=-9}^{+8} a(i)_k E^{\phi z}_{l,m+1+i} + \sum_{i=-9}^{+9} c(i)_k E^{\psi z}_{l,m+1/2+1+i}\Big) \tag{3.8}
$$

$$
{}_{k+1/2}H^{\phi y}_{l+1/2,m} = {}_{k-1/2}H^{\phi y}_{l+1/2,m} + \frac{\Delta t}{\mu \Delta x}\sum_{i=-9}^{+8} a(i)_k E^{\phi z}_{l+1+i,m} \tag{3.9}
$$

The wavelet coefficient of the E_z , H_y and H_x are updated by the following equations.

$$
\begin{aligned}
{}_{k+1}E^{\psi z}_{l,m+1/2} = {}_{k}E^{\psi z}_{l,m+1/2} + \frac{\Delta t}{\varepsilon}\Big[\frac{1}{\Delta x}\sum_{i=-9}^{+8} a(i)_{k+1/2} H^{\psi y}_{l+1/2+i,m+1/2} \\
- \frac{1}{\Delta y}\Big(\sum_{i=-9}^{+9} c(i)_{k+1/2} H^{\phi x}_{l,m-1/2+i} \\
+ \sum_{i=-9}^{+8} b(i)_{k+1/2} H^{\psi x}_{l,m+1+i}\Big)\Big]
\end{aligned}
\tag{3.10}
$$

$$ {}_{k+1/2}H^{\psi x}_{l,m} = {}_{k-1/2}H^{\psi x}_{l,m} - \frac{\Delta t}{\mu \Delta y}\left(\sum_{i=-9}^{+8} b(i)\, {}_{k}E^{\psi z}_{l,m+1/2+i} + \sum_{i=-9}^{+9} c(i)\, {}_{k}E^{\phi z}_{l,m-1+i}\right) \tag{3.11} $$

$$ {}_{k+1/2}H^{\psi y}_{l+1/2,m+1/2} = {}_{k-1/2}H^{\psi y}_{l+1/2,m+1/2} + \frac{\Delta t}{\mu \Delta x}\sum_{i=-9}^{+8} a(i)\, {}_{k}E^{\psi z}_{l+1+i,m+1/2} \tag{3.12} $$

Without loss of generality, one resolution level of wavelet is used to expand the y direction of fields.

3.1.1 The Difference between the S-MRTD updating equations and W-MRTD updating equations

Comparing with the S-MRTD updating algorithm, the scaling coefficients updating equations of the W-MRTD have one term, which is depending on the wavelet coefficients. Taking the scaling coefficient of E_z as an example, the S-MRTD updating equation is

$$ {}_{k+1}E^{\phi z}_{l,m} = {}_{k}E^{\phi z}_{l,m} + \frac{\Delta t}{\varepsilon}\left[\frac{1}{\Delta x}\sum_{i=-9}^{+8} a(i)_{k+1/2} H^{\phi y}_{l+1/2+i,m} - \frac{1}{\Delta y}\sum_{i=-9}^{+8} a(i)_{k+1/2} H^{\phi x}_{l,m+1/2+i}\right] \tag{3.13} $$

The scaling coefficient of E_z updating equation in W-MRTD is

$$
{}_{k+1}E^{\phi z}_{l,m} = {}_{k}E^{\phi z}_{l,m} + \frac{\Delta t}{\varepsilon}\Big[\frac{1}{\Delta x}\sum_{i=-9}^{+8} a(i)_{k+1/2} H^{\phi y}_{l+1/2+i,m} - \frac{1}{\Delta y}\sum_{i=-9}^{+8} a(i)_{k+1/2} H^{\phi x}_{l,m+1/2+i}\Big] - \underline{\frac{\Delta t}{\varepsilon \Delta y}\sum_{i=-9}^{+9} c(i)_{k+1/2} H^{\psi x}_{l,m+1+i}} \quad (3.14)
$$

As seen in equation (3.14), the last summation of the scaling coefficients updating equation of E_z in W-MRTD depends on the wavelet coefficients of the H_x. Hence, by setting the wavelet coefficients of H_x to zero, equation (3.14) becomes equation (3.13). In general, the scaling coefficients updating equations of the electric field depend on the wavelet coefficients of the magnetic field. Similarly, the scaling coefficients of the magnetic field depend on the wavelet coefficients of the electric field. In next section, we will discuss the possibility of removing those wavelet coefficients inside the W-MRTD updating equations so that the W-MRTD updating equations become the S-MRTD updating equations.

3.1.2 Removal of the wavelet coefficients in W-MRTD updating equations

Once the wavelet coefficients in the W-MRTD are removed in certain regions, the updating equations of W-MRTD become the updating equations of S-MRTD. Then, we would have a mixture of two different MRTD schemes as in figure 3.3.

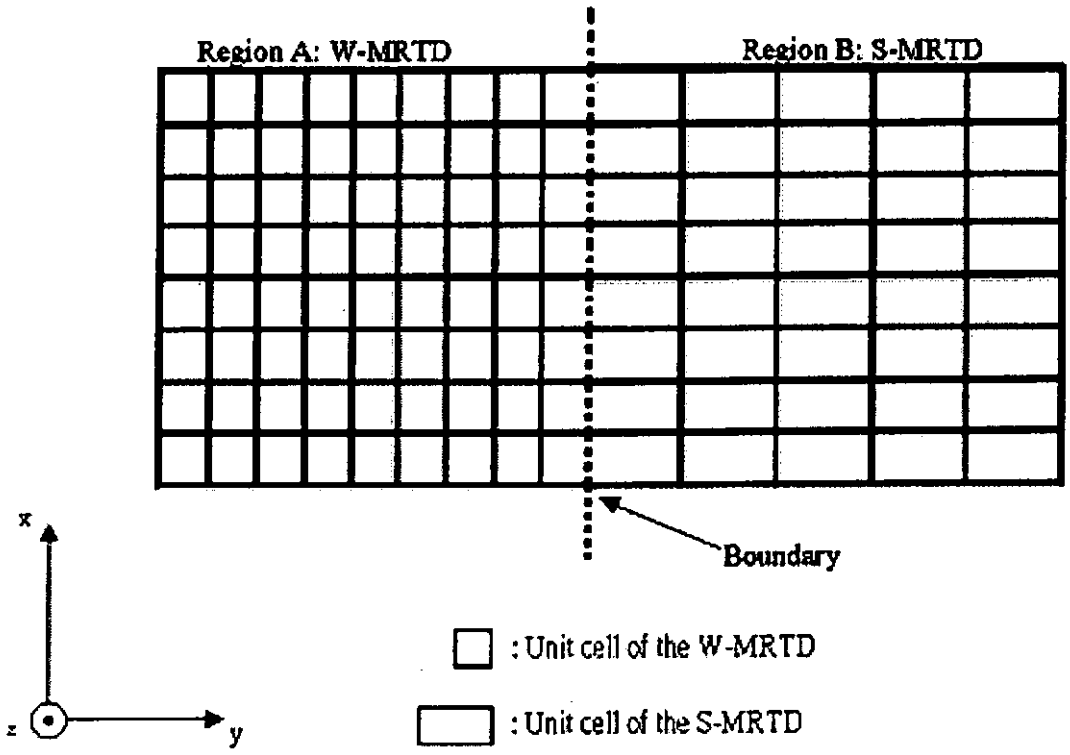

Figure 3.3. A mixture of S-MRTD and W-MRTD in two dimensional space

Hence, the possibility of having refined grids in certain regions using S-MRTD depends on how those wavelet coefficients in the W-MRTD updating equations are removed. In figure 3.3, the W-MRTD updating equation is used in region A. In region B, all the wavelet coefficients are set to zero so that the W-MRTD updating equations becomes the S-MRTD equations. However, when the numerical wave of the wavelet coefficients propagate from region A to region B, this numerical wave apparently collide an barrier with zero electric potential at the boundary as depicted in figure 3.4.

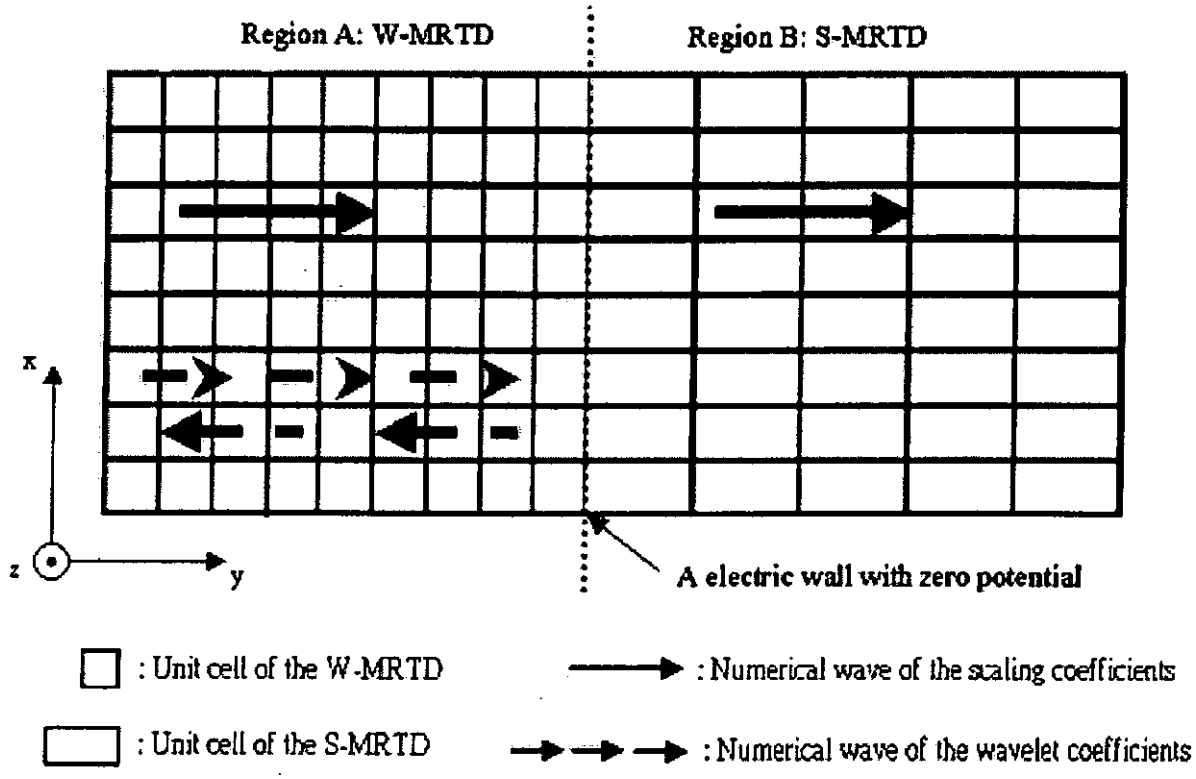

Figure 3.4 The numerical wave propagation of both scaling coefficients and wavelets coefficients in W-MRTD and S-MRTD

Since the scaling coefficients updating equations of W-MRTD contain wavelet coefficients, the non-physical reflection of the wavelet coefficients corrupt the results of the scaling coefficients updating equations in W-MRTD. Since the boundary between the W-MRTD and S-MRTD is invisible to the scaling coefficients, the numerical wave of the scaling coefficients can travel to region B form region A. Hence, the error, induced by the non-physical reflection at the boundary, affect the results at region B. Therefore, it is not possible to get correct result if we only set the all the wavelet coefficients at region B to zero.

In order to get accurate result, the non-physical reflection of the wavelet coefficients wave at the boundary has to be minimized. In the next section, the Anisotropic Perfectly Matched layer (APML) is used for the removal of the numerical wave of wavelet coefficients at the boundary.

3.2 APML as an selective absorpting medium

Anisotropic perfectly matched layer (APML) is one of the boundary condition, which has been used in Yee's Finite Difference Time Domain for open region field problems [39-40]. It has shown to be successful in minimizing the reflection wave from the outer boundary. After the theory of the MRTD has been published in 1994, MRTD has been applied in many different field problems. By then, APML has been used in MRTD for the truncation of grid points [41]. In this section, we will use APML to remove the non-physical reflection at the boundary between the W-MRTD and S-MRTD.

3.2.1 Formulation of the W-MRTD updating equations inside an APML

First, we have to derive the W-MRTD updating equations inside an APML. To simplify the discussion, the APML is assumed to be inserted at the end of the computational domain in positive y direction. From the theory of APML given in [39],

APML consists of lossy material with spatial variant conductivity. The propagation of the electromagnetic wave inside the APML is governed by the following equations.

$$\begin{bmatrix} 0 & -\partial z & \partial y \\ \partial z & 0 & -\partial x \\ -\partial y & \partial x & 0 \end{bmatrix} \begin{bmatrix} H_x \\ H_y \\ H_z \end{bmatrix} = -j\omega\mu_o S \begin{bmatrix} E_x \\ E_y \\ E_z \end{bmatrix} \tag{3.15}$$

$$\begin{bmatrix} 0 & -\partial z & \partial y \\ \partial z & 0 & -\partial x \\ -\partial y & \partial x & 0 \end{bmatrix} \begin{bmatrix} E_x \\ E_y \\ E_z \end{bmatrix} = j\omega\varepsilon_o S \begin{bmatrix} H_x \\ H_y \\ H_z \end{bmatrix} \tag{3.16}$$

where $S = \begin{bmatrix} 1+\dfrac{\sigma}{j\omega\varepsilon_O} & 0 & 0 \\ 0 & \dfrac{1}{1+\dfrac{\sigma}{j\omega\varepsilon_O}} & 0 \\ 0 & 0 & 1+\dfrac{\sigma}{j\omega\varepsilon_O} \end{bmatrix}$, ω is the angular frequency, ε_o and μ_o are the permittivity and permeability of air, σ is the conductivity. In free space, the conductivity σ is zero. Inside the APML, the conductivity is spatial variant along in y direction and is given by

$$\sigma = c_0 \frac{\varepsilon_0}{\Delta t}\left(\frac{i}{N_p}\right)^m . \tag{3.17}$$

where N_p is the Number of cells of the APML, m=2 ~ 4 and c_0=0.8~1.6 [14]. For simplicity, a two-dimensional TM wave is considered. Hence, equation (3.15) becomes

$$\frac{\partial}{\partial x}H_y - \frac{\partial}{\partial y}H_x = j\omega\varepsilon_o\left(1+\frac{\sigma}{j\omega\varepsilon_o}\right)E_z \tag{3.18}$$

$$\frac{\partial}{\partial x}E_z = j\omega\mu_o\left(\frac{1}{1+\frac{\sigma}{j\omega\varepsilon_o}}\right)H_y \tag{3.19}$$

$$\frac{\partial}{\partial y}E_z = -j\omega\mu_o\left(1+\frac{\sigma}{j\omega\varepsilon_o}\right)H_x \tag{3.20}$$

Now, we can start to derive the W-MRTD updating equation inside the APML. We consider the following equation.

$$\frac{\partial}{\partial x}H_y - \frac{\partial}{\partial y}H_x = j\omega\varepsilon_o\left(1+\frac{\sigma}{j\omega\varepsilon_o}\right)E_z \tag{3.21}$$

After rearrangment, the equation (3.21) becomes

$$\frac{\partial}{\partial x}H_y - \frac{\partial}{\partial y}H_x = j\omega\varepsilon_o E_z + \sigma E_z \tag{3.22}$$

By replacing the $j\omega$ with $\frac{\partial}{\partial t}$ in equation (3.22), we get

$$\frac{\partial}{\partial x}H_y - \frac{\partial}{\partial y}H_x = \frac{\partial}{\partial t}\varepsilon_o E_z + \sigma E_z \tag{3.23}$$

We multiply the equation (3.23) by $\phi_{l'}(x)\cdot\phi_{m'}(y)\cdot h_{k'+1/2}(t)$ in both sides and integrate with respect to x-axis, y-axis and time axis. The L.H.S of equation (3.23) becomes

$$\int_{-\infty}^{+\infty}\int_{-\infty}^{+\infty}\int_{-\infty}^{+\infty}\left(\frac{\partial}{\partial x}H_y-\frac{\partial}{\partial y}H_x\right)\cdot\phi_{l'}(x)\cdot\phi_{m'}(y)\cdot h_{k'+1/2}(t)\,dxdydt$$

$$=\left(\frac{1}{\Delta x}\sum_{i=-9}^{+8}a(i)_{k+1/2}H^{\phi y}_{l+1/2+i,m}-\right.$$

$$\left.\frac{1}{\Delta y}\left[\sum_{i=-9}^{+8}a(i)_{k+1/2}H^{\phi x}_{l,m+1/2+i}+\sum_{i=-9}^{+9}c(i)_{k+1/2}H^{\psi x}_{l,m+1+i}\right]\right)\Delta x\Delta y\Delta t \qquad (3.24)$$

The R.H.S of equation (3.23) becomes

$$\int_{-\infty}^{+\infty}\int_{-\infty}^{+\infty}\int_{-\infty}^{+\infty}\left(\frac{\partial}{\partial t}\varepsilon_o E_z-\sigma E_z\right)\cdot\phi_{l'}(x)\cdot\phi_{m'}(y)\cdot h_{k'+1/2}(t)\,dxdydt$$

$$=\varepsilon_o\int_{-\infty}^{+\infty}\int_{-\infty}^{+\infty}\int_{-\infty}^{+\infty}\frac{\partial}{\partial t}E_z\cdot\phi_{l'}(x)\cdot\phi_{m'}(y)\cdot h_{k'+1/2}(t)\,dxdydt-$$

$$\int_{-\infty}^{+\infty}\int_{-\infty}^{+\infty}\int_{-\infty}^{+\infty}\sigma E_z\cdot\phi_{l'}(x)\cdot\phi_{m'}(y)\cdot h_{k'+1/2}(t)\,dxdydt$$

$$=\varepsilon_o\left({}_{k+1}E^{\phi z}_{l,m}-{}_{k}E^{\phi z}_{l,m}\right)\Delta x\Delta y-\int_{-\infty}^{+\infty}\int_{-\infty}^{+\infty}\int_{-\infty}^{+\infty}\sigma E_z\cdot\phi_{l'}(x)\cdot\phi_{m'}(y)\cdot\frac{h_{k'+1}(t)+h_{k'}(t)}{2}\,dxdydt$$

$$=\varepsilon_o\left({}_{k+1}E^{\phi z}_{l,m}-{}_{k}E^{\phi z}_{l,m}\right)\Delta x\Delta y-\frac{\sigma}{2}\left({}_{k+1}E^{\phi z}_{l,m}+{}_{k}E^{\phi z}_{l,m}\right)\Delta x\Delta y\Delta t$$

$$=\left({}_{k+1}E^{\phi z}_{l,m}\left(1-\frac{\sigma\Delta t}{2\varepsilon_o}\right)-{}_{k}E^{\phi z}_{l,m}\left(1+\frac{\sigma\Delta t}{2\varepsilon_o}\right)\right)\Delta x\Delta y\varepsilon_o \qquad (3.25)$$

After the rearrangment in both sides, we obtain the scaling coefficient updating equation of E_z field.

$$ {}_{k+1}E^{\phi x}_{l,m} = \left(\frac{1-\frac{\sigma\Delta t}{2\varepsilon_o}}{1+\frac{\sigma\Delta t}{2\varepsilon_o}} \right) {}_{k}E^{\phi x}_{l,m} + \frac{\Delta t}{\varepsilon_o}\frac{1}{1+\frac{\sigma\Delta t}{2\varepsilon_o}} \left(\frac{1}{\Delta x}\sum_{i=-9}^{+8} a(i)_{k+1/2} H^{\phi y}_{l+1/2+i,m} - \right. $$

$$ \frac{1}{\Delta y}\left[\sum_{i=-9}^{+8} a(i)_{k+1/2} H^{\phi x}_{l,m+1/2+i}\right] \quad . \quad (3.26) $$

$$ \left. + \sum_{i=-9}^{+9} c(i)_{k+1/2} H^{\psi x}_{l,m+1+i} \right] \Bigg) $$

After we get the scaling coefficients of the updating equation of the E_z field, we start to derive the scaling coefficients updating equations of the H_y . Rewriting the equation (3.19)

$$ \frac{\partial}{\partial x} E_z = j\omega\mu_o \left(\frac{1}{1+\frac{\sigma}{j\omega\varepsilon_o}} \right) H_y \qquad (3.27) $$

However, H_y field can't be updated using this equation because of its nonlinear frequency dependence. To get the update equation of H_y , a temperory function $\hat{B}_y(r,t)$ is intoduced, which is defined as

$$\hat{B}_y = \mu_o \left(\frac{1}{1 + \frac{\sigma}{j\omega\varepsilon_o}} \right) H_y . \tag{3.28}$$

By subsituting the equation (3.28) to equation (3.27), equation (3.27) becomes

$$\frac{\partial}{\partial x} E_z = j\omega \hat{B}_y . \tag{3.29}$$

By replacing $j\omega$ by $\frac{\partial}{\partial t}$ in equation (3.29), the equation (3.29) becomes

$$\frac{\partial}{\partial x} E_z = \frac{\partial}{\partial t} \hat{B}_y . \tag{3.30}$$

This function $\hat{B}_y(r,t)$ is also expanded into scaling functions and wavelet functions That is,

$$\hat{B}_y(r,t) = \sum_{k,l,m,n=-\infty}^{\infty} [{}_{k+1/2}\hat{B}^{\phi y}_{l+1/2,m} \cdot \phi_m(y) + {}_{k+1/2}\hat{B}^{\psi y}_{l,m+1/2,n+1/2} \cdot \psi_{m+1/2}(y)] \cdot \phi_{l+1/2}(x) \cdot h_{k+1/2}(t) \tag{3.31}$$

Therefore, the scaling coefficient updating equation of $\hat{B}_y(r,t)$ can be obtained by integrating the equation (3.30) with $\phi_{l'+1/2}(x) \cdot \phi_{m'}(y) \cdot h_{k'}(t)$ to both sides and using

the orthogonal relationship as stated in chapter 2. The scaling coefficients updating equations of $\hat{B}_y(r,t)$ is

$$\hat{B}^{\phi y}_{k+1/2,l+1/2,m} = \hat{B}^{\phi y}_{k-1/2,l+1/2,m} + \frac{\Delta t}{\Delta x}\sum_{i=-9}^{+8} a(i)_k E^{\phi z}_{l+1+i,m} \quad . \tag{3.32}$$

The aim of introducing the temporary function $\hat{B}_y(r,t)$ is to update the H_y field in equation (3.27). Since the scaling coefficients of $\hat{B}_y(r,t)$ are determined by the equation (3.32), we can use the scaling coefficients of $\hat{B}_y(r,t)$ to calculate the scaling coefficients of the H_y field. To get the H_y updating equation, we consider the following equation.

$$\hat{B}_y = \mu_o \left(\frac{1}{1 + \frac{\sigma}{j\omega\varepsilon_o}} \right) H_y \tag{3.33}$$

By rearranging the equation (3.33), it becomes

$$j\omega\hat{B}_y + \frac{\sigma}{\varepsilon_o}\hat{B}_y = j\omega\mu_o H_y \quad . \tag{3.34}$$

Again, we replace the $j\omega$ by $\frac{\partial}{\partial t}$ in equation (3.34). The equation (3.34) becomes

$$\frac{\partial}{\partial t}\hat{B}_y + \frac{\sigma}{\varepsilon_o}\hat{B}_y = \mu_o \frac{\partial}{\partial t} H_y \quad . \tag{3.35}$$

To discretize the above equation, we multiply the equation (3.35) by $\phi_{l+1/2}(x) \cdot \phi_m(y) \cdot h_{k+1/2}(t)$ to both sides and then integrate it with respect to x, y, and t. Hence, the L.H.S. of equation (3.35) becomes

$$\int_{-\infty}^{+\infty}\int_{-\infty}^{+\infty}\int_{-\infty}^{+\infty}(\frac{\partial}{\partial t}\hat{B}_y + \frac{\sigma}{\varepsilon_o}\hat{B}_y) \cdot \phi_{l'+1/2}(x) \cdot \phi_{m'}(y) \cdot h_{k'+1/2}(t)dxdydt$$

$$= \int_{-\infty}^{+\infty}\int_{-\infty}^{+\infty}\int_{-\infty}^{+\infty}\frac{\partial}{\partial t}\hat{B}_y \cdot \phi_{l'+1/2}(x) \cdot \phi_{m'}(y) \cdot h_{k'+1/2}(t)dxdydt +$$

$$\int_{-\infty}^{+\infty}\int_{-\infty}^{+\infty}\int_{-\infty}^{+\infty}\frac{\sigma}{\varepsilon_o}\hat{B}y \cdot \phi_{l'+1/2}(x) \cdot \phi_{m'}(y) \cdot h_{k'+1/2}(t)dxdydt$$

$$=({}_{k+1/2}\hat{B}^{\phi y}_{l+1/2,m} - {}_{k-1/2}\hat{B}^{\phi y}_{l+1/2,m})\Delta x\Delta y +$$

$$\int_{-\infty}^{+\infty}\int_{-\infty}^{+\infty}\int_{-\infty}^{+\infty}\frac{\sigma}{\varepsilon_o}\hat{B}y \cdot \phi_{l'+1/2}(x) \cdot \phi_{m'}(y) \cdot \frac{h_{k'+1}(t) + h_{k'}(t)}{2}dxdydt$$

$$=({}_{k+1/2}\hat{B}^{\phi y}_{l+1/2,m} - {}_{k-1/2}\hat{B}^{\phi y}_{l+1/2,m})\Delta x\Delta y$$

$$+ (\frac{\sigma\Delta t}{2\varepsilon_o}{}_{k+1/2}\hat{B}^{\phi y}_{l+1/2,m} + \frac{\sigma\Delta t}{2\varepsilon_o}{}_{k-1/2}\hat{B}^{\phi y}_{l+1/2,m})\Delta x\Delta y$$

$$= (1 + \frac{\sigma\Delta t}{2\varepsilon_o})_{k+1/2}\hat{B}^{\phi y}_{l+1/2,m} - (1 - \frac{\sigma\Delta t}{2\varepsilon_o})_{k-1/2}\hat{B}^{\phi y}_{l+1/2,m} \quad (3.36)$$

The R.H.S. of the equation (3.35) becomes

$$\int_{-\infty}^{+\infty}\int_{-\infty}^{+\infty}\int_{-\infty}^{+\infty}(\mu_o\frac{\partial}{\partial t}Hy) \cdot \phi_{l'+1/2}(x) \cdot \phi_{m'}(y) \cdot h_{k'+1/2}(t)dxdydt$$

$$= \mu_o({}_{k+1/2}H^{\phi y}_{l+1/2,m} - {}_{k-1/2}H^{\phi y}_{l+1/2,m})\Delta x\Delta y \ . \tag{3.37}$$

By rearranging these two sides, we get the scaling coefficients updating equation of H_y field.

$$\begin{aligned} {}_{k+1/2}H^{\phi y}_{l,m+1/2} = {}_{k-1/2}H^{\phi y}_{l,m+1/2} + \frac{1}{\mu_o}\frac{1}{1+\frac{\sigma\Delta t}{2\varepsilon_o}}\Bigg(\left(1+\frac{\sigma\Delta t}{2\varepsilon_o}\right)_{k+1/2}\hat{B}^{\phi y}_{l+1/2,m} \\ -\left(1-\frac{\sigma\Delta t}{2\varepsilon_o}\right)_{k-1/2}\hat{B}^{\phi y}_{l+1/2,m}\Bigg) \end{aligned} \tag{3.38}$$

Hence, we get the scaling coefficients updating equations of E_z and H_y. The scaling coefficients updating equation of H_x can be derived using the similar method. The scaling coefficients updating equation of H_x is stated as follows.

$$\begin{aligned} {}_{k+1/2}H^{\phi x}_{l,m+1/2} = \left(\frac{1-\frac{\phi\Delta t}{2\varepsilon_o}}{1+\frac{\phi\Delta t}{2\varepsilon_o}}\right)_{k-1/2}H^{\phi x}_{l,m+1/2} - \frac{\Delta t}{\mu_o}\frac{1}{1+\frac{\phi\Delta t}{2\varepsilon_o}}\Bigg(\frac{1}{\Delta y}[\sum_{i=-9}^{+8}a(i)_k E^{\phi z}_{l,m+1+i} + \\ \sum_{i=-9}^{+9}c(i)_k E^{\psi z}_{l,m+1+i}]\Bigg) \end{aligned} \tag{3.39}$$

We have demonstrated the derivation of the scaling coefficients updating equations inside the APML. The derivation of the wavelet coefficients updating equations is similar and it is skipped for simplicity. The wavelet coefficients updating equations inside the APML are stated as follows.

$$
{}_{k+1}E^{\psi z}_{l,m+1/2} = \left(\frac{1-\frac{\sigma\Delta t}{2\varepsilon_o}}{1+\frac{\sigma\Delta t}{2\varepsilon_o}}\right) {}_{k}E^{\psi z}_{l,m+1/2} + \frac{\Delta t}{\varepsilon_o}\frac{1}{1+\frac{\sigma\Delta t}{2\varepsilon_o}}\left(\frac{1}{\Delta x}\sum_{i=-9}^{+8} a(i)_{k+1/2} H^{\psi y}_{l+1/2+i,m+1/2} - \right.
$$

$$
\frac{1}{\Delta y}\left[\sum_{i=-9}^{+9} c(i)_{k+1/2} H^{\phi x}_{l,m-1/2+i} \right. \qquad (3.40)
$$

$$
\left.\left. + \sum_{i=-9}^{+8} b(i)_{k+1/2} H^{\psi x}_{l,m+1/2+1+i}\right]\right)
$$

$$
{}_{k+1/2}H^{\psi x}_{l,m} = \left(\frac{1-\frac{\phi\Delta t}{2\varepsilon_o}}{1+\frac{\phi\Delta t}{2\varepsilon_o}}\right) {}_{k-1/2}H^{\psi x}_{l,m} - \qquad (3.41)
$$

$$
\frac{\Delta t}{\mu_o}\frac{1}{1+\frac{\phi\Delta t}{2\varepsilon_o}}\left(\frac{1}{\Delta y}\left[\sum_{i=-9}^{+9} c(i)_k E^{\phi z}_{l,m-1+i} + \sum_{i=-9}^{+8} b(i)_k E^{\psi z}_{l,m+1/2+i}\right]\right)
$$

$$
{}_{k+1/2}H^{\psi y}_{l+1/2,m+1/2} = {}_{k-1/2}H^{\psi y}_{l+1/2,m+1/2} + \qquad (3.42)
$$

$$
\frac{1}{\mu_o}\frac{1}{1+\frac{\phi\Delta t}{2\varepsilon_o}}\left(\left(1+\frac{\sigma\Delta t}{2\varepsilon_o}\right)_{k+1/2}\hat{B}^{\psi y}_{l+1/2,m+1/2} - \right.
$$

$$
\left.\left(1-\frac{\sigma\Delta t}{2\varepsilon_o}\right)_{k+1/2}\hat{B}^{\psi y}_{l+1/2,m+1/2}\right)
$$

$$
{}_{k+1/2}\hat{B}^{\psi y}_{l+1/2,m+1/2} = {}_{k-1/2}\hat{B}^{\psi y}_{l+1/2,m+1/2} + \frac{\Delta t}{\Delta x}\sum_{i=-9}^{+8} a(i)_k E^{\psi z}_{l+1+i,m+1/2} \qquad (3.43)
$$

3.2.2.The use of the wavelet coefficients updating equation for APML

The non-physical reflection between the W-MRTD and the S-MRTD can be removed if the numerical wave of the wavelet coefficients can be absorbed at the boundary. From the W-MRTD updating equations inside the APML in last part, it can be seen that the both scaling coefficients and wavelet coefficients are updated independently. That is, the APML absorb the numerical wave of the wavelet coefficients and the numerical wave of the scaling coefficients separately. This allows the use of the wavelet coefficients updating equation for AML alone while the scaling coefficients can be updated using other method. In next part, we propose a new computational scheme, which is called sub-gridding MRTD. In this scheme, the S-MRTD and W-MRTD are joined together and APML is placed at the boundary between the W-MRTD and S-MRTD to absorb the non-physical reflection.

3.3 A sub-gridding MRTD

As discussed before, the W-MRTD and S-MRTD cannot be joined together because the existence of non-physical reflection at the boundary affect the simulation result accuracy. Making use of the APML, the non-physical reflection can be removed. The APML is placed at the boundary is depicted in figure 3.5.

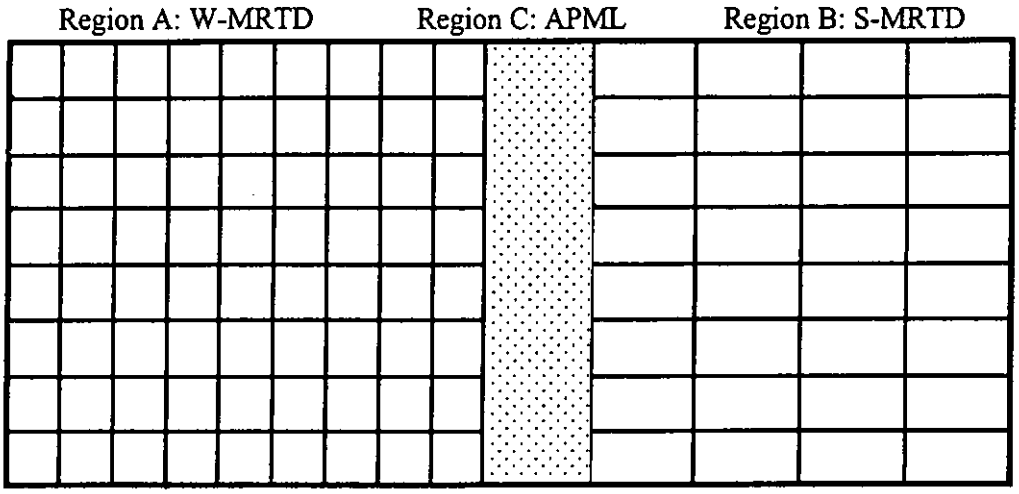

Figure 3.5 The insertion of APML between the W-MRTD and S-MRTD.

As we want to remove the numerical wave of wavelet coefficients at the boundary without creating non-physical reflection, the wavelet coefficients updating equations in the APML are used at region C (figure 3.5). Hence, when the numerical wave of the wavelet coefficients travel from the W-MRTD to the S-MRTD, the region C will appear as an open end. In other words, numerical wave of wavelet coefficients is absorbed. However, the APML cannot completely absorb the numerical wave [39], a small reflection exists at the end of the APML. This mechanism is illustrated in figure 3.6.

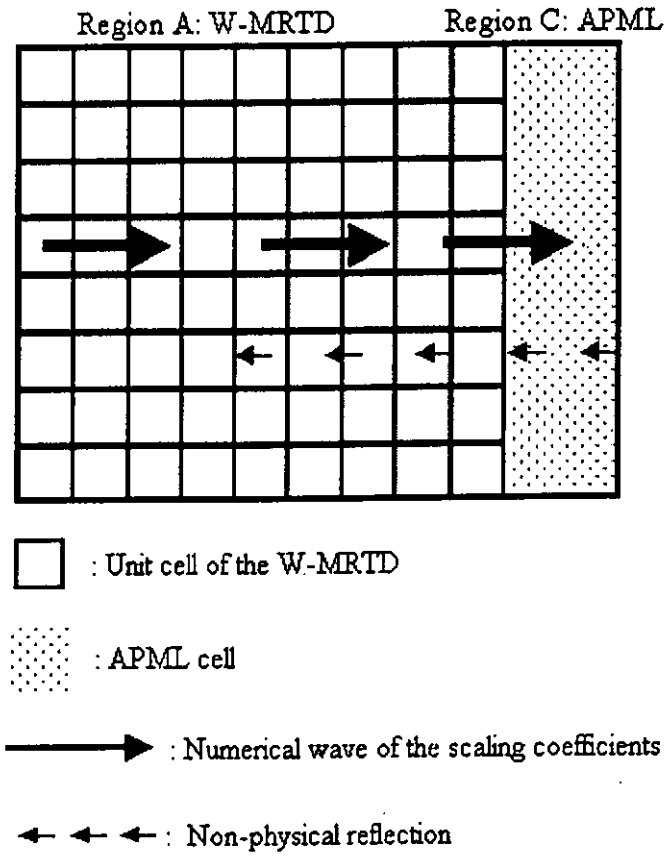

Figure 3.6. The reflection of numerical wave of wavelet coefficients at the end of APML

For the numerical wave of the scaling coefficients, it travels from the W-MRTD to the S-MRTD and is affected by the boundary (figure 3.7).

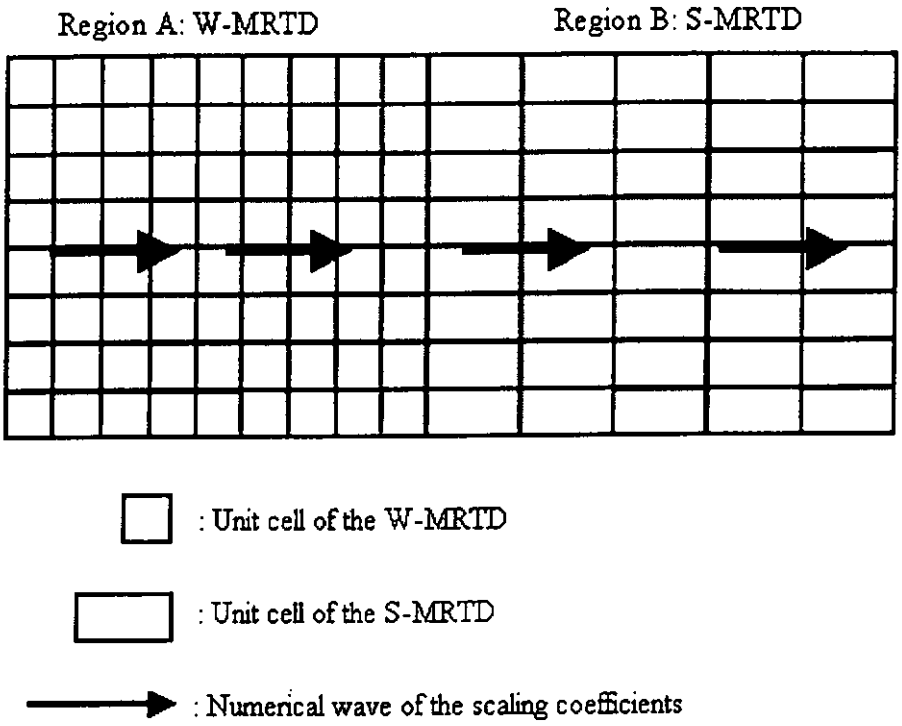

Figure 3.7 The propagation of the numerical wave of the scaling coefficients inside the W-MRTD and S-MRTD

Summarizing the above discussion, a new computational scheme is proposed, in which combines the S-MRTD scheme and the W-MRTD scheme with the insertion of the APML at the boundary. Hence, we can compute the field with different scale of grid density. This computational scheme is called sub-gridding MRTD.

3.3.1 The formulation of sub-gridding MRTD scheme

Basically, the sub-gridding MRTD is composed of three regions as seen in figure 3.8 Region I is the dense grid region, which corresponds to the W-MRTD. Region II is the coarse grid region, which corresponds to the S-MRTD and APML is placed in region III.

Region I: dense grid region	Region III: APML	Region II: dense grid region
Updated by the Wy-MRTD updating equation	Updated by the wavelet coefficients updating equation inside APML While the scaling coefficient is updated by Wy-MRTD	Updated by the S-MRTD updating equation

Figure 3.8 The updating scheme of the sub-gridding MRTD

In region I, the fields component are expanded by both scaling functions and wavelet functions. Consider E_z field as an example, the E_z field is expanded by both the scaling functions and the wavelet functions, Therefore, we can write

$$E_z(r,t) = \sum_{k,l,m,n=-\infty}^{\infty} [\, {}_k E^{\phi\phi}_{l,m} \phi_m(y) + {}_k E^{\psi z}_{l,m+1/2} \psi_{m+1/2}(y)] \phi_l(x) h_k(t) \ . \qquad (3.44)$$

The numerical wave is composed of both scaling coefficients and wavelet coefficients. Hence, the scaling coefficients of the E_z field in this region are updated by

$$
\begin{aligned}
{}_{k+1}E^{\phi z}_{l,m} = {}_{k}E^{\phi z}_{l,m} + \frac{\Delta t}{\varepsilon}\Big[\frac{1}{\Delta x}\sum_{i=-9}^{+8} a(i)_{k+1/2} H^{\phi y}_{l+1/2+i,m} \\
- \frac{1}{\Delta y}\Big(\sum_{i=-9}^{+8} a(i)_{k+1/2} H^{\phi x}_{l,m+1/2+i} \\
+ \sum_{i=-9}^{+9} c(i)_{k+1/2} H^{\psi x}_{l,m+1+i}\Big)\Big]
\end{aligned}
\tag{3.45}
$$

and the wavelet coefficients of E_z field are updated by

$$
\begin{aligned}
{}_{k+1}E^{\psi z}_{l,m+1/2} = {}_{k}E^{\psi z}_{l,m+1/2} + \frac{\Delta t}{\varepsilon}\Big[\frac{1}{\Delta x}\sum_{i=-9}^{+8} a(i)_{k+1/2} H^{\psi y}_{l+1/2+i,m+1/2} \\
- \frac{1}{\Delta y}\Big(\sum_{i=-9}^{+9} c(i)_{k+1/2} H^{\phi x}_{l,m-1/2+i} \\
+ \sum_{i=-9}^{+8} b(i)_{k+1/2} H^{\psi x}_{l,m+1+i}\Big)\Big]
\end{aligned}
\tag{3.46}
$$

For region II, it is a coarse grid region in which the fields are expanded by scaling function only. Therefore, the E_z field can be written as

$$
E_z(r,t) = \sum_{k,l,m=-\infty}^{\infty} {}_{k}E^{\phi z}_{l,m}\,\phi_l(x)\phi_m(y)h_k(t)\,. \tag{3.47}
$$

In this region, the numerical wave is composed of scaling coefficients only. Hence, the scaling coefficients of E_z field are governed by the following updating equation.

$$ {}_{k+1}E^{\phi z}_{l,m} = {}_{k}E^{\phi z}_{l,m} + \frac{\Delta t}{\varepsilon}\left[\frac{1}{\Delta x}\sum_{i=-9}^{+8} a(i)_{k+1/2} H^{\phi y}_{l+1/2+i,m} - \frac{1}{\Delta y}\sum_{i=-9}^{+8} a(i)_{k+1/2} H^{\phi x}_{l,m+1/2+i}\right] \tag{3.48} $$

For region III, an absorbing layer is placed for the removal of the non-physical reflection due to wavelet coefficients. This layer is composed of a substance with spatial variant conductivity. The conductivity is taken as $\sigma = c_0 \frac{\varepsilon_0}{\Delta t}\left(\frac{i}{N_p}\right)^m$ where m = 2 ~ 4 and c_0 =0.8~1.6 [14]. Again, considering the E_z field as an example, the scaling coefficients of E_z field are updated by

$$ {}_{k+1}E^{\phi z}_{l,m} = {}_{k}E^{\phi z}_{l,m} + \frac{\Delta t}{\varepsilon}\left[\frac{1}{\Delta x}\sum_{i=-9}^{+8} a(i)_{k+1/2} H^{\phi y}_{l+1/2+i,m} - \frac{1}{\Delta y}\sum_{i=-9}^{+8} a(i)_{k+1/2} H^{\phi x}_{l,m+1/2+i}\right] \tag{3.49} $$

It implies that the scaling coefficients of E_z in this region are updated using the S-MRTD scheme in this region. While the wavelet coefficients are updated by

$$ {}_{k+1}E^{\psi c}_{l,m+1/2} = \left(\frac{1-\frac{\sigma\Delta t}{2\varepsilon_o}}{1+\frac{\sigma\Delta t}{2\varepsilon_o}}\right) {}_{k}E^{\psi c}_{l,m+1/2} + \frac{\Delta t}{\varepsilon_o}\frac{1}{1+\frac{\sigma\Delta t}{2\varepsilon_o}}\left(\frac{1}{\Delta x}\sum_{i=-9}^{+8} a(i)_{k+1/2} H^{\psi y}_{l+1/2+i,m+1/2} - \frac{1}{\Delta y}\left[\sum_{i=-9}^{+9} c(i)_{k+1/2} H^{\phi x}_{l,m-1/2+i} + \sum_{i=-9}^{+8} b(i)_{k+1/2} H^{\psi x}_{l,m+1/2+i+j}\right]\right) \tag{3.50} $$

To ensure we can get the stable results, the time step is chosen as

$$\Delta t = \frac{0.1c}{\sqrt{\left(\frac{1}{\Delta x}\right)^2 + \left(\frac{1}{\Delta y}\right)^2}} \text{ where } c = 3 \times 10^8.$$

3.4. Summary

In this chapter, we have discussed the propagation of the numerical wave inside the MRTD computational domain. In order to compute the field accurately, a new computation scheme is formed by joining the W-MRTD and S-MRTD. However, there is a non-physical reflection at the boundary due to the wavelet coefficients. To remove the non-physical reflection, an APML is placed at the boundary so that only the wavelet coefficients updating equation for APML is used. Hence, the numerical wave of the scaling coefficients propagates through the boundary while the numerical wave of the wavelet coefficients will be terminated at the boundary. The above computation method lead to our proposed sub-gridding MRTD.

In brief, our proposed sub-gridding MRTD constitutes three parts. They are the dense grid region, coarse grid region and the boundary. The dense grid region corresponds to the W-MRTD while the coarse grid region corresponds to the S-MRTD. APML is used at the boundary between the dense grid regions and the coarse grids region.

Chapter 4

The application of the sub-gridding MRTD for two dimensional field problems

The aim of this chapter is to verify the sub-gridding MRTD by applying this computational scheme to some two-dimensional field problems. The propagation of the electromagnetic pulse inside an extra large two-dimensional cavity is considered. Also, we have studied the resonant frequency of a small size two-dimensional cavity using the sub-gridding MRTD. The results have been compared with those obtained by S-MRTD and W-MRTD.

4.1. The propagation of the electromagnetic pulse inside the cavity.

As discussed in last chapter, a sub-gridding MRTD is divided the whole area into three parts. To investigate the performance of sub-gridding MRTD, the propagation of a electromagnetic pulse inside these three regions is studied. A two-dimensional cavity with size 63.75m×63.75m is considered. To ensure a plane wave is traveled in y-direction inside the cavity, a row source of Blackman Harris window function is used for pulse excitation as shown in figure 4.1.

4.1.1 The source is excited inside the dense grid region

When the electromagnetic pulse propagates from the dense grid region to the coarse grid region, the numerical wave of the wavelet coefficients should be absorbed. In order to verify this property, A row source of Blackman Harris window function is excited at the dense grid region as shown in figure 4.1. The mathematical representation of Blackman Harris window function is as follow.

$$f_b(t) = \begin{cases} W(t) & t_c - N \le t \le t_c + N \\ 0 & \text{otherwise} \end{cases}$$

where N is the width of the pulse, t_c is the excition time and $W(t)$ is given by

$$W(t) = 0.35875 + 0.48829\cos(\frac{\pi(t-t_c)}{N}) + 0.14128\cos(\frac{2\pi(t-t_c)}{N}) + 0.01168\cos(\frac{3\pi(t-t_c)}{N}) \quad (4.1)$$

The APML with 4 cells is used at the boundary between the dense grid region and the coarse grid region. The time response is observed at four different locations inside the cavity. They are Point A, Point B, Point C and Point D. Both Point A and Point B are located in the dense grid region and Point C and Point D are located in the coarse grid region. Both S-MRTD and W-MRTD are used to simulate the same cavity and the time response is also observed at the same positions. The simulation takes 3000 time steps and the time step (Δt) is 1.125ρs.

4.1.1.1 Cell size is one half of the wavelength

In this simulation, Blackman Harris window function of cut-off frequency 20GHz is used as shown in figure 4.1. For a 20GHz electromagnetic wave, its wavelength is 0.015m. The cell size is set to one half of the wavelength.

The comparisons of time response of the signal obtained by the sub-gridding MRTD inside the dense grid region and W-MRTD are shown in figure 4.4 and figure 4.6. The comparisons of frequency response of the signal obtained by the sub-gridding MRTD inside the dense grid region and W-MRTD are shown in figure 4.5 and figure 4.7. The difference between the results can be seen in the frequency spectrum of the signal beyond 20GHz in figure 4.5 and figure 4.7.

The time response of the signal obtained by the sub-gridding MRTD inside the coarse grid region is compared with the S-MRTD in figure 4.8 and figure 4.10. The comparisons of frequency response of the signal obtained by sub-gridding MRTD inside the dense grid region and W-MRTD are shown in figure 4.9 and figure 4.11. The difference between the results can be seen in the frequency spectrum of the signal beyond 20GHz in figure 4.9 and figure 4.11.

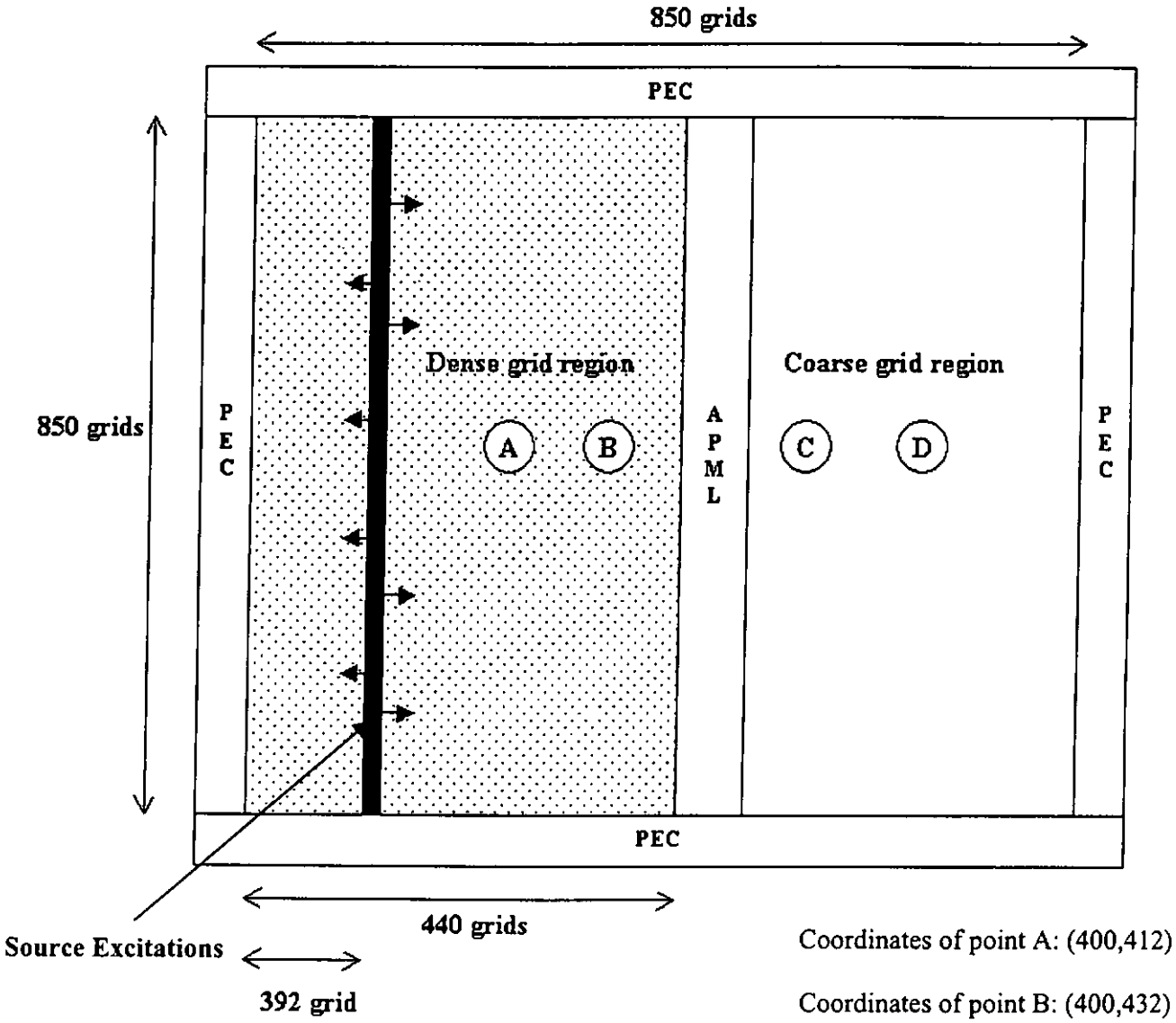

Figure 4.1 The geometry of the two dimensional cavity using the sub-gridding MRTD with 4 cells APML boundary (the source is excited at dense grid region)

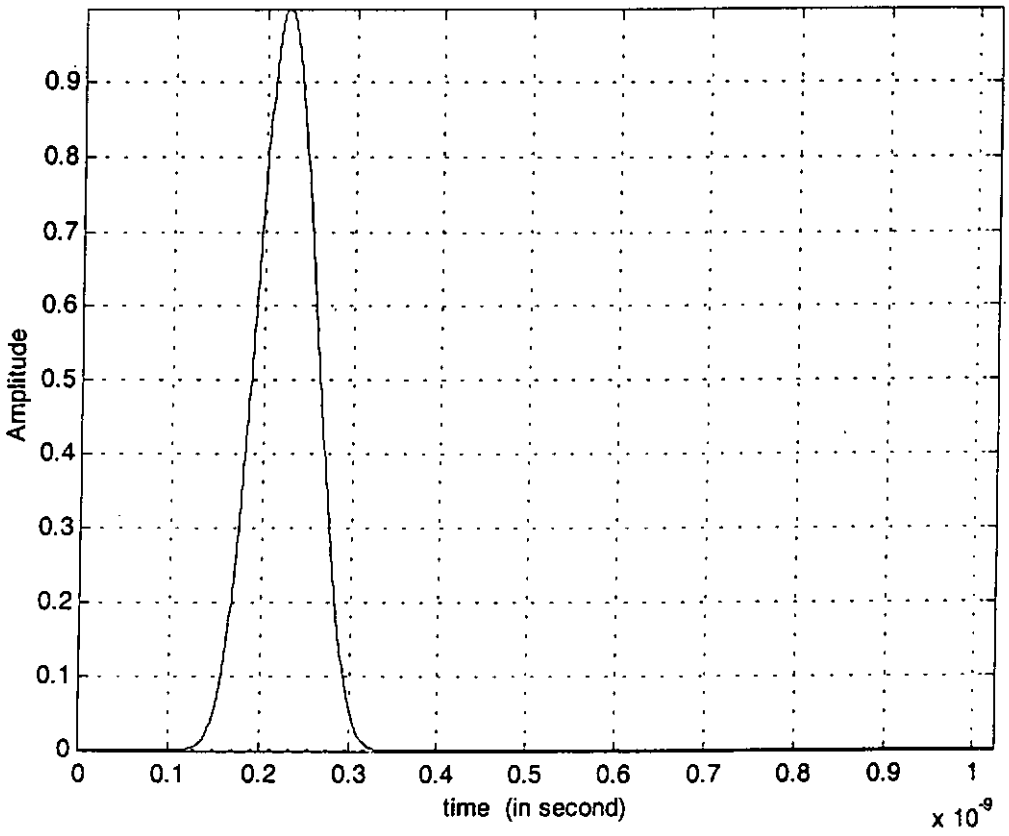

Figure 4.2. The time domain of a blackman harris window function of cut-off frequency 20GHz

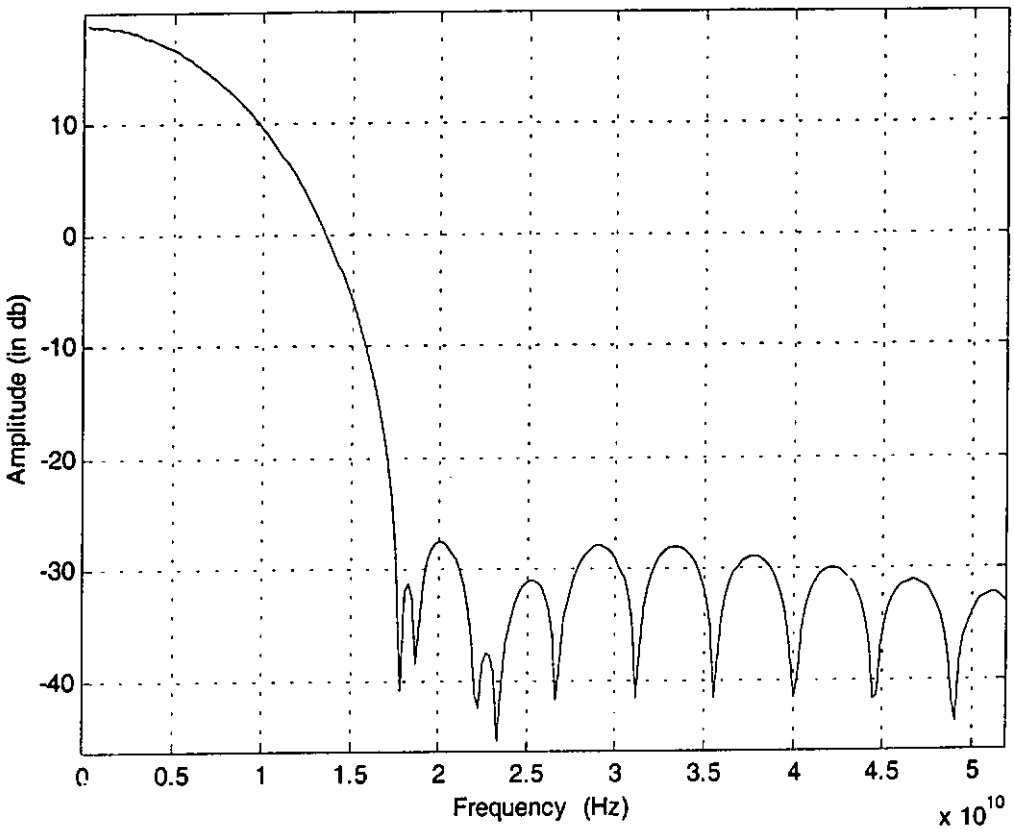

Figure 4.3. The frequency domain of blackman harris window function of cut-off frequency 20GHz

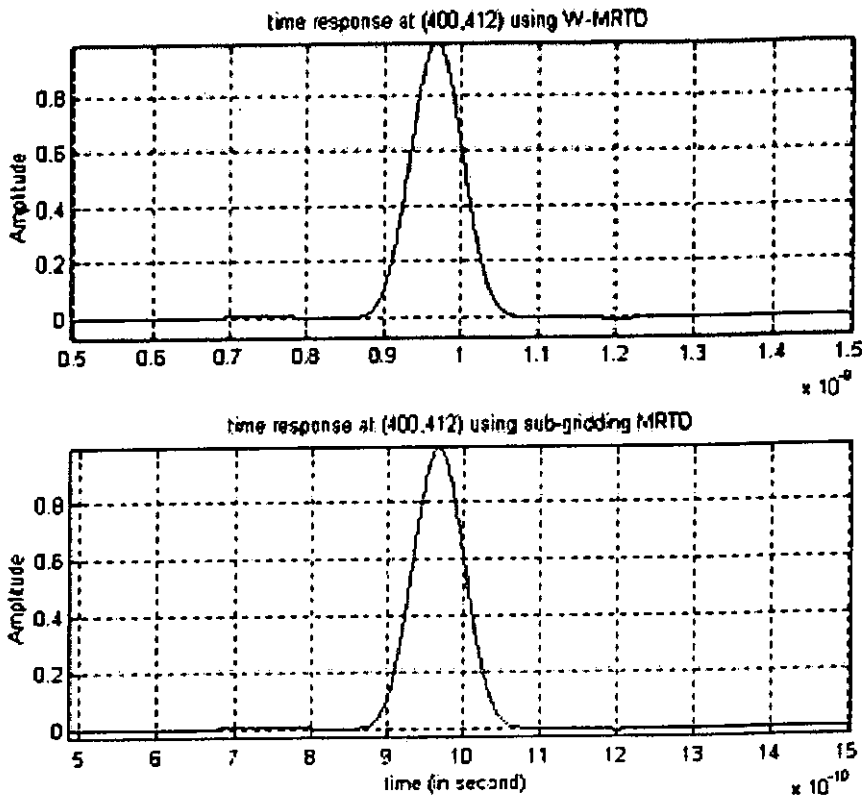

Figure 4.4. The comparsion of time response at point A using the W-MRTD and sub-gridding MRTD with cell size=0.5λ (The source is excited at the dense grid region)

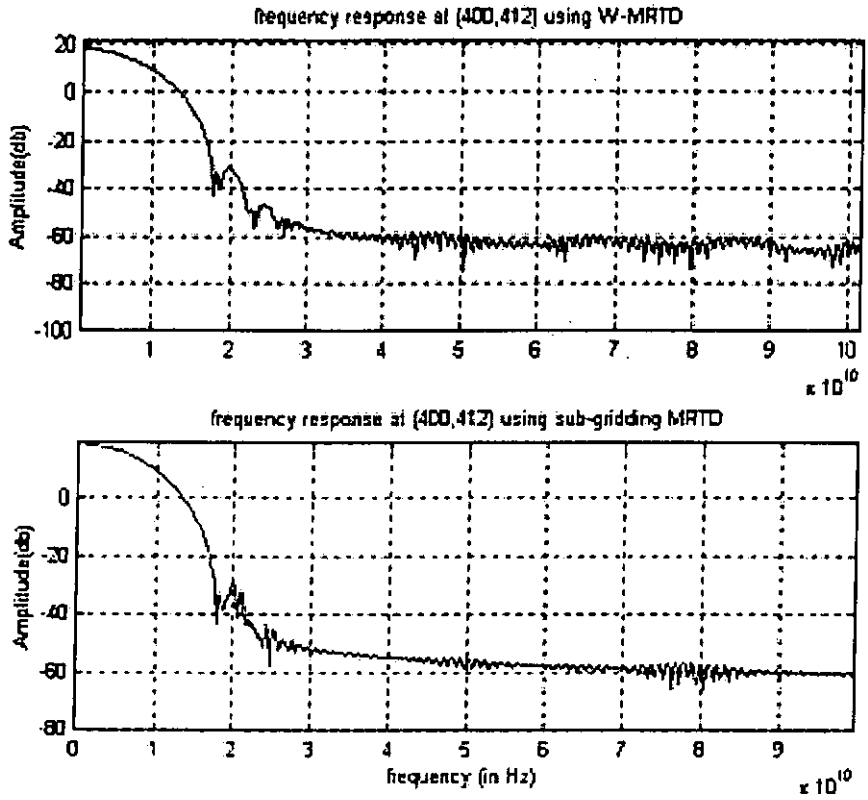

Figure 4.5 The comparsion of frequency response at point A using the W-MRTD and sub-gridding MRTD with cell size=0.5λ (The source is excited at the dense grid region)

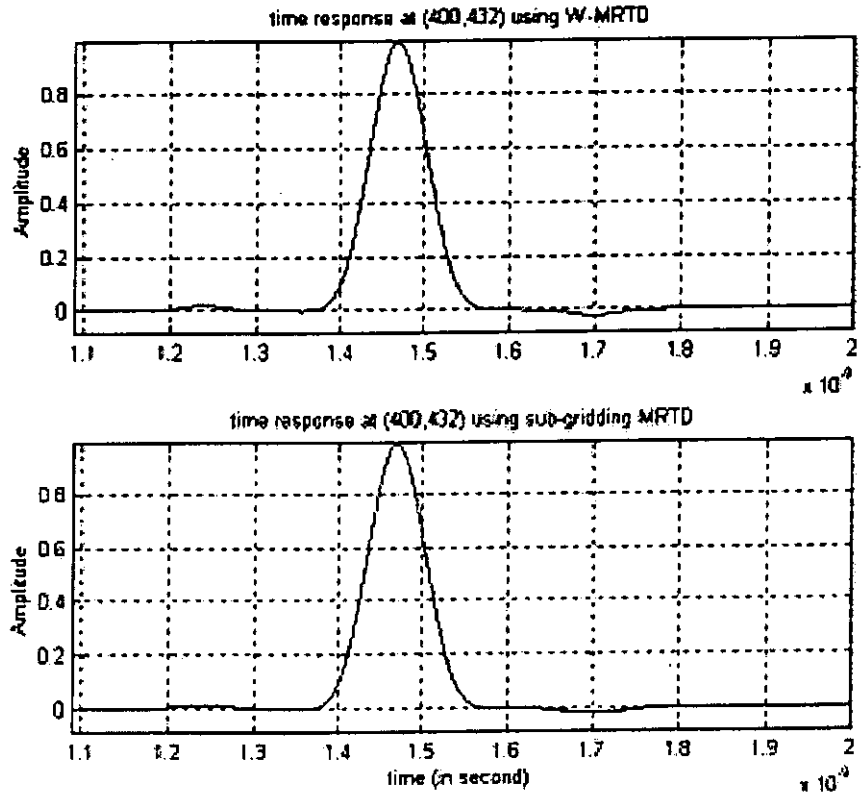

Figure 4.6 The comparsion of time response at point B using the W-MRTD and sub-gridding MRTD with cell size=0.5λ (The source is excited at the dense grid region)

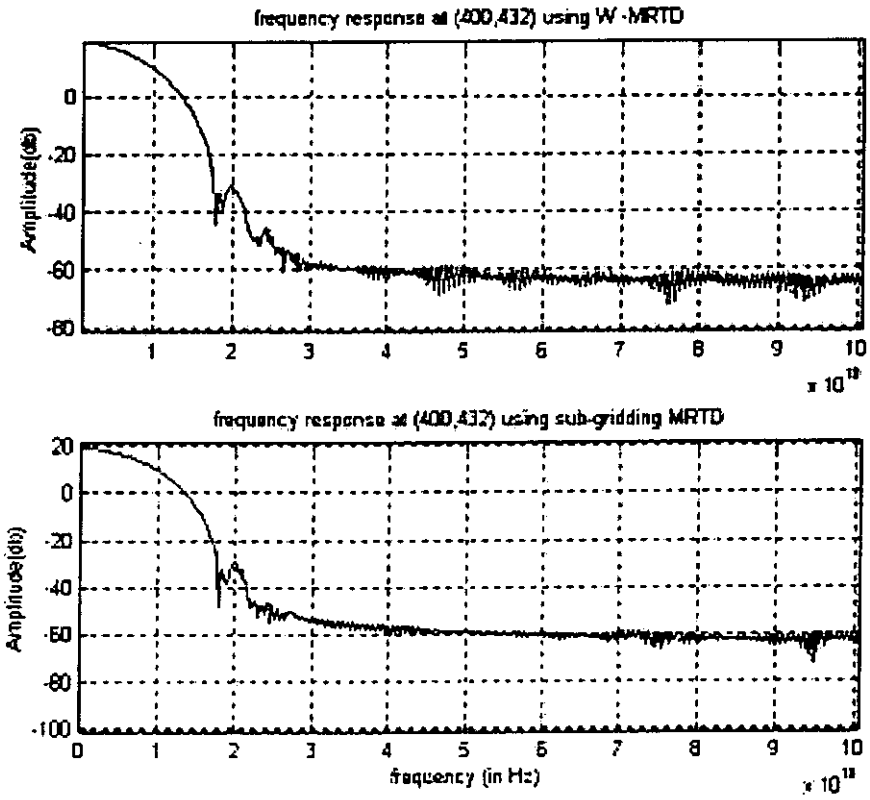

Figure 4.7 The comparsion of frequency response at point B using the W-MRTD and sub- gridding MRTD with cell size=0.5λ (The source is excited at the dense grid region)

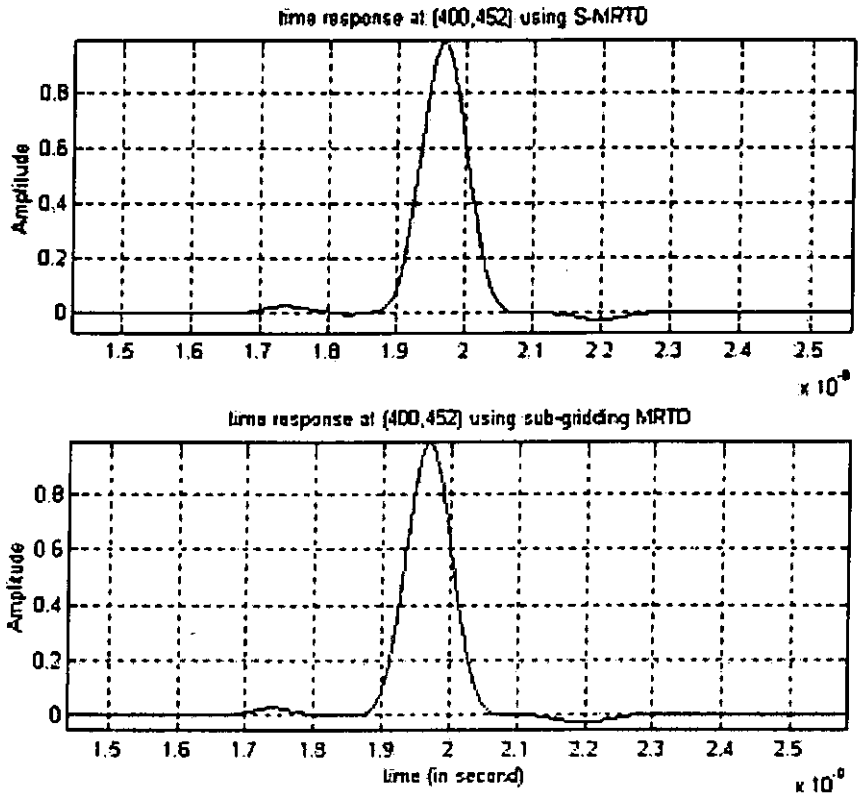

Figure 4.8. The comparsion of time response at point C using the S-MRTD and sub-gridding MRTD with cell size=0.5λ (The source is excited at the dense grid region)

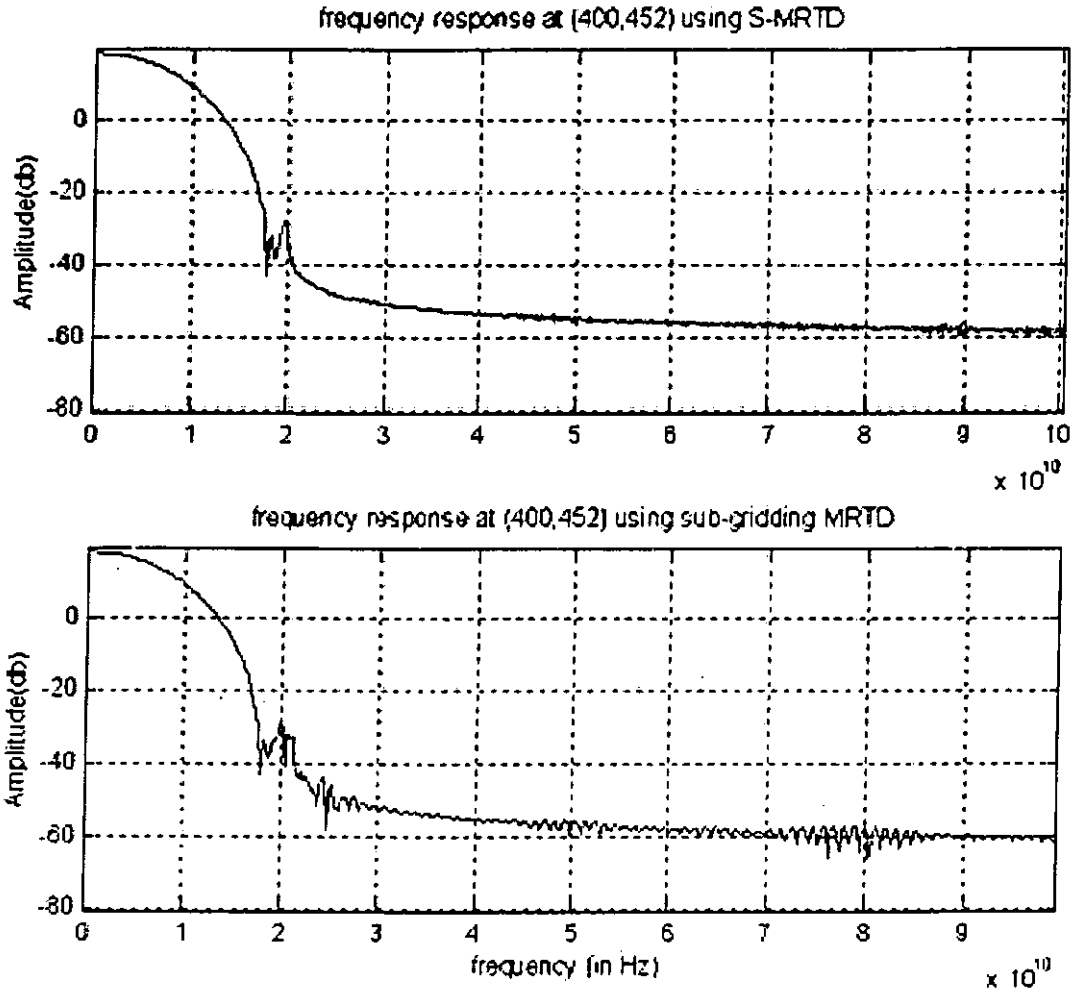

Figure 4.9. The comparsion of frequency response at point C using the S-MRTD and sub- gridding MRTD with cell size=0.5λ (The source is excited at the dense grid region)

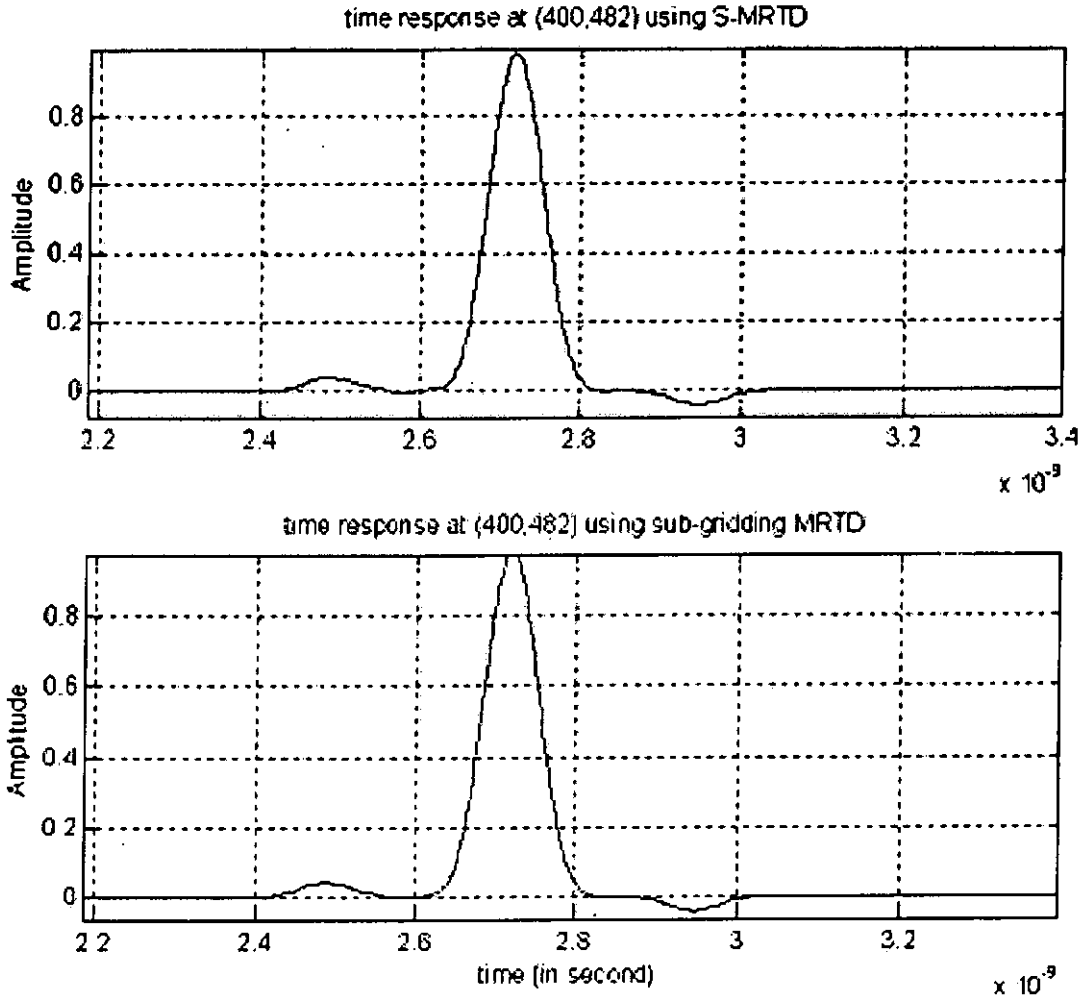

Figure 4.10. The comparsion of time response at point D using the S-MRTD and sub-gridding MRTD with cell size=0.5λ (The source is excited at the dense grid region)

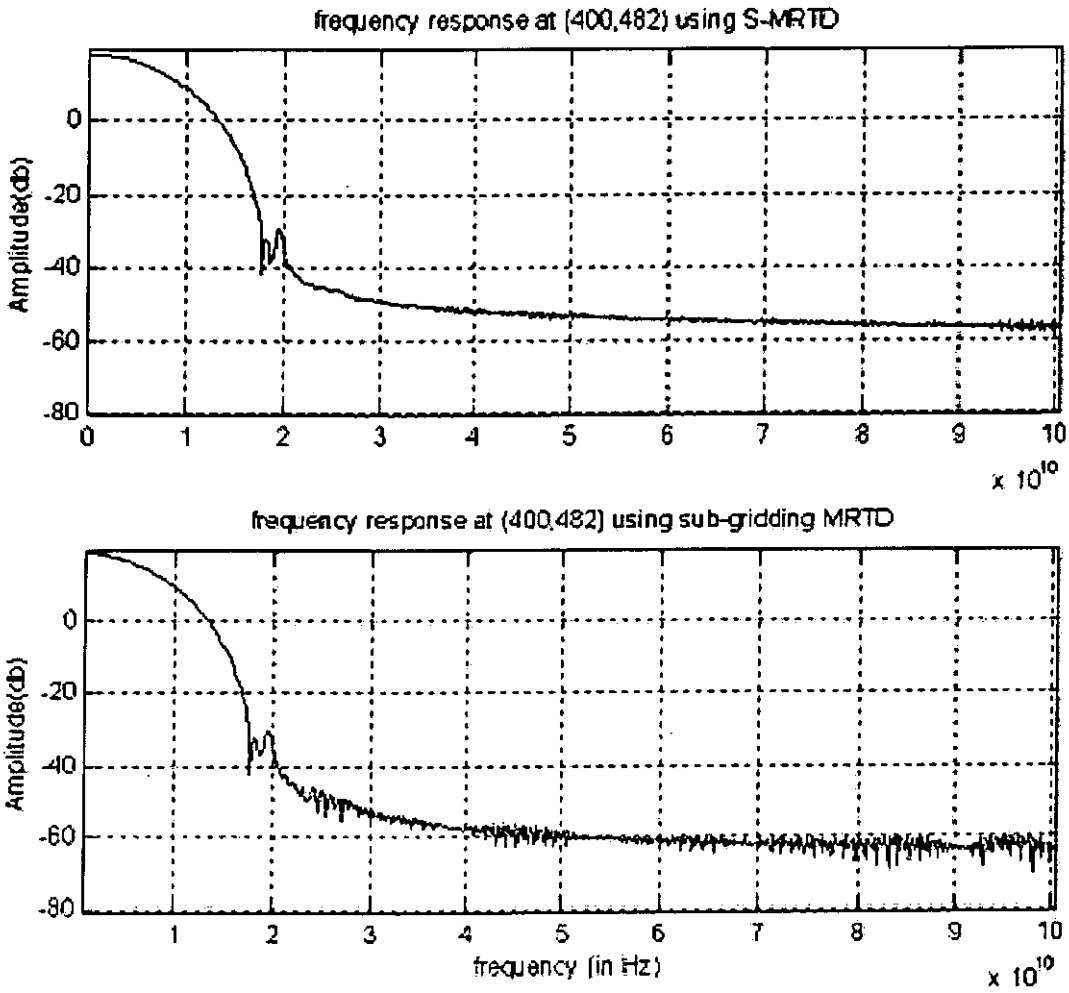

Figure 4.11. The comparsion of frequency response at point D using the S-MRTD and sub-gridding MRTD with cell size=0.5λ (The source is excited at the dense grid region)

4.1.1.2 Cell size is one tenth of the wavelength

In this simulation, a Blackman Harris window function of cut-off frequency 4GHz is used for excitation while other parameters remain unchange. For a 4GHz electromagnetic wave, its wavelength is 0.075m. The cell size is set to one tenth of the wavelength.

For the dense grid region, the time response of the signal is computed using the sub-gridding MRTD. The simulation results obtained by the sub-gridding MRTD are compared with those obtained by the W-MRTD in figure 4.14 and figure 4.16. The comparisons of frequency response of the signal obtained by the sub-gridding MRTD inside the dense grid region and the W-MRTD are shown in figure 4.15 and figure 4.17. For frequency above 10GHz, the signal obtained by sub-gridding MRTD is different from those obtained by W-MRTD as shown in figure 4.15 and figure 4.17.

The time response of the signal inside the coarse grid region obtained by the sub-gridding MRTD region is compared with those obtained by the S-MRTD in figure 4.18 and figure 4.20. The comparisons of frequency response of the signal obtained by the sub-gridding MRTD inside the coarse grid region and the S-MRTD are shown in figure 4.19 and figure 4.21. For frequency above 4GHz, the signal obtained by sub-gridding MRTD is different from those obtained by S-MRTD as in figure 4.19 and figure 4.21.

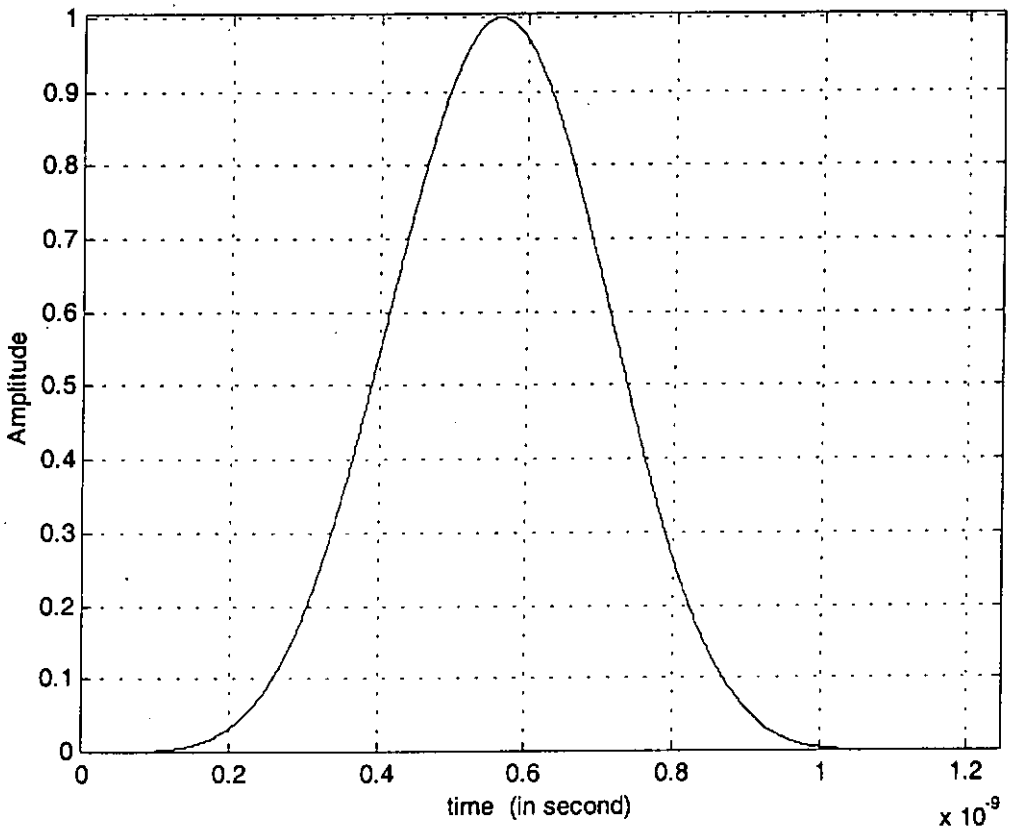

Figure 4.12. The time domain of Blackman Harris window function of cut-off frequency 4GHz

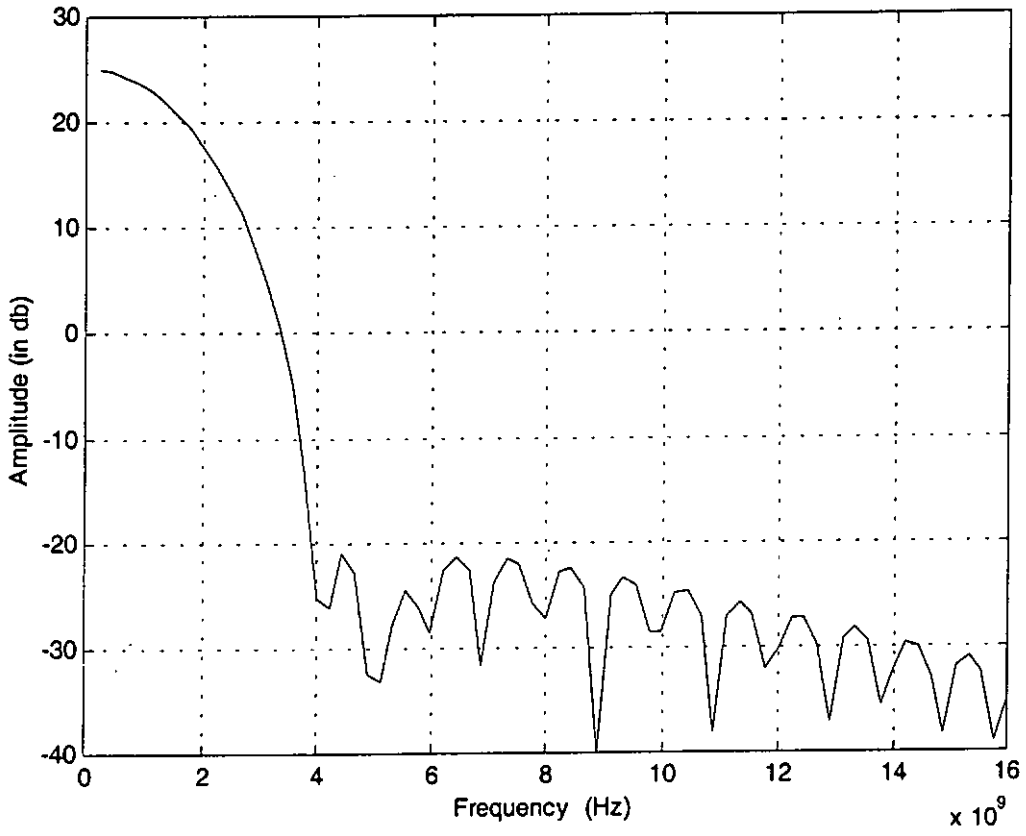

Figure 4.13. The frequency domain of Blackman Harris window function of cut-off frequency 4GHz

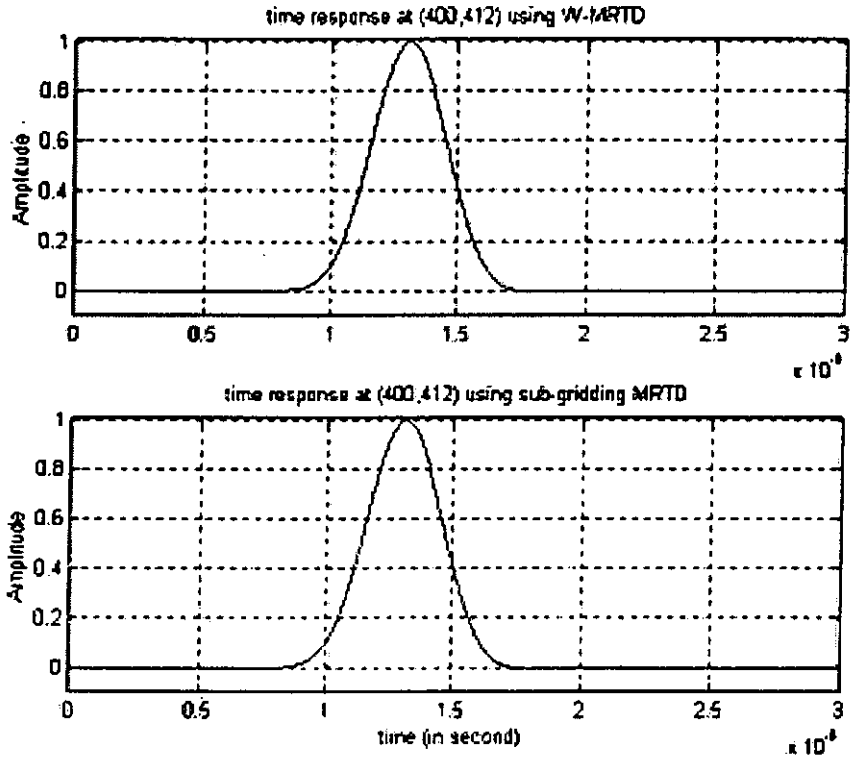

Figure 4.14. The comparsion of time response at point A using the W-MRTD and sub- gridding MRTD with cell size=0.1λ (The source is excited at the dense grid region)

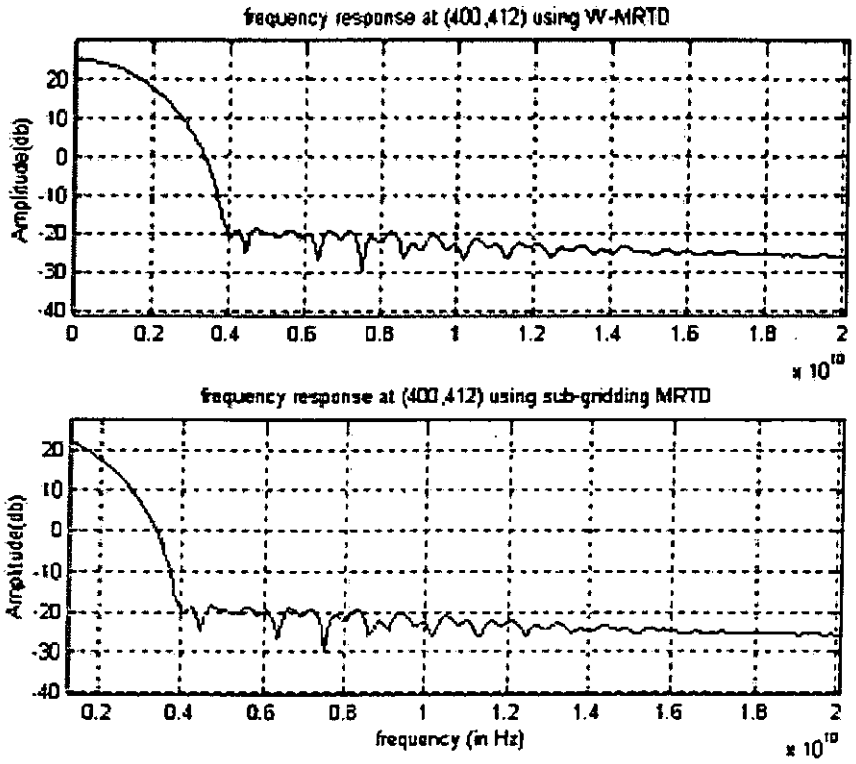

Figure 4.15. The comparsion of frequency response at point A using the W-MRTD and sub gridding MRTD with cell size=0.1λ (The source is excited at the dense grid region)

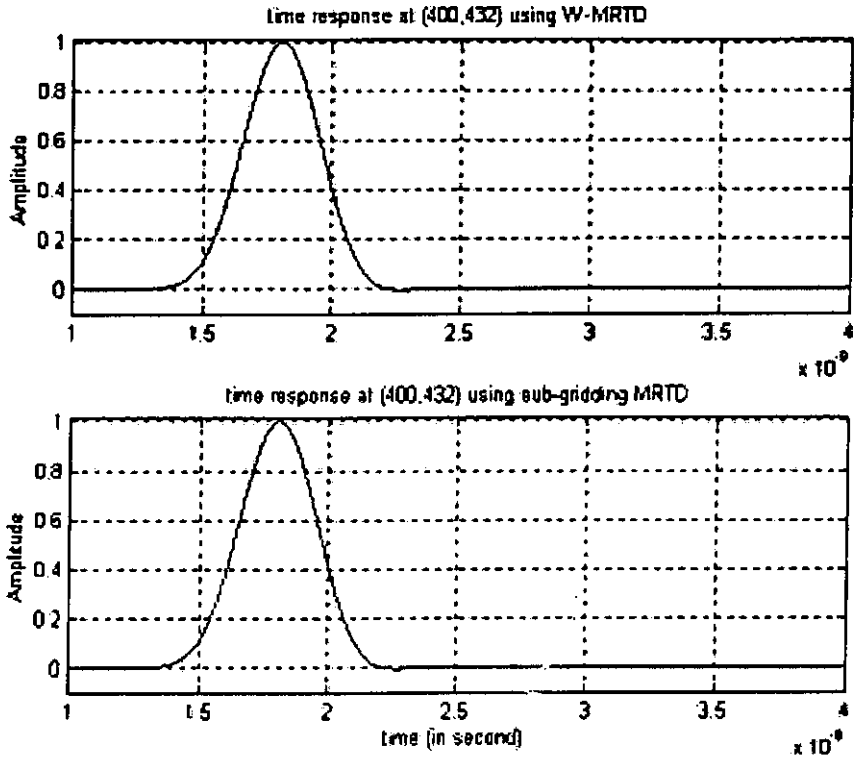

Figure 4.16. The comparsion of time response at point B using the W-MRTD and sub-gridding MRTD with cell size=0.1λ (The source is excited at the dense grid region)

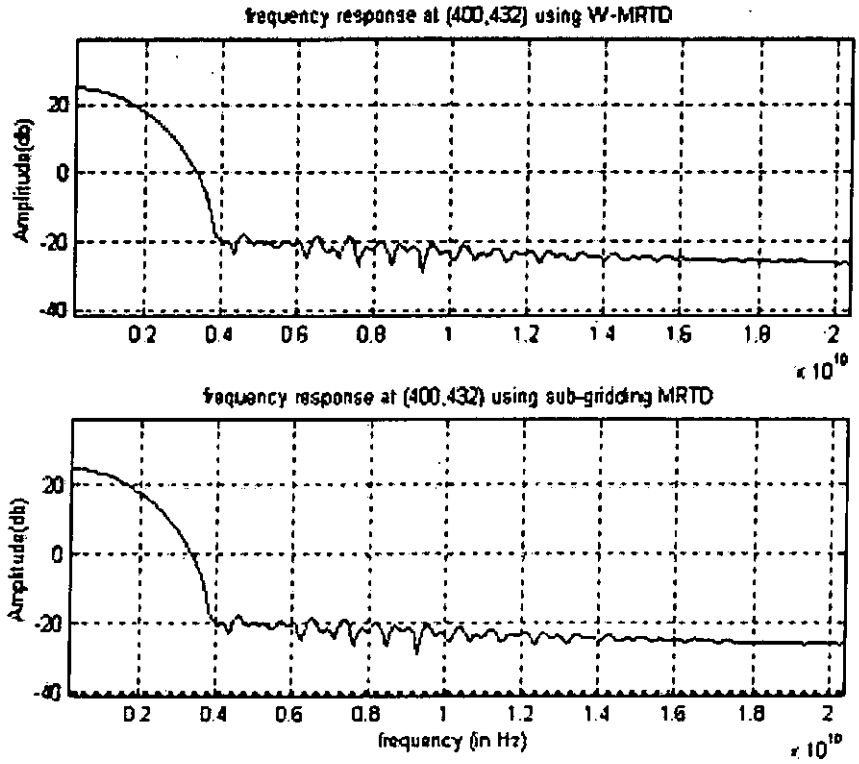

Figure 4.17. The comparsion of frequency response at point B using theW-MRTD and sub-gridding MRTD with cell size=0.1λ (The source is excited at the dense grid region)

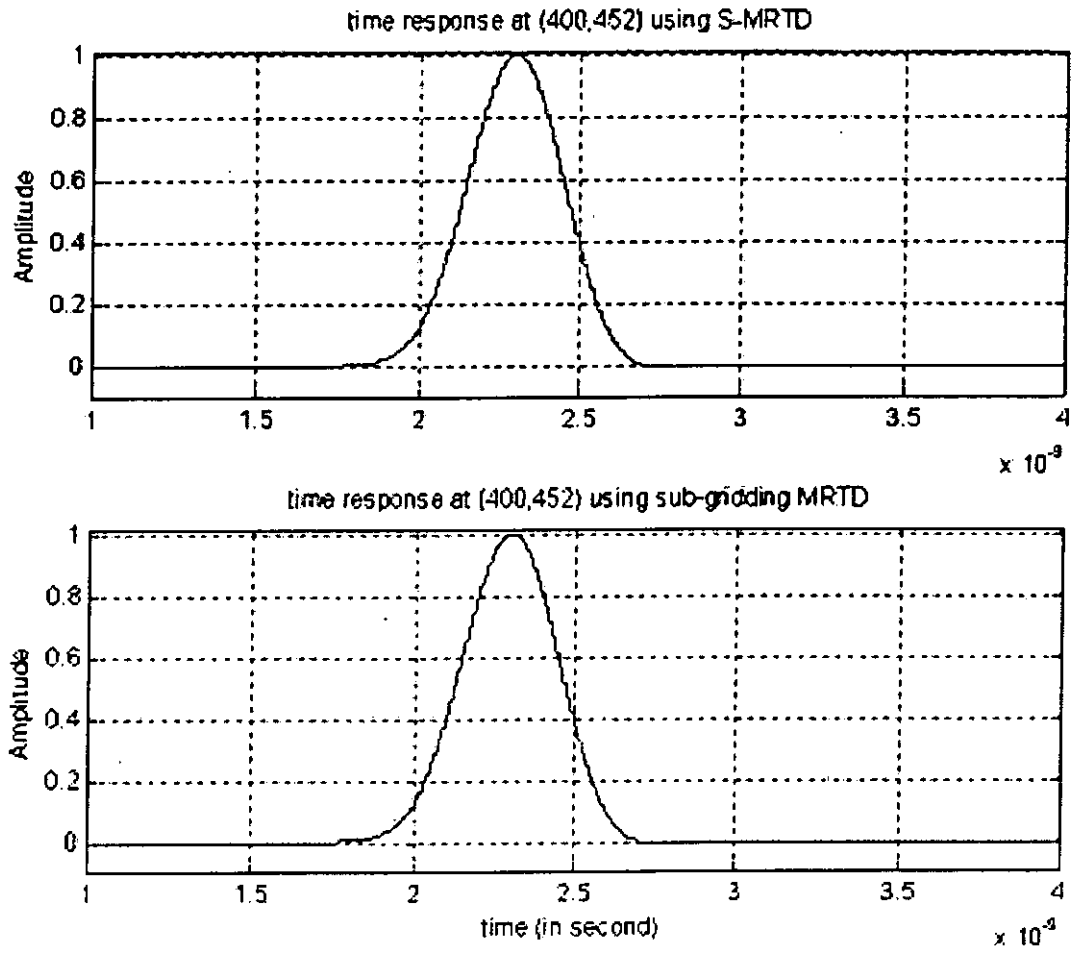

Figure 4.18. The comparsion of time response at point C using the S-MRTD and sub-gridding MRTD with cell size=0.1λ (The source is excited at the dense grid region)

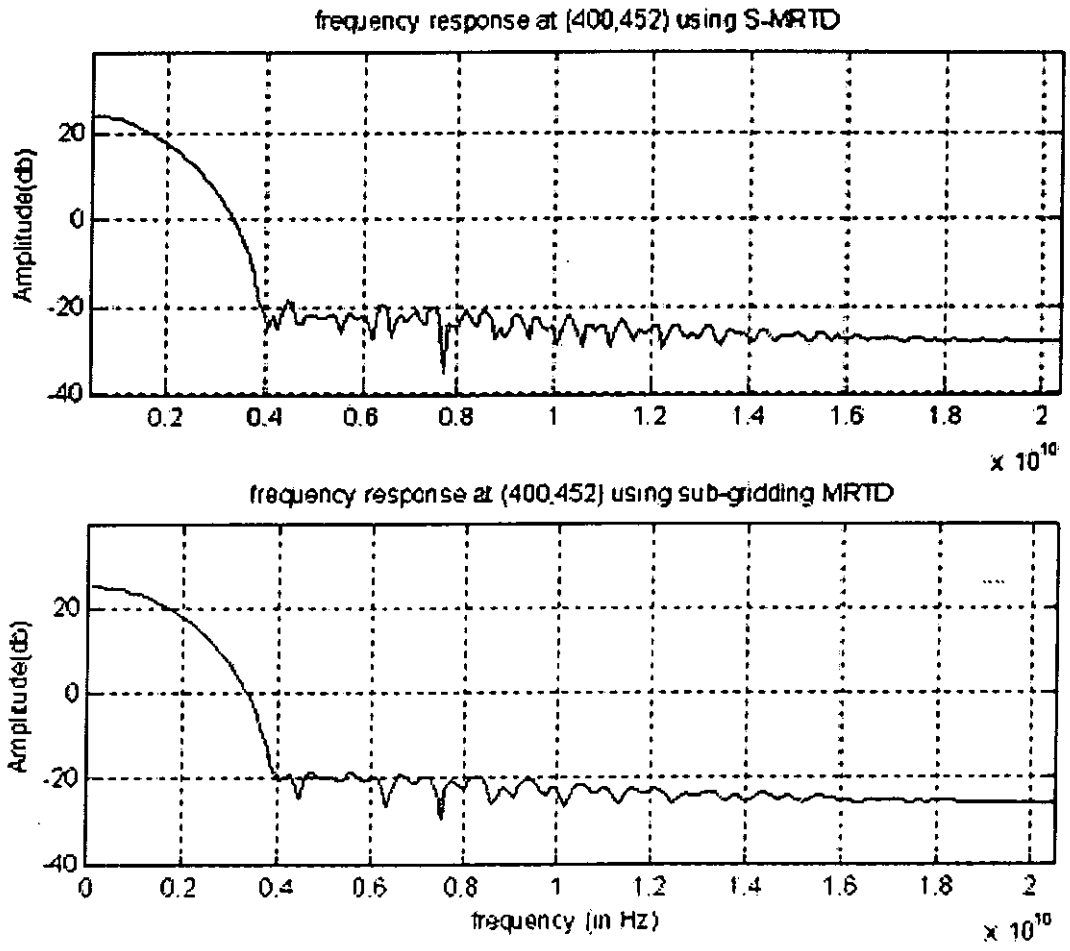

Figure 4.19. The comparsion of frequency response at point C using the S-MRTD and sub-gridding MRTD with cell size=0.1λ (The source is excited at the dense grid region)

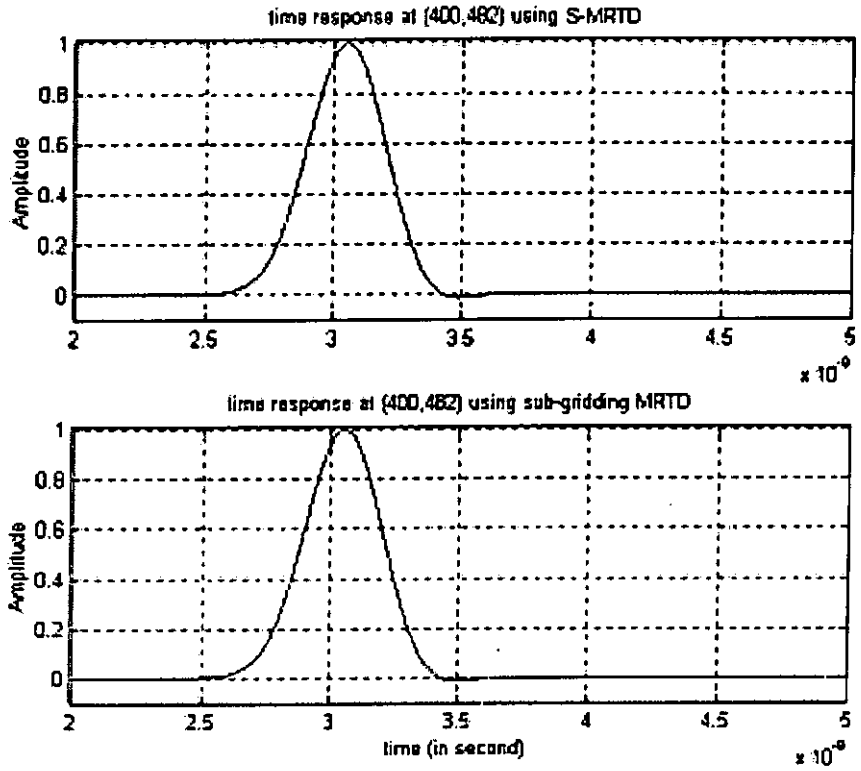

Figure 4.20. The comparsion of time response at point D using the S-MRTD and sub-gridding MRTD with cell size=0.1λ (The source is excited at the dense grid region)

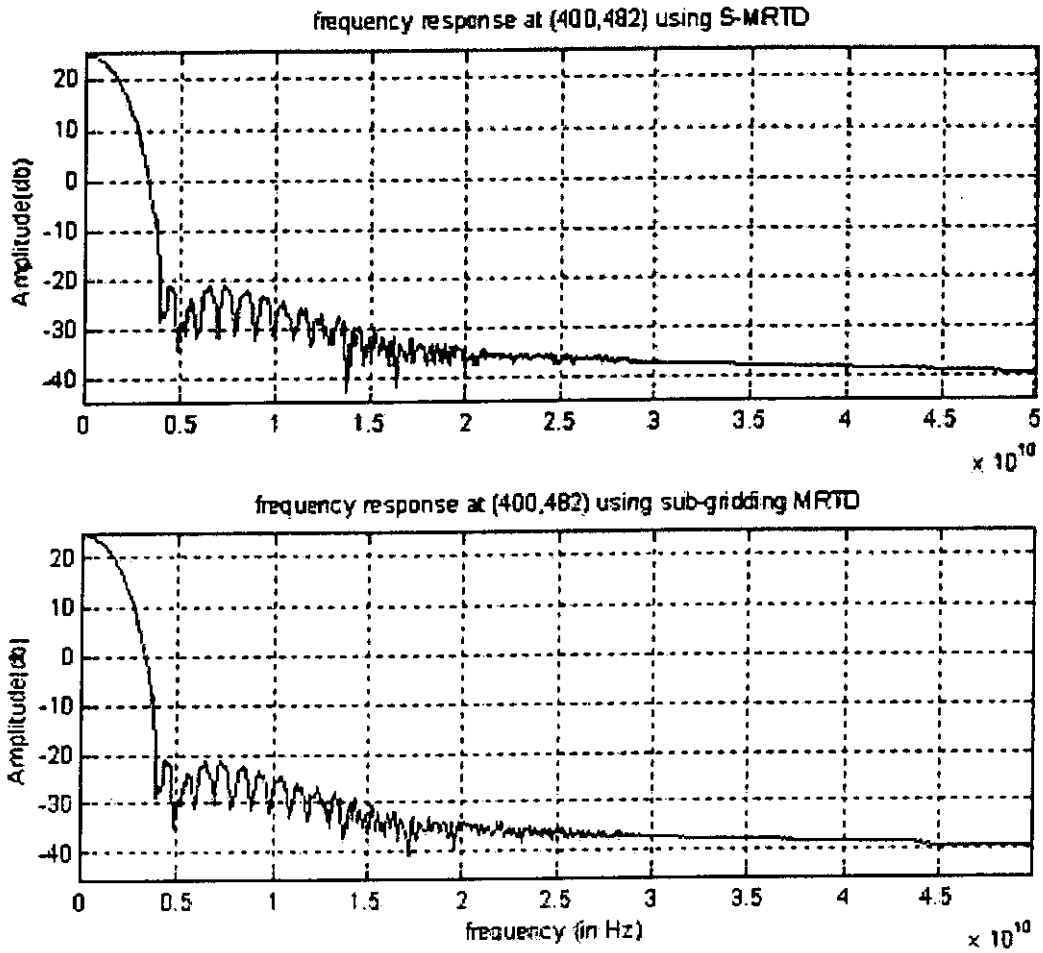

Figure 4.21. The comparsion of frequency response at point D using the S-MRTD and sub-gridding MRTD with cell size=0.1λ (The source is excited at the dense grid region)

When the pulse travel from the dense grid region to the coarse grid region, the results indicate that the sub-gridding MRTD obtains almost the same results as both obtained by the W-MRTD and S-MRTD especially when the cell size is one tenth of the wavelength. In the last chapter, we mentioned that the APML in the region III is used to remove the numerical wave due to the wavelet coefficients. Also, it is invisible to the numerical wave of the scaling coefficients. In order to verify this property, a pulse is excited inside the coarse grid region in next section.

4.1.2 The source is excited inside the coarse grid region

A row source of Blackman Harris window function is excited at point D as in figure 4.22. The APML with 4 cells is inserted at 440 cells counting from the left boundary in as in figure 4.22. The time response is observed at four locations inside the cavity. Three locations inside the dense grid region are observed. Other point is located in the coarse grid region. The results have been compared by the S-MRTD and W-MRTD using the same parameters. For comparison, two different cell sizes have been considered. Both simulations run 3000 times step and time step (Δt) is 1.125ps.

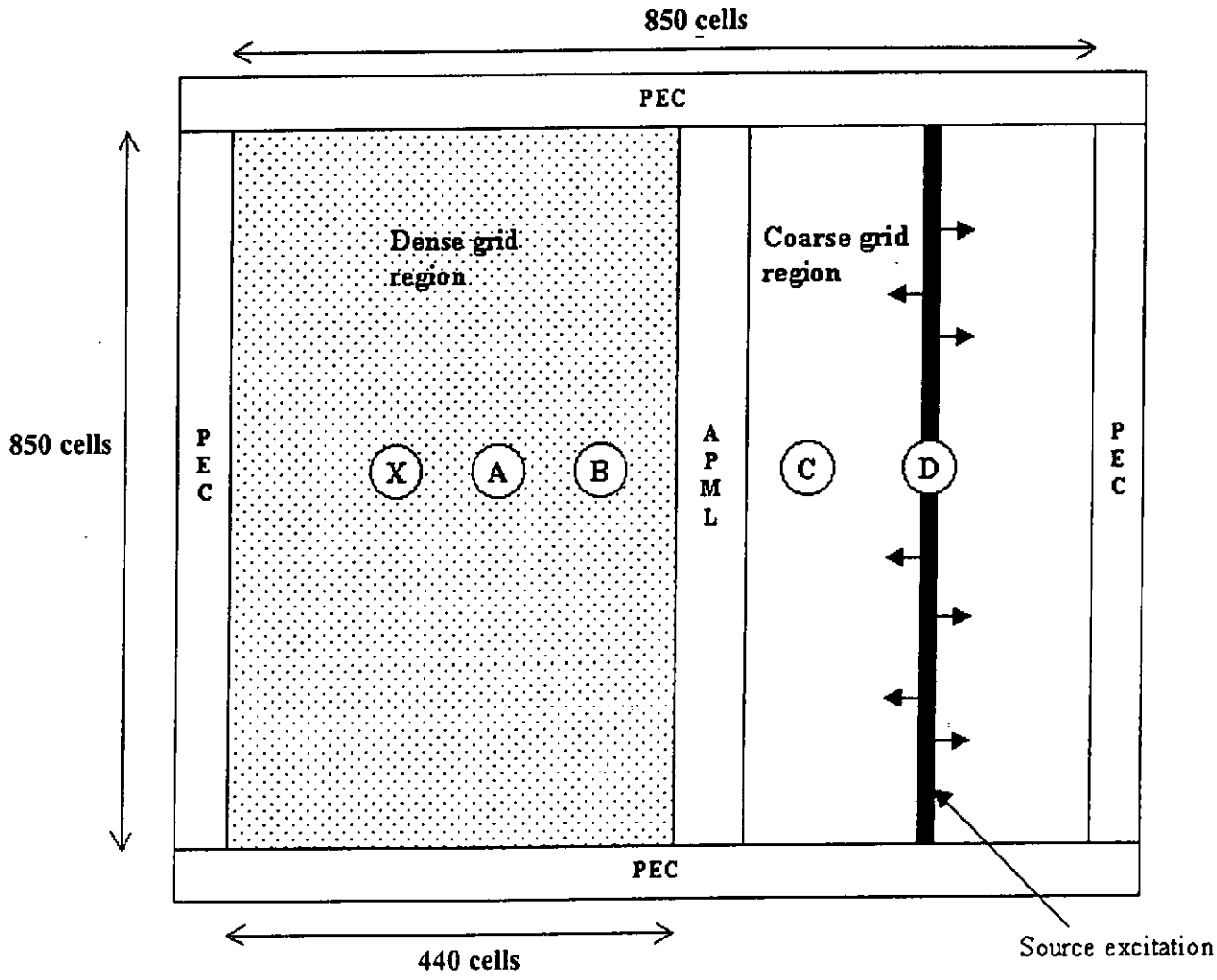

Coordinates of point X: (400,392)

Coordinates of point A: (400,412)

Coordinates of point B: (400,432)

Coordinates of point C: (400,452)

Coordinates of point D: (400,482)

Figure 4.22. The geometry of the two dimensional cavity using sub-gridding MRTD with 4 cells in the APML boundary (the source is excited at the coarse grid region)

4.1.2.1 Cell size is one half of the wavelength

In this simulation, a Blackman Harris window function of 20GHz cut-off frequency is used as the excitation. The grid size is 0.0075m, which is one half of the wavelength.

The time response is plotted inside the dense grid region of sub-gridding MRTD and compared with those obtained by the W-MRTD in figure 4.25, figure 4.27 and figure 4.29. The comparison of frequency response of the signal obtained by sub-gridding MRTD inside the dense grid region and W-MRTD is shown in figure 4.26, figure 4.28 and figure 4.30. The difference between the results can be seen in the frequency spectrum of the signal beyond 20GHz as in figure 4.26, figure 4.28 and figure 4.30.

The time response obtained inside the coarse grid region of sub-gridding MRTD is compared with the S-MRTD as shown in figure 4.23. For frequency above 20GHz, the signal obtained by the sub-gridding MRTD is different from those by the S-MRTD. It can be seen in the frequency response in figure 4.24.

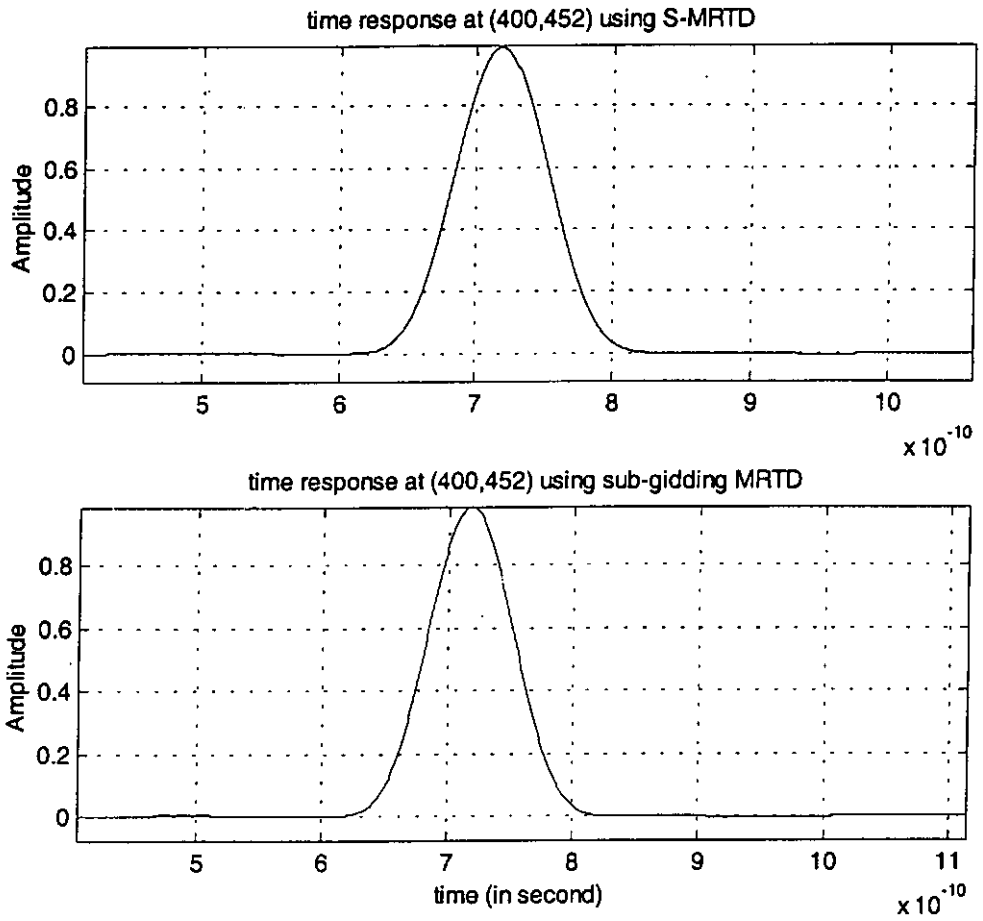

Figure 4.23. The comparsion of time response at point C using the S-MRTD and sub-gridding MRTD with cell size=0.5λ (the source is excited at the coarse grid region)

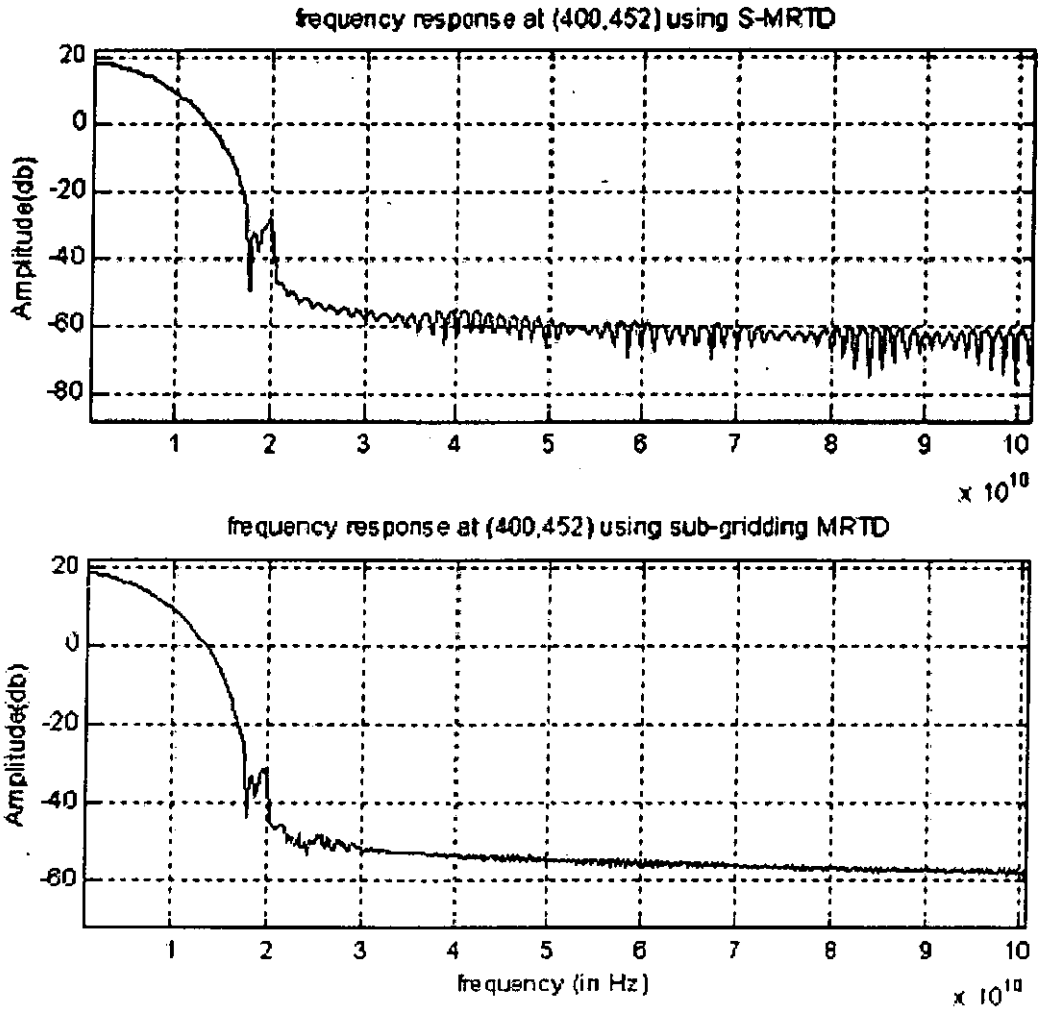

Figure 4.24. The comparsion of frequency response at point C using the S-MRTD and sub-gridding MRTD with cell size=0.5λ (the source is excited at the coarse grid region)

Pao Yue-Kong Library
PolyU • Hong Kong

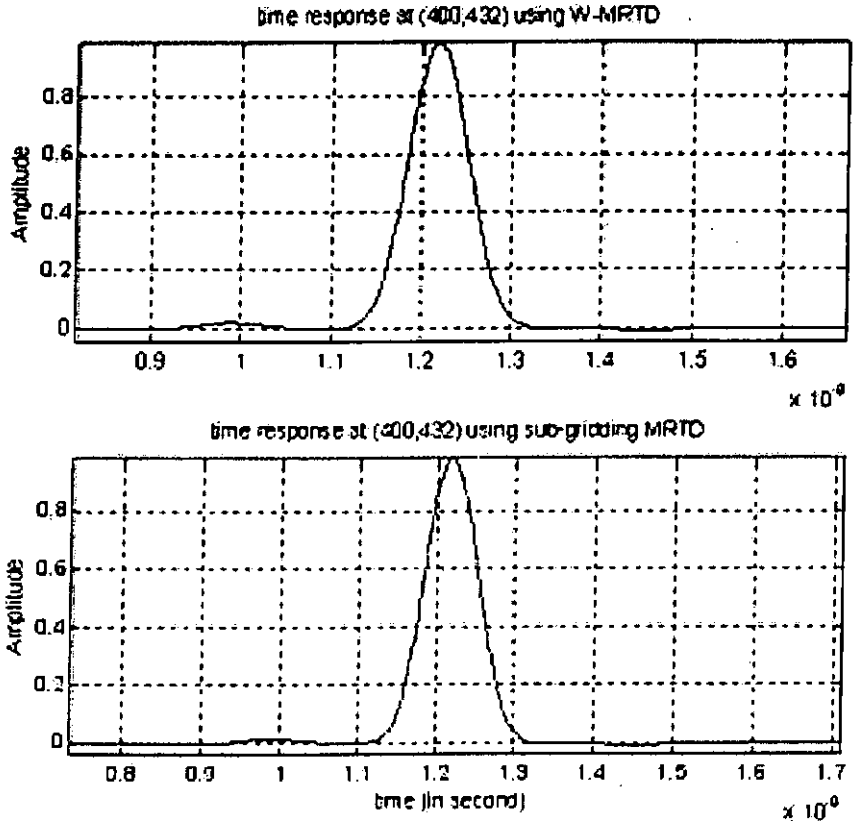

Figure 4.25 The comparsion of time response at point B using the W-MRTD and sub-gridding MRTD with cell size=0.5λ (the source is excited at the coarse grid region)

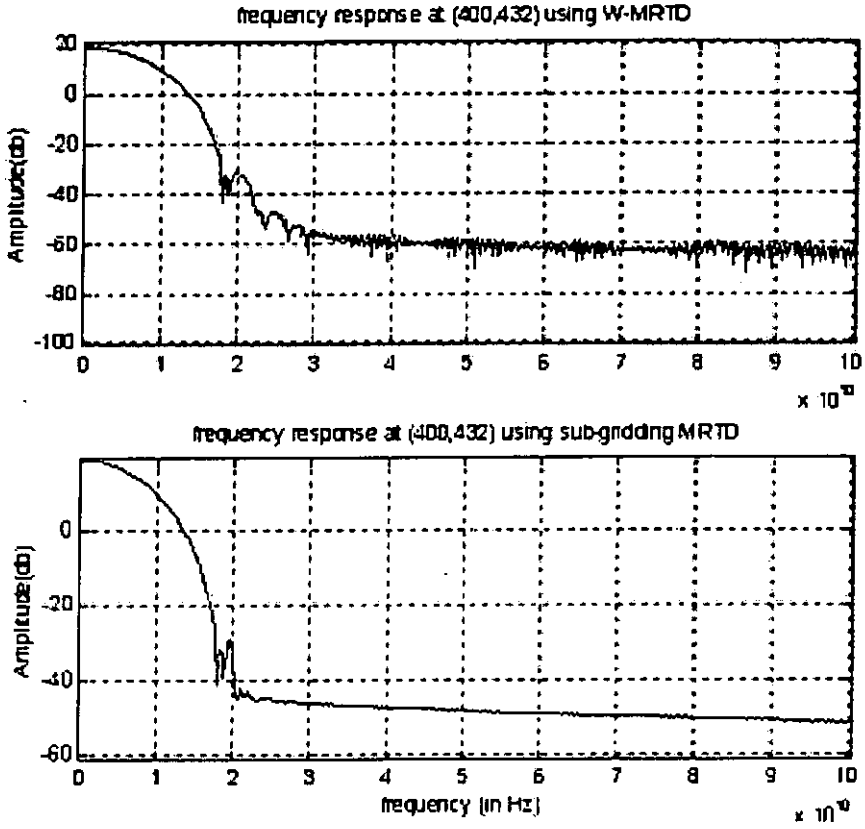

Figure 4.26. The comparsion of frequency response at point B using the W-MRTD and sub-gridding MRTD with cell size=0.5λ (the source is excited at the coarse grid region)

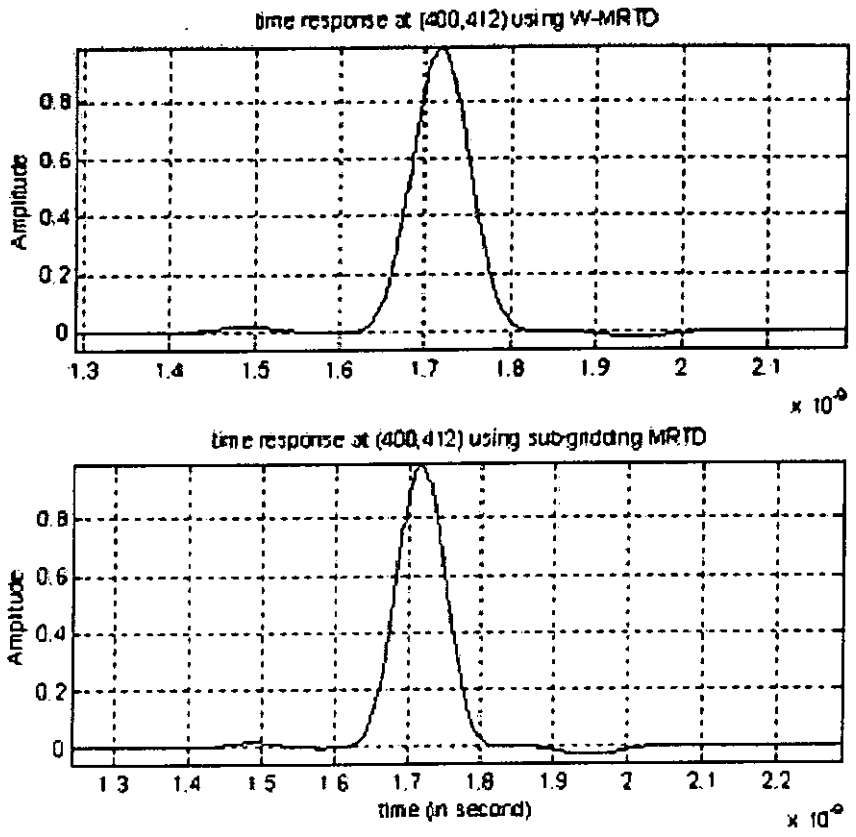

Figure 4.27. The comparsion of time response at point A using the W-MRTD and sub-gridding MRTD with cell size=0.5λ (the source is excited at the coarse grid region)

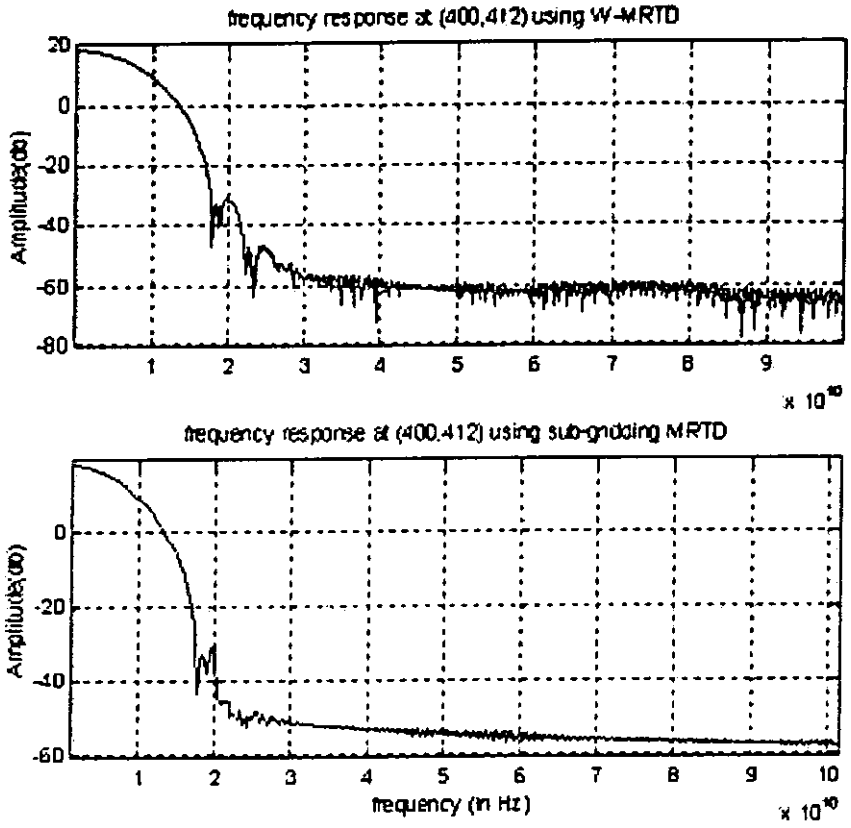

Figure 4.28. The comparsion of frequency response at point A using W-MRTD and sub-gridding MRTD with cell size=0.5λ (the source is excited at the coarse grid region)

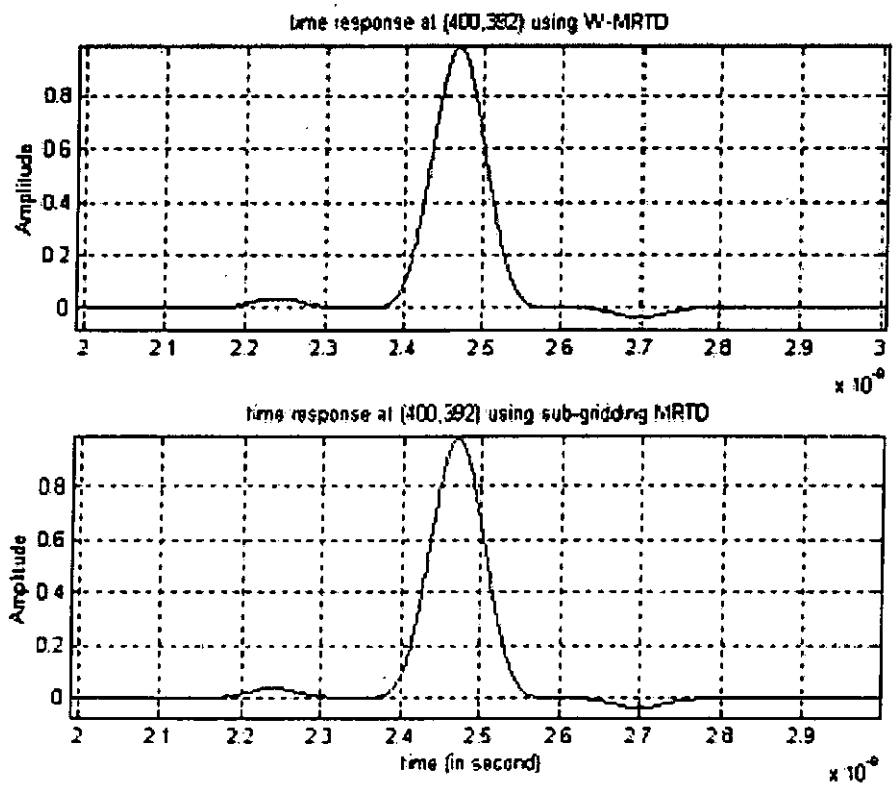

Figure 4.29. The comparsion of time response at point X using W-MRTD and sub-gridding MRTD with cell size=0.5λ (the source is excited at the coarse grid region)

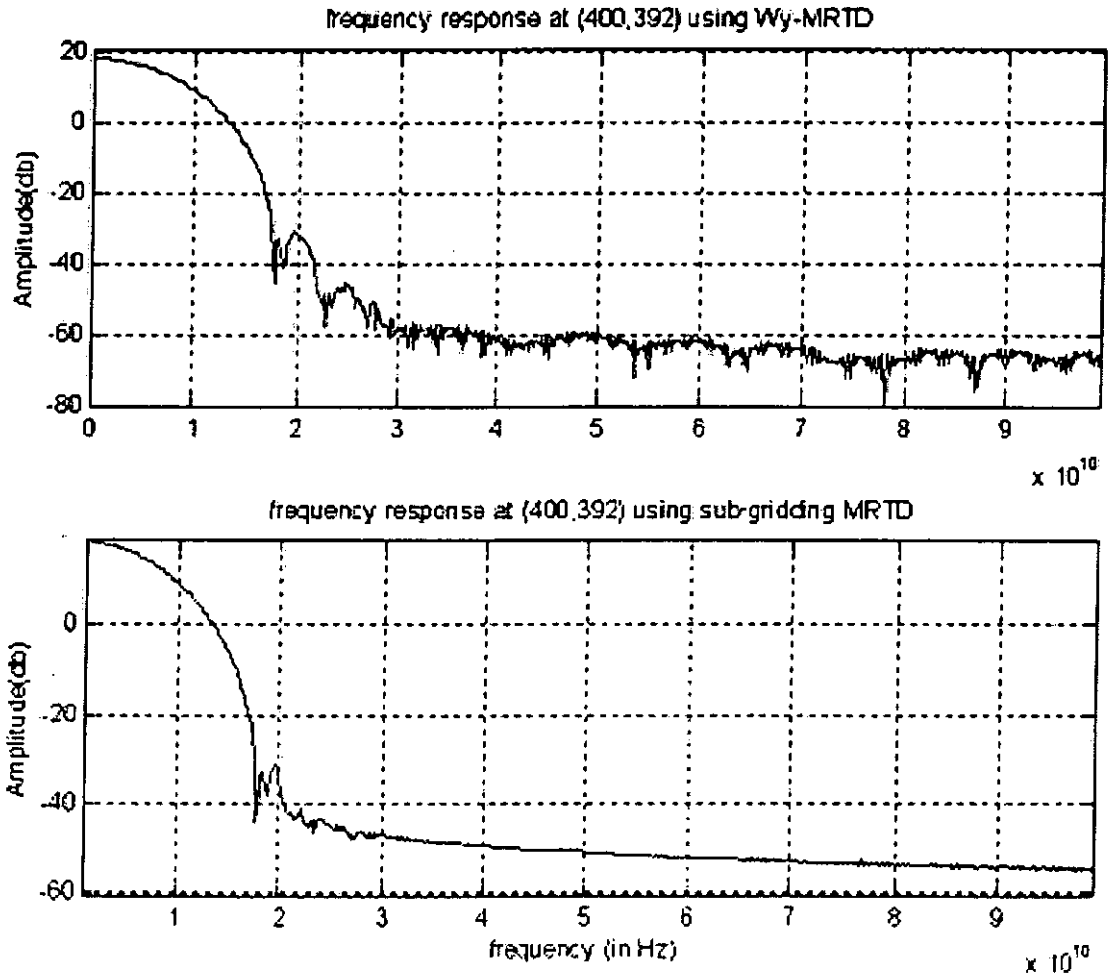

Figure 4.30. The comparsion of frequency response at point X using W-MRTD and sub-gridding MRTD with cell size=0.5λ (the source is excited at the coarse grid region)

4.1.2.2 Cell size is one tenth of the wavelength

In this simulation, a Blackman Haris window function of 4GHz cutoff frequency is used as the excitation while other parameters remain unchange. The cell size is 0.0075m, which is one tenth of the wavelength.

The time response is observed inside the dense grid region of sub-gridding MRTD and compared with those obtained by the W-MRTD as shown in figure 4.33, figure 4.35 and figure 4.37. The comparison of frequency response of the signal obtained by the sub-gridding MRTD inside the dense grid region and W-MRTD is seen in figure 4.34, figure 4.36 and figure 4.38. For frequency above 15GHz, the signal obtained by sub-gridding MRTD is different from that of W-MRTD.

The time response obtained inside the coarse grid region of sub-gridding MRTD is compared with the S-MRTD in figure 4.32. For frequency above 15GHz, the signal obtained by sub-gridding MRTD is different from those obtained by the S-MRTD. This can be seen in figure 4.32.

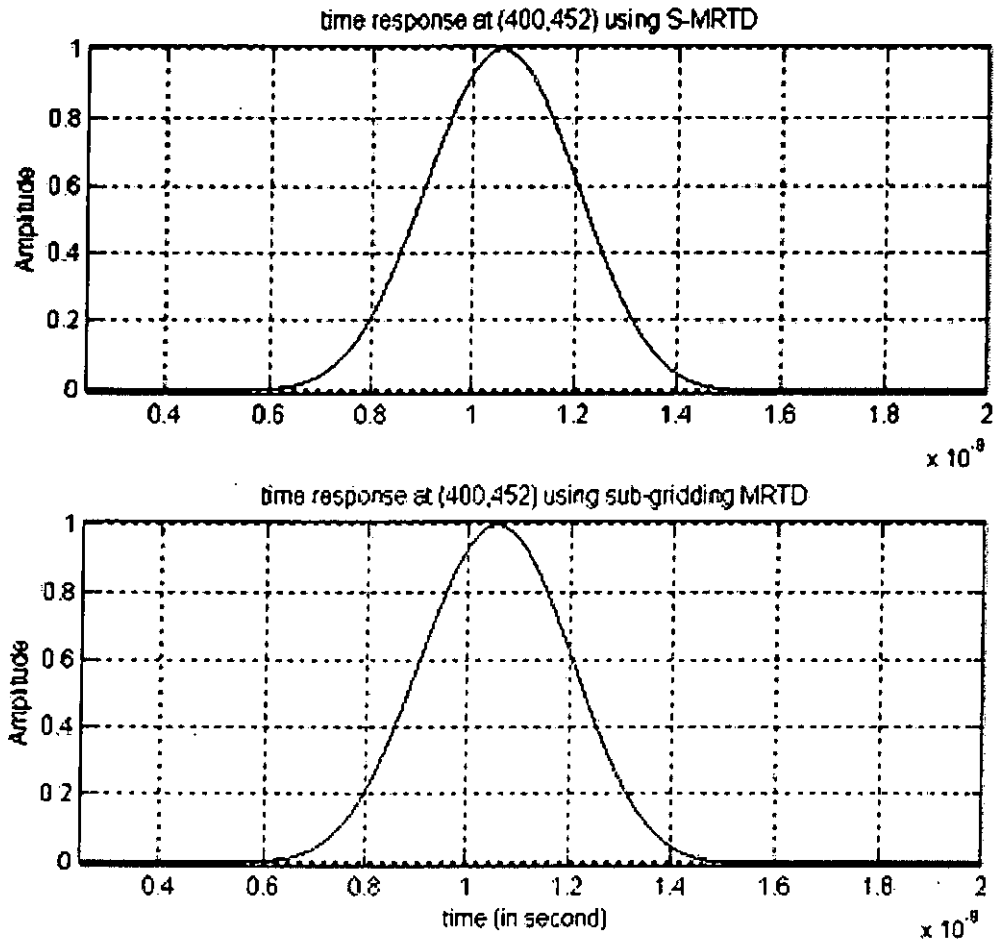

Figure 4.31. The comparison of time response at point C using the S-MRTD and sub-gridding MRTD with cell size=0.1λ (the source is excited at the coarse grid region)

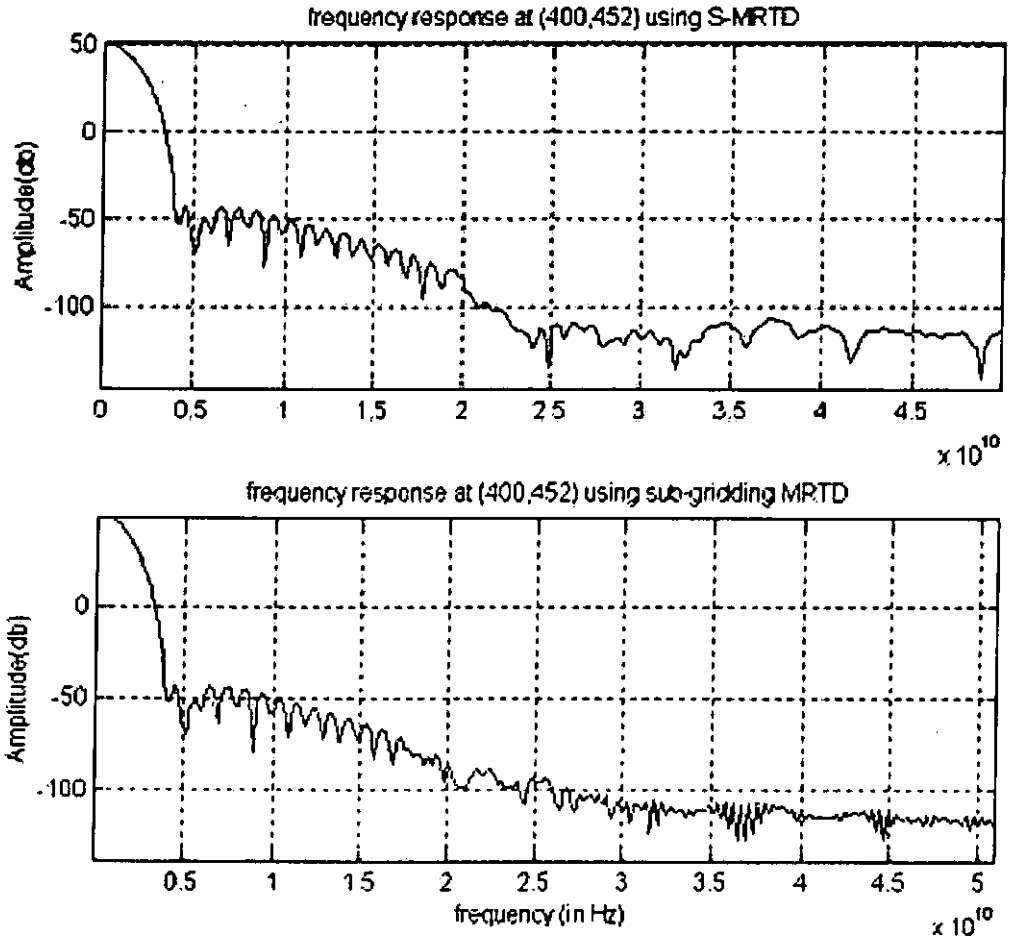

Figure 4.32. The comparsion of frequency response at point C using the S-MRTD and sub-gridding MRTD with cell size=0.1λ (the source is excited at the coarse grid region)

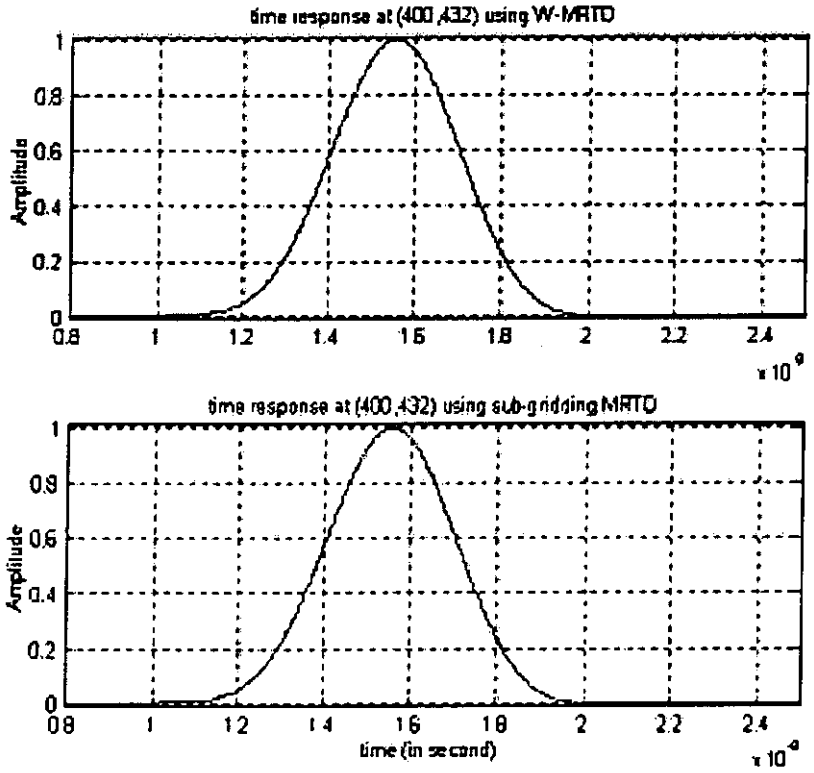

Figure 4.33. The comparsion of time response at point B using the W-MRTD and sub-gridding MRTD with cell size=0.1λ (the source is excited at the coarse grid region)

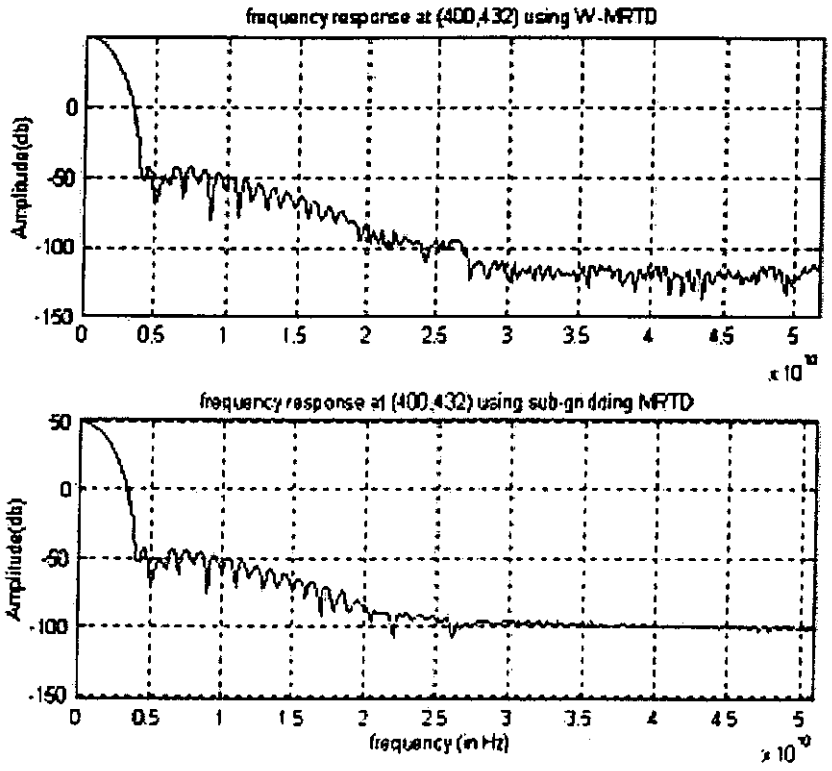

Figure 4.34. The comparsion of frequency response at point B using the W-MRTD and sub-gridding MRTD with cell size=0.1λ (the source is excited at the coarse grid region)

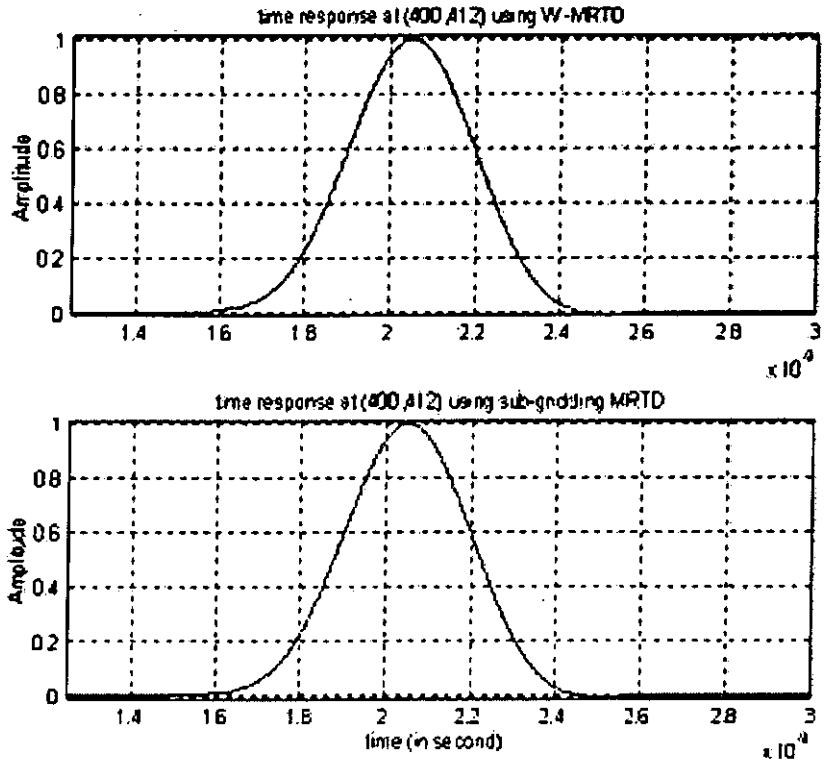

Figure 4.35. The comparsion of time response at point A using the W-MRTD and sub- gridding MRTD with cell size=0.1λ (the source is excited at the coarse grid region)

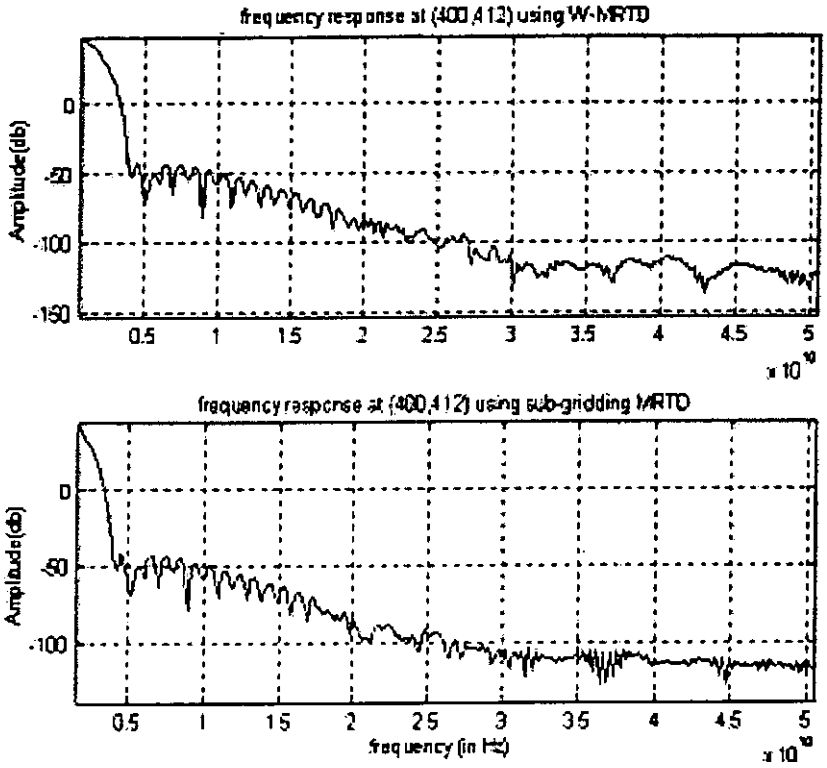

Figure 4.36. The comparsion of frequency response at point A using the W-MRTD and sub-gridding MRTD with cell size=0.1λ (the source is excited at the coarse grid region)

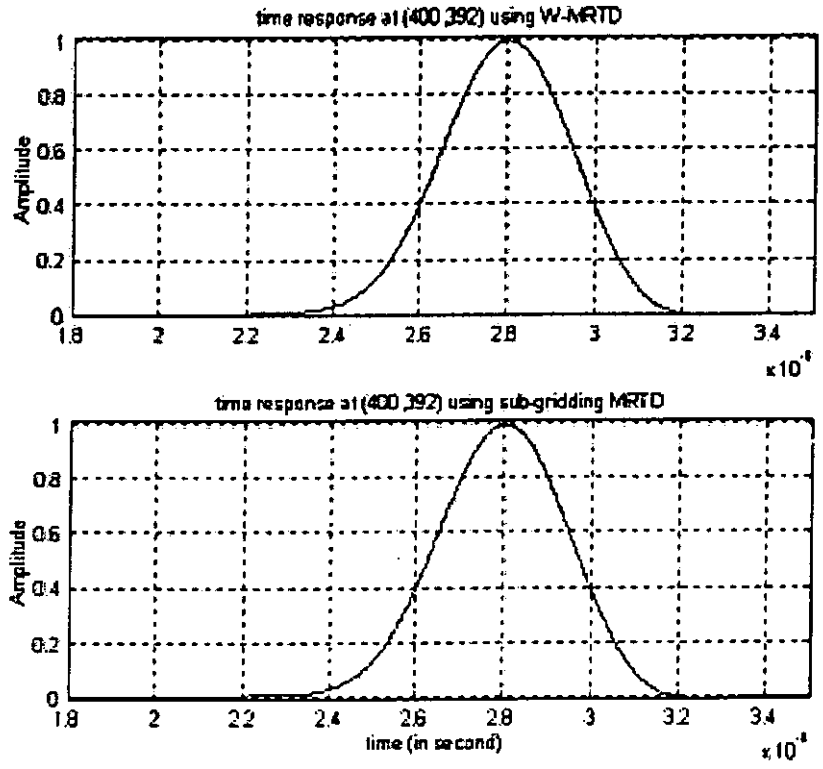

Figure 4.37. The comparsion of time response at point X using W-MRTD and sub-gridding MRTD with cell size=0.1λ (the source is excited at the coarse grid region)

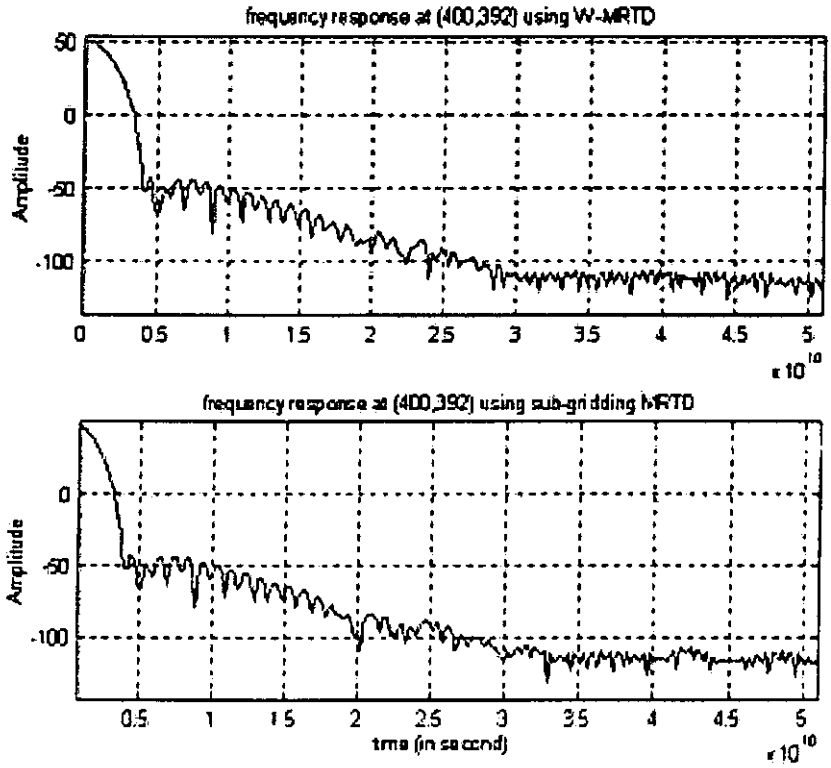

Figure 4.38. The comparsion of frequency response at point X using W-MRTD and sub-gridding MRTD with cell size=0.1λ (the source is excited at the coarse grid region)

From the above simulations results, it is noticed that the results obtained by sub-gridding MRTD are very close to the W-MRTD and the S-MRTD in both the dense grid region and coarse grid region.

When the grid size is one half of the wavelength, the results obtained by sub-gridding MRTD inside the dense grid region are compatible with those obtained by W-MRTD. We found that the results obtained by the sub–gridding MRTD are much closer to the results obtained by W-MRTD when finer grid is used. Only small difference is seen in the frequency spectrum beyond the cutoff frequency of the source. Hence, in these simulations, we found that sub-gridding MRTD can provide similar accuracy with the W-MRTD while it use less computational resources comparing with the W-MRTD.

For the coarse grid region, the results obtained by sub-gridding MRTD are very close to those obtained by the S-MRTD. Again, when a finer grid is used, the results obtained by sub-gridding MRTD are much closer to those obtained by the S-MRTD. The deviation of these results can be seen in frequency components beyond the cutoff frequency of the Blackman Harris window source. Hence, in these simulations, we found that the APML boundary can be used as an interface between the dense grid region and the coarse grid region.

In previous simulations, we have applied a sub-gridding MRTD to study two dimensional propagation problems. The results indicate that sub-gridding MRTD can get a similar result compared with those obtained by the S-MRTD and W-MRTD.

Although it increases the computation complexity at the boundary, it requires fewer grids to compute the field. In the next part, we will compare the accuracy of sub-gridding MRTD with both the S-MRTD and W-MRTD by studying the resonance frequency of a two dimensional cavity.

4.2 Resonant frequencies of a two-dimensional air filled cavity

A two dimensional air filled cavity is a closed structure, which is surrounding by conducting walls with air inside as shown in figure 4.39. When there is an excitation of electromagnetic pulse, the pulse will propagate inside the cavity and reflected by the conducting walls. The reflected wave will either cancel out or superimpose with the incoming wave. Only certain frequencies of the wave exist in the cavity. These frequencies are said to be resonant frequencies of the cavity, which is independent to the source of excitation. Instead, it depends on the dimension of the cavity and the dielectric substance inside the cavity. The resonance frequency of the cavity is given by

$$f_{mn} = \frac{C}{2}\sqrt{\left(\frac{m}{a}\right)^2 + \left(\frac{n}{b}\right)^2} \qquad \text{(Hz)} \qquad (4.2)$$

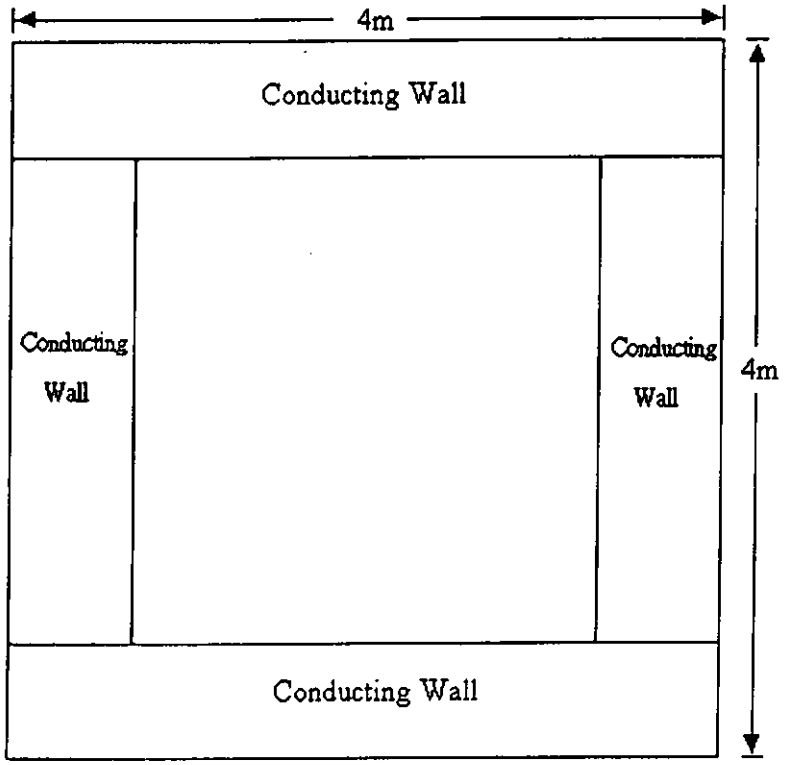

Figure 4.39. The Geometry of the two-dimensional air filled cavity

Our aim of this simulation is to compare the memory resources and computation time of sub-gridding MRTD with the S-MRTD, W-MRTD and traditional FDTD by investigating the resonance frequencies of the cavity. A two-dimensional air-filled cavity with size 4m×4m has been considered. The source of excitation is 300MHz. Hence, the wavelength (λ) is 1m. For comparison, the time response of the cavity is observed from t=0 to t=2.357μs and the parameters are chosen to keep the percentage error of the first seven resonant frequency below 1%. Two different cell sizes are used for comparison. The time response of the signal is plotted as in figure 4.40. The time response is then transformed into frequency domain (figure 4.41).

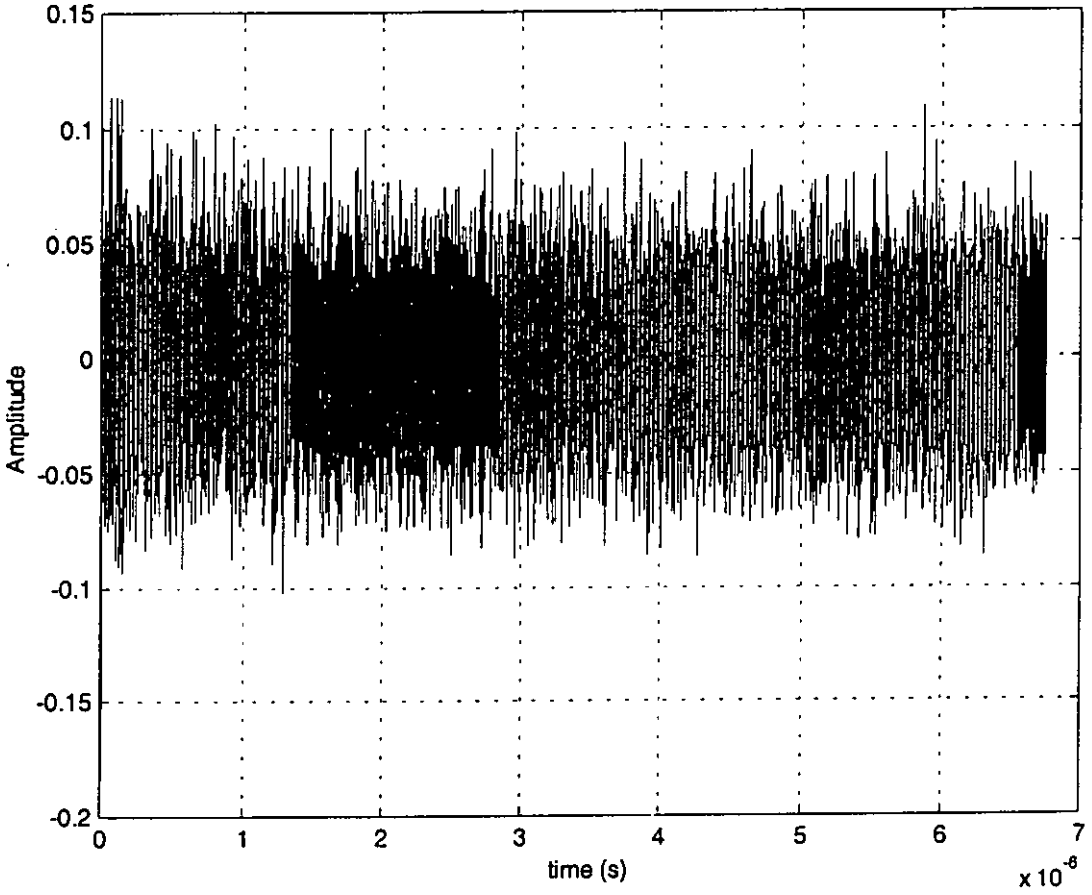

Figure 4.40. Magnitude of the E_z component in time domain calculated by sub-gridding MRTD inside a two dimensional air filled cavity (4m×4m).

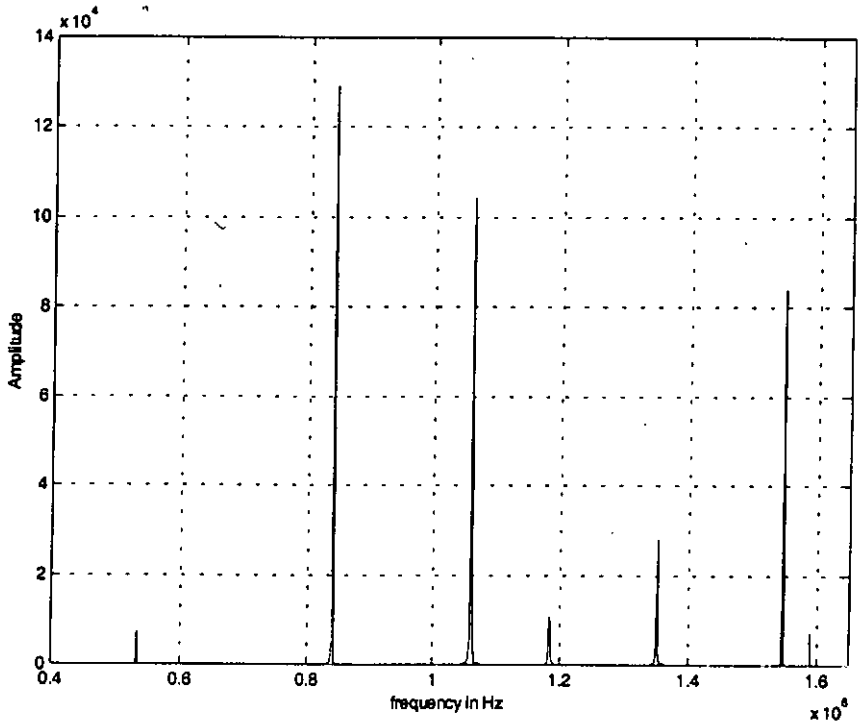

Figure 4.41. Magnitude of the E_z component in frequency domain calculated by sub-gridding MRTD inside a two dimensional air filled cavity (4m×4m).

For the FDTD analysis of the cavity, uniform mesh with Δx=0.1m is used, which corresponds to $\lambda/10$. This results in a total number of 1200 grid points. Since each FDTD cells contain three field components. They are, $E_z^n, H_x^{n+1/2}$ and $H_y^{n+1/2}$. Hence, the total number of variable that needs to update in each time step is 4800. In order to satisfy the FDTD stability condition in equation (1.14), the time step is choose as 23.6ps. The FDTD algorithm uses 629 seconds to simulate the time response of the cavity from t=0 to t=2.357μs. The results of the FDTD simulation are in Table 4.1.

Resonant frequency for an air-filled cavity (4m×4m)		
Cell size (Δx) : 0.1m	Time step (Δt) :23.6ρs (from t=0 to2.357μs)	
Computation Time: 629s	Platform: Linux on Pentium 166MHz computer	
Analytical values (MHz)	FDTD	
	Absolute values (MHz)	Relative error (%)
53.03	53.0	-0.06
83.85	83.6	-0.3
106.07	106.1	0.03
118.59	118.4	-0.16
135.21	134.9	-0.23
154.62	154.0	-0.4
159.10	158.2	-0.57

Table 4.1. The resonant frequency for an air filled cavity (4m×4m) using the FDTD with cell size (Δx)=0.1m and the time step (Δt) = 23.6ρs.

For the analysis of the cavity with S-MRTD scheme, a S-MRTD cell with Δx=0.2m is used, which corresponds to λ /5. This results in a total number of 400 grid points. As seen in figure 3.1, there are three fields components in each S-MRTD cell, hence the total number of variable stored in the computer in each time step is 1200. In order to satisfy the stability condition in equation (2.81), the time step is set as 100ρs. The S-MRTD algorithm uses 164 seconds to simulate the time response of the cavity from t=0 to t=2.357μs. The results of the S-MRTD simulation are in Table 4.2

Resonant frequency for an air-filled cavity (4m×4m)		
Cell size (Δx) : 0.2m	Time step (Δt) :100ρs (from t=0 to2.357μs)	
Computation Time: 164s	Platform: Linux on Pentium 166MHz computer	
Analytical values (MHz)	S-MRTD	
	Absolute values (MHz)	Relative error (%)
53.03	53.5	0.87
83.85	84.1	0.30
106.07	106.5	0.41
118.59	118.5	-0.08
135.21	135.4	0.14
154.62	154.7	0.05
159.10	159.4	-0.19

Table 4.2. The resonant frequency for an air filled cavity (4m×4m) using the S-MRTD with cell size (Δx)=0.2m and the time step (Δt) = 100ρs.

Analysing the cavity with the W-MRTD scheme, a W-MRTD cell with Δx=0.4m is used, which corresponds to λ /2.5. Compared with S-MRTD, the total number of grid point is reduced to 100. As seen in figure 3.2, there are six fields components in the cell. Hence, the total number of variables stored in the computer in each time step is 600. The time step is set as 100ps to satisfy the stability condition in equation (2.81). The W-MRTD algorithm uses 116 seconds to complete the simulation. The results of the W-MRTD simulation are in Table 4.3.

Resonant frequency for an air-filled cavity (4m×4m)		
Cell size (Δx) : 0.4m	Time step (Δt) :100ps (from t=0 to2.357μs)	
Computation Time: 116s	Platform: Linux on Pentium 166MHz computer	
Analytical values (MHz)	W-MRTD	
	Absolute values (MHz)	Relative error (%)
53.03	53.5	0.87
83.85	84.0	0.18
106.07	106.7	0.59
118.59	118.8	0.17
135.21	135.8	0.44
154.62	154.7	0.05
159.10	160.3	-0.75

Table 4.3. The resonant frequency for an air filled cavity (4m×4m) using the W-MRTD with cell size (Δx)=0.4m and the time step (Δt) = 100ps.

For the analysis of the cavity with sub-gridding MRTD scheme, a mesh with Δx=0.4m is used, which corresponds to λ /2.5. The sub-gridding MRTD model of the cavity can be seen in figure 4.42. The number of grid points in the dense grid region and the coarse grid region are 40 and 60 respectively. Also, there are 40 grid points in the APML region with 4 cells. With six fields components in each cells inside the dense grid region, the number of variable stored in the computer in this region is 240. For the coarse grid region, only three fields components need to calculate in each cell. Thus, the number of variable stored in the computer in the coarse grid region is 180. For the APML region, only two wavelet coefficients need to update in each time step. Hence, the number of variable stored in the computer in the APML region is 80.

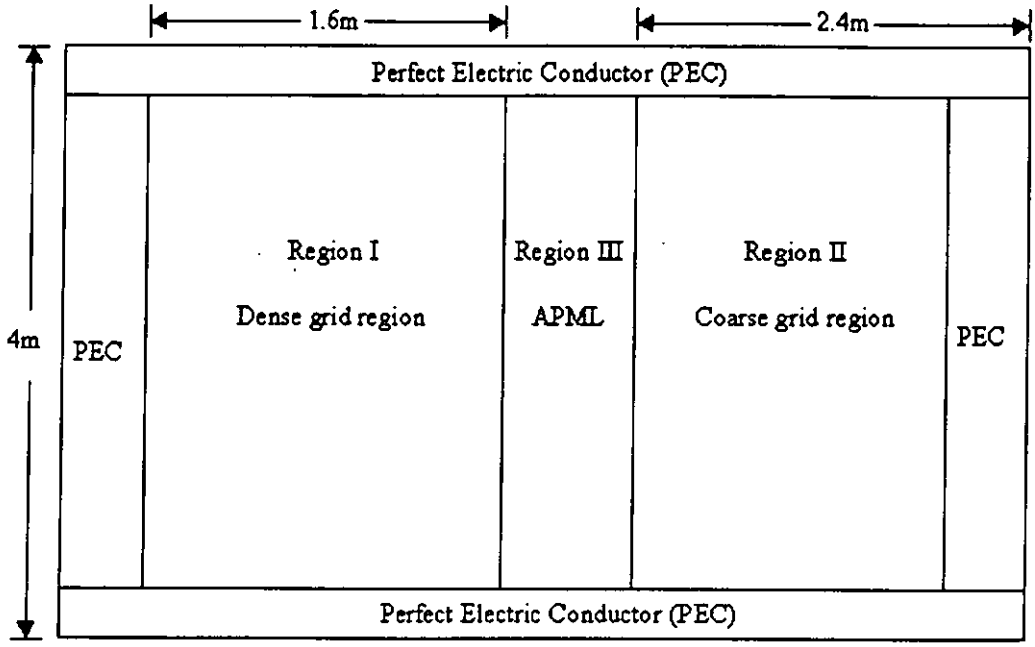

Figure 4.42. A sub-gridding MRTD model of the two dimensional air filled cavity

This results in a total number of 500 variables, which is stored in the computer in each time step. The time step is set as 100ps so as to satisfy the stability condition in equation (2.81). The sub-gridding MRTD uses 110 seconds to complete the simulation and the results of the sub-gridding MRTD simulation are in Table 4.4.

Resonant frequency for an air-filled cavity (4m×4m)		
Cell size (Δx) : 0.4m	Time step (Δt) :100ps (from t=0 to2.357μs)	
Computation Time: 110s	Platform: Linux on Pentium 166MHz computer	
Analytical values (MHz)	Sub-gridding MRTD	
	Absolute values (MHz)	Relative error (%)
53.03	53.0	-0.06
83.85	84.0	0.18
106.07	106.1	0.03
118.59	118.8	0.17
135.21	135.3	0.07
154.62	154.5	-0.08
159.10	159.0	-0.06

Table 4.4. The resonant frequency for an air filled cavity (4m×4m) using the sub-gridding MRTD with cell size (Δx)=0.4m and the time step (Δt) = 100ps.

From the simulation results, it can be conclude that the sub-gridding MRTD provides a good accuracy in measuring the resonant frequencies of the cavity. Also, It consumes less computational resources and use less computation time, compared with FDTD, S-MRTD and W-MRTD in Table 4.5. Compared with the FDTD, there is a 90% reduction in memory resources in the sub-gridding MRTD. With the same order of accuracy, the sub-gridding MRTD consumes 17% of the computation time of the FDTD. Compared with other MRTD scheme such as S-MRTD and W-MRTD, the memory resources of the sub-gridding MRTD reduce to 60% and 23% of those consumed by the S-MRTD and W-MRTD respectively. Besides, the sub-gridding MRTD saves 35% and 6% of the computation time consumed by the S-MRTD and W-MRTD respectively.

Platform: Linux on Pentium 166MHz computer	Computation time (in seconds)	Relative error (<1%)	Memory resources (Number of variables)
FDTD	629s	<1%	4800
S-MRTD	164s	<1%	1200
W-MRTD	116s	<1%	600
Sub-gridding-MRTD	110s	<1%	500

Table 4.5. Comparison of the sub-gridding MRTD method to S-MRTD, W-MRTD and FDTD in terms of memory resources and computation times with the relative error below 1%

4.3 Summary

In this chapter, we have applied the proposed sub-gridding MRTD to some two-dimensional field problems. The propagation of electromagnetic wave inside the cavity is considered. The time response are observed and compared with those results obtained by the S-MRTD and W-MRTD. Also, we have compared the memory resources and the computation time of sub-gridding MRTD with traditional FDTD, S-MRTD and W-MRTD by studing the resonant frequencies of an air-filled cavity.

Chapter 5

Further development

In this thesis, we have applied the sub-gridding MRTD to study the propagation of the electromagnetic wave. Also, the sub-gridding is used to calculate the resonance frequencies of a cavity. The sub-gridding MRTD can obtain similar degree of accuracy as W-MRTD while the sub-gridding MRTD use less computational resources than the W-MRTD.

Throughout the thesis, only one APML is inserted to separate the dense grid region and the coarse grid region. In future, two APML regions will be inserted so that the dense grid region is separated by the APML in both positive direction and negative direction. Besides, we will consider the possibility of increasing the grid density by using wavelets to expand both x –coordinate and y- coordinate in the sub-gridding MRTD. APML regions will be inserted in such a way that the dense grid region will be completely surrounded by the APML. Hence the sizes of the dense grid region can be adjusted in both x-direction and y-direction easily.

In future, we will apply the sub-gridding MRTD to analyze the microwave structure. To model the structures involve dielectric media, we have to solve extra sets of equation, which involve the calculation of permitivity matrix and electric flux vector(D). In the following text, we will describe the general concepts of incorporating the $\boldsymbol{D}$ field and permitivity matrix $\varepsilon(r,t)$ to the sub-gridding MRTD algorithm. At first, we have to break down the Maxwell's equation in (2.2) into the following two equations.

$$\nabla \times \boldsymbol{H} = \frac{\partial}{\partial t}\boldsymbol{D} \tag{5.1}$$

and

$$\boldsymbol{D} = \varepsilon(r,t)\boldsymbol{E} \tag{5.2}$$

, where $\boldsymbol{D}$ is the electric flux vector. $\varepsilon(r,t)$ is permittivity tensor, assuming it is anisotropic media. The space and time dependent permitivity tensor can be simplicity to which is given by

$$\varepsilon(r,t) = \begin{bmatrix} \varepsilon_{xx}(r,t) & 0 & 0 \\ 0 & \varepsilon_{yy}(r,t) & 0 \\ 0 & 0 & \varepsilon_{zz}(r,t) \end{bmatrix} \tag{5.3}$$

.Hence, the resultant $\boldsymbol{D}$ field will be written as follow.

$$\begin{aligned} D_x &= \varepsilon_{xx}(r,t)E_x \\ D_y &= \varepsilon_{yy}(r,t)E_y \\ D_z &= \varepsilon_{zz}(r,t)E_z \end{aligned} \tag{5.4}$$

To obtain the sub-gridding MRTD model, we have to discretize equation (x.x) by moment method. Using D_x field as an example, D_x field in the dense grid region will be written as

$$D_x(r,t) = \sum_{k,l,m,n=-\infty}^{\infty} [\ {}_k D^{\phi\alpha}_{l+1/2,m,n} \phi_m(y) + {}_k D^{\psi\alpha}_{l+1/2,m+1/2,n} \psi_{m+1/2}(y)] \phi_{l+1/2}(x) \phi_n(z) h_k(t) \quad (5.5)$$

For the coarse grid region, D_x field will be written as

$$D_x(r,t) = \sum_{k,l,m,n=-\infty}^{\infty} {}_k D^{\phi\alpha}_{l+1/2,m,n} \phi_m(y) \phi_{l+1/2}(x) \phi_n(z) h_k(t) \quad (5.6)$$

The updating equation of the D_x field can be determined by method mentioned in chapter 2. In order to calculate the E_x, we have to discretize the equation (x.). Hence, we will get the following equations.

In the dense grid region,

$$\begin{aligned} {}_k D^{\phi\alpha}_{l+1/2,m,n} = \sum_{k,l,m,n=-\infty}^{\infty} & \varepsilon x^{\phi\alpha}_{l,l'} \cdot \varepsilon y^{\phi\alpha}_{m,m'} \cdot \varepsilon z^{\phi\alpha}_{n,n'} \cdot \varepsilon t^{\phi\alpha}_{k,k'} \cdot {}_k E^{\phi\alpha}_{l'+1/2,m',n'} \\ & + \varepsilon x^{\phi\alpha}_{l,l'} \cdot \varepsilon y^{ix}_{m,m'} \cdot \varepsilon z^{\phi\alpha}_{n,n'} \cdot \varepsilon t^{\phi\alpha}_{k,k'} \cdot {}_k E^{\psi\alpha}_{l'+1/2,m'+1/2,n'} \end{aligned} \quad (5.7)$$

$$\begin{aligned} {}_k D^{\psi\alpha}_{l+1/2,m+1/2,n} = \sum_{k,l,m,n=-\infty}^{\infty} & \varepsilon x^{\phi\alpha}_{l,l'} \cdot \varepsilon y^{lx}_{m,m'} \cdot \varepsilon z^{\phi\alpha}_{n,n'} \cdot \varepsilon t^{\phi\alpha}_{k,k'} \cdot {}_k E^{\phi\alpha}_{l'+1/2,m',n'} \\ & + \varepsilon x^{\phi\alpha}_{l,l'} \cdot \varepsilon y^{\psi\alpha}_{m,m'} \cdot \varepsilon z^{\phi\alpha}_{n,n'} \cdot \varepsilon t^{\phi\alpha}_{k,k'} \cdot {}_k E^{\psi\alpha}_{l'+1/2,m'+1/2,n'} \end{aligned} \quad (5.8)$$

,where $\varepsilon x^{\phi\alpha}_{l,l'}, \varepsilon y^{lx}_{m,m'}, \varepsilon y^{\psi\alpha}_{m,m'}, \varepsilon z^{\phi\alpha}_{n,n'}$ and $\varepsilon t^{\phi\alpha}_{k,k'}$ are determined by the following relations

$$\varepsilon p^{\phi\alpha}_{l,l'} = \frac{1}{\Delta p} \int_{-\infty}^{+\infty} \varepsilon_{xx}(r,t) \phi_l(p) \phi_{l'}(p) dp \quad \text{where } p = x, y, z$$

$$\varepsilon t^{\phi\alpha}_{k,k'} = \frac{1}{\Delta p} \int_{-\infty}^{+\infty} \varepsilon_{xx}(r,t) h_k(t) h_{k'}(t) dt$$

$$\varepsilon y^{lx}_{m,m'} = \frac{1}{\Delta y} \int_{-\infty}^{+\infty} \varepsilon_{xx}(r,t) \phi_m(y) \psi_{m'}(y) dy$$

$$\varepsilon y^{\psi\alpha}_{m,m'} = \frac{1}{\Delta y}\int_{-\infty}^{+\infty} \varepsilon_{xx}(r,t)\psi_m(y)\psi_{m'}(y)dy \tag{5.9}$$

For the coarse grid region, since the D field and E field are expanded by scaling function only, hence the relations between the ${}_kD^{\phi\alpha}_{l+1/2,m,n}$ and ${}_kE^{\phi\alpha}_{l+1/2,m,n}$ is determined by

$${}_kD^{\phi\alpha}_{l+1/2,m,n} = \sum_{kJ,m,n=-\infty}^{\infty} \varepsilon x^{\phi\alpha}_{l,j'} \cdot \varepsilon y^{\phi\alpha}_{m,m'} \cdot \varepsilon z^{\phi\alpha}_{n,n'} \cdot \varepsilon t^{\phi\alpha}_{k,k'} \cdot {}_{k'}E^{\phi\alpha}_{l'+1/2,m',n'} \tag{5.10}$$

Hence, to perform a sub-gridding MRTD analysis on a particular field problem, we have to first calculate the permitivity matrix in the MRTD domain, such as $\varepsilon x^{\phi\alpha}_{l,j'}$, $\varepsilon y^{Ix}_{m,m'}$, $\varepsilon y^{\psi\alpha}_{m,m'}$, $\varepsilon z^{\phi\alpha}_{n,n'}$ and $\varepsilon t^{\phi\alpha}_{k,k'}$. The calculations of these matrix are only depends on the structure of the field problem. Thus, these matrixes can be stored in the computer for future use.

Chapter 6

Conclusions

In this thesis, we have proposed a new computational scheme, which is called sub-gridding MRTD. The sub-gridding MRTD consists of regions with different resolutions. For the coarse grid region, the fields are expanded by the scaling functions with respect to the spatial coordinates. The fields are updated by the S-MRTD updating equations inside this region. For the dense grid region, the fields are expanded by the scaling functions and wavelet functions with respect to the spatial coordinates. The fields are updated by the W-MRTD updating equations inside this region. It is found that there is a non-physical reflection at the boundary between the coarse grid region and the dense grid region. By the use of an Anisotropic Perfectly Matched Layer (APML), the non-physical reflection can be removed.

In order to investigate the performance of sub-gridding MRTD, the propagation of the electromagnetic pulse inside an extra large two-dimensional cavity has been considered. The results are obtained in both the dense grid region and coarse grid

region. We have compared the results obtained by sub-gridding MRTD with those obtained by the S-MRTD and the W-MRTD.

It is found that the results obtained by the sub-gridding MRTD in the dense grid region are very closed to those obtained by the W-MRTD so that only small difference can be seen in the higher frequency component. When a finer grid is used, the results obtained by sub-gridding MRTD are even closer to the results obtained by W-MRTD. For the coarse grid region, the results obtained by sub-gridding MRTD are almost the same as that obtained by the S-MRTD. The deviation of the results is seen in the higher frequency spectrum.

It can be seen that the results obtained by the sub-gridding MRTD inside the dense grid region are very closed to the results obtained by W-MRTD. Although it increases the computation complexity at the boundary, it requires fewer cells to compute the field and it can get almost identical results obtained by the W-MRTD. Also, We found that the results obtained inside the coarse grid region are very close to the results obtained by S-MRTD. This implies that the APML join the dense grid region and the coarse grid region successfully.

We have also compared the memory resources and the computation time of the sub-gridding MRTD to the tradition FDTD, S-MRTD and W-MRTD by studying the resonance frequencies of a two-dimensional cavity and the percentage error of the first seven modes of the resonant frequencies are kept below 1%.

The results indicates that the sub-gridding MRTD provides a good accuracy in measuring the resonant frequencies of the cavity, while in consumes less memory resources and fast computation time, compared with FDTD, S-MRTD and W-MRTD. Compared with the FDTD, there is a 90% reduction in memory resources in the sub-gridding MRTD. With the same order of accuracy, the sub-gridding MRTD consumes 17% of the computation time of the FDTD. For the other MRTD scheme such as S-MRTD and W-MRTD, the memory resources of the sub-gridding MRTD reduce to 60% and 23% of those consumed by the S-MRTD and W-MRTD respectively. Besides, the sub-gridding MRTD saves 35% and 6% of the computation time consumed by the S-MRTD and W-MRTD respectively.

It can be concluded that the sub-gridding MRTD can obtain accurate results with less memory resources and fast computation time. Although it increases the computation complexity at the boundary between the dense grid region and the coarse grid region, it use less computational resources but has a similar accuracy compared with the W-MRTD.

References

1. Navarro, E.A.and Such, V., "Study of TE and TM modes in waveguides of arbitrary cross-section using an FD-TD formulation Microwaves," IEEE Proceedings of Antennas and Propagation, vol.139, Dec. 1992, pp. 491-494.

2. Olivier, J.C.; McNamara, D.A, "Finite-difference time-domain (FD-TD) analysis of discontinuities in homogeneous dispersive waveguides," Electronics Letters, vol. 25, 20 July 1989, pp.1006 –1007.

3. Reineix, A.and Jecko, B, "Analysis of microstrip patch antennas using finite difference time domain method," IEEE Transactions on Antennas and Propagation, vol. 37, Nov. 1989 , pp. 1361-1369.

4. Olivier, J.C. and McNamara, D.A., "Analysis of multiport rectangular waveguide devices using pulsed finite-difference time-domain (FDTD) technique," Electronics Letters, vol. 28, 16 Jan. 1992, pp. 129 –131.

5. Leveque, P., Reineix, A. and Jecko, B., "Modelling of dielectric losses in microstrip patch antennas: application of FDTD method," Electronics Letters, vol. 28, 12 March 1992, pp. 539 –541.

6. Wagner, R.L.; Otto, G.P.; and Chew, W.C , "Fast waveguide mode computation using wavelet-like basis functions." IEEE Microwave and Guided Wave Letters Vol: 3, July 1993 , pp. 208 -210.

7. R.F. Harrington, *Field computation by Moment Methods.* New York: IEEE Press, c1993.

8. K.S.Yee, "Numerical solution of initial boundary value problems involving Maxwell's equations in isotropic media", IEEE Transactions on Antennas and Propagation. vol AP-14, May 1966, pp. 302-307.

9. Krumpholz, M and Linda P. B. Katehi, "MRTD: New Time-Domain Schemes Based on Multiresolution Analysis", IEEE Transactions on Microwave Theory and Technique, vol. 44, April 1996, pp. 555-571.

10. S.S. Zivanovix, K.S. Yee, and K.K. Mei, "A subgridding method for the time domain finite difference method to solve Maxwell's equations", IEEE Transaction on Microwave Theory and Technique, vol. 29, March 1991, pp 471-479.

11. M.Okoniewski, E. Okoniewska, and M.A. Stuchly, " Three dimensional subgridding algorithm for FDTD", IEEE Transaction on Antennas Propagation, vol 45, March 1997, pp 422-429.

12. L.S. Kim and W.J.R Hoefer, " A local mesh refinement algorithm for the time domain finite difference method using Maxwell's curl equations", IEEE Transaction on Microwave Theory and Technique, vol 38, Jun,1990, pp. 812-815.

13. E. Tentzeris, Krumpholz, M and Katechi, "Application of MRTD to printed transmission lines", IEEE Antennas and Propagation Society International Symposium 1996. AP-S. Digest, vol. 1, 1996, pp.634 -637.

14. Qunsheng Cao and Yinchao Chen, "MRTD Analysis of a Transient Electromagnetic Pulse Propagating through a Dielectric Layer", International Journal of Electronics, 1999, vol. 86, pp.459-474.

15. Robertson, R., Tentzeris, E.M.and Katehi, L.P.B. , "Modeling of membrane patch antennas using MRTD analysis," IEEE AP-S Digest, 1997, vol.1 , 1997 , pp. 126 –129.

16. Zhizhang Chen and Jiazong Zhang, "An efficient eigen-based spatial-MRTD method for computing resonant structures," IEEE Microwave and Guided Wave Letters Volume: 9, Sept. 1999 , pp. 333 –335.

17. Tentzeris, E.M., Robertson, R., Krumpholz, M.and Katehi, L.P.B., "Application of the PML absorber to the MRTD technique," AP-S. Digest, Antennas and Propagation Society International Symposium 1996, vol. 1 , 1996 , pp. 634 –637.

18. PML absorbing boundary conditions for the characterization of open microwave circuit components using multiresolution time-domain techniques (MRTD) Tentzeris, E.M.; Robertson, R.L.; Harvey, J.F.; Katehi, L.P.B. Antennas and Propagation, IEEE Transactions on Volume: 47 11 , Nov. 1999 , pp.1709 –1715.

19. Krumpholz, M., Katehi, L.P.B. Robertson, R. and Tentzeris, E , "MRTD analysis of dielectric cavity structures," Microwave Symposium Digest, 1996., IEEE MTT-S International Volume: 3 , 1996 , Page(s): 1861 –1864.

20. Goverdhanam, K. and Katehi, L.P.B., "Applications of Haar wavelet based MRTD scheme in the characterization of 3D microwave circuits," IEEE MTT-S Digest, vol. 4, pp. 1475 –1478.

21. Shlager, K.L.and Schneider, J.B., "Analysis of the dispersion properties of the multiresolution time-domain (MRTD) scheme," IEEE AP-S Digest, vol. 4, pp. 2144 –2147.

22. Tentzeris, E.M., Robertson, R.L., Harvey, J.F. and Katehi, L.P.B., "PML absorbing boundary conditions for the characterization of open microwave circuit components using multiresolution time-domain techniques (MRTD)," IEEE Transactions on Antennas and Propagation, vol. 47, Nov. 1999, pp. 1709 -1715.

23. Krumpholz, M., Winful, H.G.and Katehi, L.P.B., "Nonlinear time-domain modeling by multiresolution time domain (MRTD)," IEEE Transactions on Microwave Theory and Techniques, vol. 45, March 1997, pp. 385 –393.

24. K. Y. Choi, W. Y. Tam "Numerical dispersion of multiresolution time domain method (W-MRTD)," Proceedings, International on Symposium Antennas and Propagation Society, July 2000, vol.1, pp.256 –259.

25. Tentzeris, E.M., Robertson, R.L., Katehi, L.P.B. and Cangellaris, "Space- and time-adaptive gridding using MRTD technique," IEEE MTT-S Digest 1997, vol.1, 1997, pp. 337 –340.

26. K. Y. Choi, W. Y. Tam, "The theory of sub-gridding MRTD", Proceedings, IEEE International Symposium on Antennas and Propagation Signal Processing, vol.1, July 2000,pp.240-243.

27. Steinberg, B.Z. and Leviatan, Y , "On the use of wavelet expansions in the method of moments (EM scattering)," IEEE Transactions on Antennas and Propagation, vol. 41, May 1993 , pp. 610 –619.

28. Krumpholz, M, C. Huber, and P. Russer, "A field theoretical comparison of FDTD and TLM," IEEE Transactions on Pattern Analysis And Machine Intelligence, vol. 11, Sept. 1995, pp.1935-1950.

29. Krumpholz, M and P. Russer, "two dimensional FDTD and TLM", International Journal of Numerical Modeling, vol. 7, Feb. 1993, pp. 141-153.

30. Chui, C. K., *An introduction to wavelets*, Boston : Academic Press, c1992 .

31. Taflove, Allen, *Computational electrodynamics: the finite-difference time-domain method*, Artech House Boston c1995.

32. I.Daubechies, "Ten lectures on Wavelets", SIAM Review.,Philadelphia,PA,1982.

33. Mallat, S.; Hwang, W.L.,"Singularity detection and processing with wavelets," IEEE Transactions of Information Theory, vol.38, March 1992, pp. 617 –643.

34. Frisch, M.and Messer, H., "The use of the wavelet transform in the detection of an unknown transient signal," IEEE Transactions on Information Theory, vol. 38, March 1992, pp. 892 –897.

35. Taflove, Allen, *Advances in Computational electrodynamics: the finite-difference time-domain method*, Artech House Boston c1998

36. Battle,G., "A block spin construction of ondelettes ,part I: Lemarie functions," Commm. Math. Phys., vol. 110, 1987, pp. 601-615.

37. Tentzeris, E.M.; Robertson, R.L.; Harvey, J.F.; Katehi, L.P.B., "Stability and dispersion analysis of Battle-Lemarie-based MRTD schemes," IEEE Transactions on Microwave Theory and techniques, vol. 47, July 1999, pp. 1004 –1013.

38. Ling, H.and Kim, H., "Wavelet analysis of backscattering data from an open-ended waveguide cavity," IEEE Microwave and Guided Wave Letters, vol. 2 , April 1992 , pp. 140 –142.

39. Gedney, S.D., "An anisotropic perfectly matched layer absorbing media for the truncation of FDTD lattices," IEEE Transactions on Antennas and Propagation, vol. 44, 1996, pp.1630-1639.

40. Gedney, S.D., "An anisotropic PML absorbing media for FDTD simulation of fields in lossy dispersive media," Electromagnetics, vol.16, 1996, pp.399-415.

41. Qunsheng Cao, Yinchao Chen and Mittra, R., "An anisotropic perfectly matched layer (APML) absorber for mesh truncation in the context of a multiresolution time domain scheme Antennas and Propagation Society," Proceedings, IEEE International Symposium 1999, vol.3, 1999, pp. 2010 -2013.